ENGINEERING OF HUMAN ACID PHOSPHATASE ENZYME SENSITIVE NANOMEDICINE FOR HIV/AIDS PREVENTION BY TOPICAL ROUTE.

A DISSERTATION IN
Pharmaceutical Science
and
Chemistry

Presented to the Faculty of the University
of Missouri-Kansas City in partial fulfillment of
the requirements for the degree

DOCTOR OF PHILOSOPHY

by

ALBERT NGUESSAN NGO

B.S. Chemical engineering, National Institute Polytechnic
Felix Houphouët-Boigny, Ivory Coast, 2008

Kansas City, Missouri, 2018

ENGINEERING OF HUMAN ACID PHOSPHATASE ENZYME SENSITIVE NANOMEDICINE FOR HIV/AIDS PREVENTION BY TOPICAL ROUTE.

Albert Nguessan Ngo, Candidate for the Doctor of Philosophy Degree

University of Missouri-Kansas City, 2018

ABSTRACT

This study is divided into two aims. Aim #1 focuses on the development and characterization of tenofovir (TFV) loaded a stimuli sensitive nanomedicine against male to female HIV/AIDS infection. Aim #2 focus on the development of a verstatile formulation for drug solid dispersion applicable to other anti HIV/AIDS active pharmaceutical agents..

In Chapter 1 and 2, an overview related to the hypothesis to be tested and a literature review is extensively discussed, respectively. Aim#1 and #2 are summarized in Chapter 3-5 and Chapter 6 respectively.

Pre-exposure propyilaxis (PrEP), using topical TFV based nanomedicine is a promising effective way to prevent male-to-women HIV/AIDS infection. It is hypothesized that human prostatic acid phosphatase (hPAP) content in semen can trigger the release of TFV loaded chitosan /TPP NPs against male to female HIV/AIDS transmission during penile-vaginal intercourse.

In Chapter 3, a response surface methodology is used to identify the optimal concentration of 3, 3, 3 trichloroacetic acid (TCA) needed for the efficient quantification of TFV released interfering with protein containing simulated vaginal and seminal fluids. The optimal concentration needed to efficiently pellet down protein is 4% w/v (a saddle point). In

these conditions, the limit of detection (LOD) and limit of quantification (LOQ) of TFV are 0.0014 mg/ mL and 0.0042 mg/mL respectively.

In Chapter 4, a method for improving the physico-chemical properties of TFV loaded chitosan/TPP NPs is engineered using a modified ionic gelation process. The NPs are characterized for the percent encapsulation efficiency (% EE), size, morphology, release mechanism and *in vitro* cytotoxicity. The spherical and nontoxic NPs size and (% EE) range from 171-379 nm, 86.3-92.7%, respectively. The NPs exhibit a sustained release following anomalous transport mechanism.

In Chapter 5, the influence of hPAP (50 Unit/mL) on the release of TFV from five different chitosan/TPP NPs formulations are engineered using the above ionic gelation process. Formulation (F1) exhibits significant TFV, released in the presence of hPAP considering the similarity factor and difference factor of 56.5 and 40.3 respectively. The NPs size, % EE, ζ and PDI are 149.3-8924.67 nm, 78.8-93.71%, 4.15-11.23 mV and 0.256-1 respectively. The optimal condition for enhanced TFV released from chitosan NPs formulation under the influence of hPAP compared to the control is obtained for chitosan concentration (1.5 mg/mL), acetic acid concentration (1.25 % v/v) and TPP concentration (3 mg/mL, TPP being a hPAP substrate), and TFV amount (5 mg), respectively. This nanoparticle formulation is a promising topical anti-HIV microbicide for HIV/AIDS prevention.

In Chapter 6, a dual versatile coating process and fast dissolving crystal solid dispersion is engineered to enhance the aqueous dissolution and dispersion of hydrophobic drugs. The motivation of this study came from the knowledge gained in the process used to improve the physico-chemical properties of chitosan NPs. Docetaxel a BCS Class 2 drug is dissolved in glacial acetic acid/SA solution and subsequently freeze-dried (C-DXT). The

relatively safe C-DXT formulation rapidly forms an aqueous non-rigid nanosuspension (mean diameter size ~ 161 nm) with a faster drug dissolution rate compared to native DXT. The difference factor (f_1) and the similarity factor (f_2) values are 547.8 and 7.1 respectively. This unique crystal solid dispersion engineering process of DXT using SA might be applicable to other anti-HIV/AIDS hydrophobic bioactive agents to enhance their safety and efficacy.

APPROVAL PAGE

The faculty listed below, appointed by the Dean of the School of Graduates Studies, have examined the dissertation titled" Engineering of Human Acid Phosphatase Enzyme Sensitive Nanomedicine for HIV/AIDS Prevention by Topical Route", presented by Albert Nguessan Ngo, candidate for the Doctor of Philosophy degree, and certify that in their opinion it is worthy of acceptance.

Supervisory Committee

Bi-Botti C. Youan, Ph.D., Committee Chair
Division of Pharmaceutical Sciences

Kathleen Kilway, Ph.D.
Department of Chemistry

William G. Gutheil, Ph.D.
Division of Pharmaceutical Sciences

James Murowchick, Ph.D.
Department of Geosciences

Jacob Marszalek, Ph.D.
School of Education

TABLE OF CONTENTS

LIST OF ILLUSTRATIONS

LIST OF TABLES

Table Page

ACKNOWLEDGMENTS

First and, foremost I would like to sincerely thank my advisor Bi-Botti C. Youan, PhD. for giving me the opportunity to work and accepting me as a graduate research assistant in his laboratory of Future Nanomedicine and Theoretical Chronopharmaceutic. I show my gratitude to his constant guidance, advice, motivation, financial support and inspiration throughout this research and dissertation coursework. I express a special gratitude to my supervisory committee member, Bi-Botti C. Youan, Ph.D., professor of pharmaceutical sciences, Kathleen Kilway, Ph.D., chair and professor of chemistry, William G. Gutheil, Ph.D. professor of pharmaceutical sciences, James Murowchick, Ph.D., professor of geochemistry and mineralogy, and Jacob Marszalek, Ph.D., associate professor and acting director of urban education research and center, for their guidance and support in their area of expertise and various aspect of this dissertation. I would like to thank also Russell B. Melchert, Ph.D., dean of school of Pharmacy and professor of pharmacology and toxicology for his tremendous support of graduate the doctoral program.

I express also a thankful to my formers and current labmates, Jean-Marc Miezan Ezoulin, PhD, Ibrahima Youm, PhD, Tao Zhang, PhD., Vivek Agrahari, PhD., Jianing Meng, PhD., Fohona Coulibaly, Danielle Thomas, Alsalhi Abdullah, and Omowumi Akinjole for productive intellectual interaction, support and friendship during my tenure in Dr. Youan's lab.

I also express my gratitude to the school of pharmacy staff especially, Yolande Joyce Johnson, executive assistant, Sharon D. Self, office support assistant, Nancy Bahner, administrative manager, Shana K. Eisentrager, Tamica Lige and Jeannie Westmoreland for

logistic support GTAs and GRAs. I also extend my thanks to the school of pharmacy faculty and all the graduate students for their support.

This work is supported by R01; award number R01 AI087304, from the national institute of allergic and infectious diseases and University of Missouri System Fast Track initiative award # 16002K.

Lastly and not the least, I would like to thank my beloved wife Laetitia Koffi for her consistent support and encouragement in the up and down cycle of life as well as my brother Seraphin N. Ndri for his financial support.

DEDICATION

This dissertation is dedicated to my entire family and relatives.

CHAPTER 1

STATEMENT OF THE PROBLEM

1.1 Overview

Human immunodeficiency virus (HIV) is a lentivirus, which is a subgroup of a retrovirus. Retro virus are types of virus that use ribonucleic acid (RNA) as its genetic material and insert a DNA copy of their genome in the host cell in order to replicate. Upon infection with HIV, there is a progressive failure of human immune system leading to the acquisition and growth of opportunistic diseases and cancers. This human health state is called acquired immunodeficiency syndrome (AIDS). HIV/AIDS is a social and economic problem. For instance, according to the World Health Organization (WHO) 2017 recent report, HIVs have infected more than 70 million people and 35 million have died since the onset of the HIV/AIDS epidemic in the early 1980. By the end of 2016, 36.7 million people are still leaving with HIV[1]. In addition, the cost for HIV prevention and treatments can reach 35 billion by 2030[2]. In the US, the estimated life time cost of HIV infected adult is 326,500 US dollar[3]. Currently, there is no vacccine to eradicate or stop the spread of HIV/AIDS, which so far might be the ideal solution to eliminate this worldwide epidemic disease[4]. The vaginal route is still a major path of women infection to HIV/AIDS. For instance the incidence of penile-vaginal HIV transmission is as high as 1 in 10 exposure[5]. In addition, male to female HIV/AIDS transmission was found to be greater than female-to-male due to the vaginal anatomy[6].

Pre-exposure propyilaxis (PrEP) using topical tenofovir gel, had an effective protection 70 -100%[7]. Beside using topical gel microbicide, polymeric nanoparticles are a promising delivery system, including chitosan-based nanoparticle[8]. Chitosan crosslinked with pentasodium

triphosphate (TPP) NPs is widely used as a carrier, for novel drug delivery and this carrier showed some intrinsic mucoadhesive properties[9]. However, Chitosan/TPP NPs exhibit a low encapsulation efficiency[10]. In addition Chitosan/TPP NPs exhibit a burst release, a failure to sustain release TFV, a highly water soluble drug [10].TPP, the crosslink of this carrier, is itself a substrate of human prostatic acid phosphatase (hPAP) [11].

Tenofovir (TFV) is a reverse transcriptase enzyme inhibitor. TFV is approved by US Food and Drugs Administration (FDA) for the treatment of HIV/AIDS[10]. Once the virus infects the target cells, especially $CD4^+$ cells, the HIV's reverse transcriptase enzyme (RTE) transcribes the virus messenger ribonucleic acid (mRNA) into deoxyribonucleic acid (DNA)[12]. This resulting in the incorporation of the virus DNA into the host genome. TFV is an inhibitor of RTE. TFV binds to RTE's active site, and subsequently, prevents the binding of the natural substrate deoxyadenosine 5' triphosphate[13]. Thus, the inhibition of the HIV's RTE stops the transcription of the HIV messenger RNA (mRNA) into complementary DNA (cDNA) resulting in the termination of HIV cDNA replication[14]. The solubility in water, logP and oral bioavailability of TFV are 13.4 mg/mL, −1.1, and, 25–39% respectively[15]. TFV is defined as a BCS class III drug and the UV absorption maximal of TVF is at 260 nm[15].

1.2 Human Prostatic Acid Phosphatase

Human prostatic acid phosphatase (hPAP, E.C.3.1.3.2) is an enzyme mainly produced by the prostate. Until now, the physiological substrate of hPAP is still unknown[16]. It is largely present in human seminal fluid[17]. Cellular human acid phosphatase (chPAP) and secreted human prostatic acid phosphatase (shPAP), (100kDa glycoprotein holding two subunits of approximately 50 kDa each), are the two forms of hPAP. [18] hPAP was in identified for the first time in 1853[19]. The

structure of hPAP and identified histidine phosphatase are alike[16]. The mechanistic underlying of hPAP catalyzes hydrolysis of phosphate monesters involves a nucleophile active site histidine moiety in the formation of a phosphoenzyme intermediate [20]. In addition, both hPAP and histidine phosphatase have identical catalytic residues positions [16-17] . The amount of hPAP produced by the epithelial cell of the prostate gland varied from 195 Unit/mL to 1428 Unit/mL of first portion semen ejaculated and from 57 Unit/mL to 241 Unit/mL in the second portion semen ejaculated[21]. The abnormal level of prostatic acid phosphatase (PAP) in the serum is linked to the occurence of prostate cancer in men[19]. hPAP has a broad substrate specificity[11]. Triphosphate (TPP) is a prefered substrate for wheat wGAP acid phophatase (wGAP) which is an analogue of acid phosphatase. The michaelis menten constant (km)and the velocity Vmax of wPAP are respecively 0.18 mM and 720 $\mu mol.min^{-1}mg^{-1}$ at pH 5.0 and temperature of 25±0.1 °C. Thus, these aforementionned values show that wPAP has a great affinity for TPP [11]. Similarly, TPP might be a prefered substrate for hPAP. The michaelis menten constant and the velocity of hPAP are still unknown. Similarly to wGAP, the activity of hPAP is pH and temperature dependent. Acid phosphatse hydrolyzes a broad wide spectrum of substrate including monoester phosphate in acidic or neutral pH[22]. The rate of denaturation of hPAP in acid pH (~5.6-5.8) is similar to that of neutral pH 7[23] at 37°C. hPAP can form amyloid fibril. This undesirable amylodoidgenic PAP fragments largely found in semen is demonstrated to promote HIV infection. Those amyloid fibril known as semen-derived enhancer of virus infection (SEVI), are known to attach HIV virion to the host cell and thereby enable their infection[24]. Currently, hPAP represents a new target against male to female HIV infection.

1.3 Statement for the Problem

Male to female HIV incidence is as high as 80% through heterosexual vaginal route. PreP using TVF gel has shown a promising result against women infection through the vaginal route[25]. However, TVF vaginal gel exhibits low patient compliance[25] and low vaginal mucoadhesion. hPAP is an enzyme found in male semen and has a variety of substrates[11]. TPP is both a substrate of hPAP and is used as crosslinker during the preparation of chitosan/TPP nanoparticle. However, the effect of hPAP on TFV loaded chitosan/TPP NPs is still unknown. In additon, proteins (e.g. hPAP) UV absorption maxima are in the range 200-280 nm[26]. The huge amount of protein (50.7 mg/mL)[27] containing human semen interferes with TFV absorbance at 260 nm[15]. In this dissertation, we plan to elucidate the optimal chitosan/TPP nanoformulation independent variable needed to release significantly TFV in the presence of hPAP in order to prevent women against HIV infection during heterosexual intimate contact.

1.4 Objectives

The main objective of this dissertation are:

1. Bioanalytical method for TFV analysis in simulated human seminal fluid interfering with seminal protein. This method allows a better quantification of the amount of TFV released under the influence of hPAP.

2. Development of sodium acetate coated TFV loaded chitosan/TPP based nanoparticles (NPs) for improved physico-chemical properties. This method allows significantly increasing the nanoparticle percent encapsulation efficiency and preparation process.

3. Optimization of Human Acid Phosphatase Triggering Tenofovir Release from Chitosan/TPP Nanoparticles using a fractional factorial design. This approach pinpoints the optimal formulation parameters needed to release significantly TFV in the presence of hPAP.

4. Engineering of fast dissolving crystal solid dispersion of drug applicable to others anti HIV microbicides. This engineered process can enhance the aqueous availability of anti HIV hydrophobic drug.

CHAPTER 2.

LITERATURE REVIEW

2.1 Timeline, Structure and Pathophysiology of HIV

2.1.1 Timeline of HIV Discovery

HIV belongs to *retroviridae* family[28]. The first scientific literature report on HIV/AIDS was in the early 1981[29] A that early stage HIV/AIDS was known as pneumocystis Pneumonia. However, all the patient health conditions worsened beside extensive treatment with trimethoprim-sulfamethoxazole (TMP/SMX), pentamidine, and acyclovir a well-known pneumocystis pneumonia anti-microbicide[29]. The surprising immunodeficiency in the entire patient population treated at that early stage appeared unusual especially when severe immunosuppression was only attributed to pneumocystis Pneumonia in the United States (US) in the early 1980[30]. In November 1984, the US Centers for Disease Control and Prevention (CDC) reported 6993 cases of the new and troublesome disease and 3442 related deaths. In the same year 1984, Dr. Robert Gallo of the National Institute of Cancer, Dr. Luc Montagnier at the Pasteur Institute and Dr. Jay Levy at the University of California San Franciscco identified the HIV and called it Human T-lymphotropic Virus type III (HTLV-III), Lymphadenopathy Related Virus (LAV) and antiretrovirus (ARV) respectively[31]. It was only in 1987 that the US president Ronald Reagan and the French prime minister Jacques Chirac publicized a joint promise on the matter regarding the first scientific report of the discovery of HTLV-III, LAV and ARV and called it Human Immunodeficiency Virus (HIV)[31].

2.1.2 Structure of HIV

HIV has a spherical shape with a diameter of about 110-146 nm[32]. The virus is composed of two copies of ribonucleic acid (RNA) and essential enzymes especially reverse transcriptase, integrase, proteases, ribonuclease and integrase. Those enzymes are fundamentally needed for the insertion of HIV's RNA in the host genome and the development of the virion. The viral envelop is made of phospholipid bilayer deriving from the host cell membrane[33]. HIV glycoprotein (gp) is a protein expressed on the surface of HIV with a molecular weight of 120 DA and 41 DA. These surface proteins are called gp120 and gp41 respectively[34]. The structure of the virus is shown in figure 2-1. HIV-1 and HIV-2 are the two main types of HIV. HIV-1 is spread worldwide whereas; HIV-2 is mainly restrained in West Africa[35]. The difference and similarities between HIV-1 and HIV-2 are shown in **table 2-1**[35].

Table 2- 1 Similarities and difference features between HIV-1 and HIV-2

Features	Similarity /difference
Basic gene arrangement	similar
Mode of transmission	similar
Replication	similar
Clinical outcomes	Both lead to HIV/AIDS
pathogenesis	Not well understood
Pathological progression	Similar
CD4 counts	HIV-2 occurs at higher CD4 counts compared to HIV-1
Immune response	There are a significant production of Interleukin 2 in HIV-2 infected patient compared to HIV-1 infected patient resulting in more protective immune system.
Plasma viral load	Plasma viral load is lower in HIV-2 infected patient.

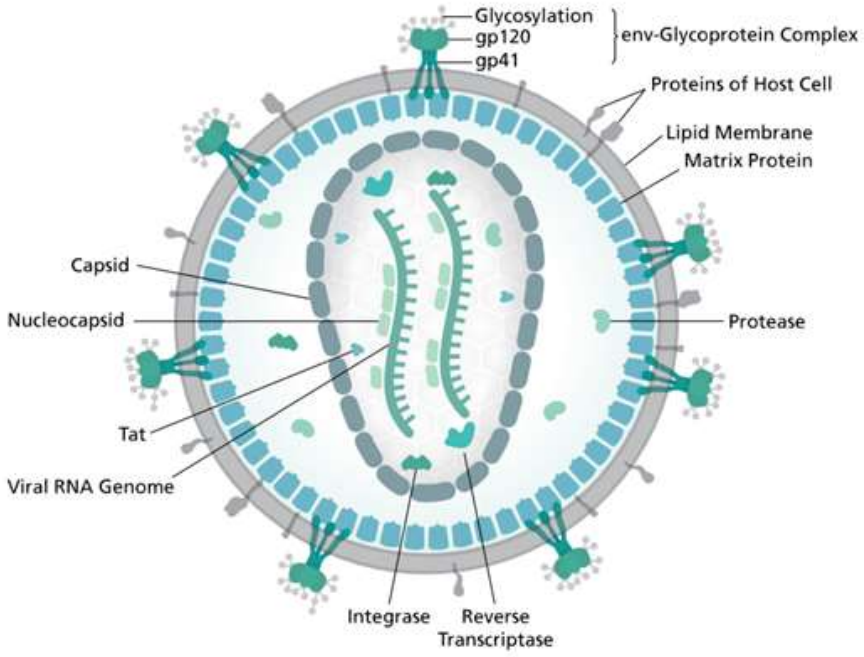

Figure 2- 1 Schematic representation of HIV virion (Adopted from Thomas Splettstoesser, 2014).

2.2 Vaginal Acquisition of HIV and Potential Topical Microbicide against HIV

2.2.1 Vaginal Acquisition

Heterosexual vaginal transmission of HIV is through vaginal or cervical route. The undamaged vaginal mucosa is made of multilayer of squamous epithelial cells[36] which unlikely will facilitate transcytosis of HIV to submucosa site after HIV exposure. However, the disturbance of the vaginal integrity and flora favors the infections to HIV[36]. Those losses of vaginal integrity are but not limited to vaginal dryness, ulcerative disease and bacterial vaginosis[37]. Upon release of HIV in the vaginal tract during heterosexual activity, the HIV cross several layers of stratified squamous vaginal epithelial cells within 2-6 hours[38]. The immediate targeted cells are T cells, macrophage and dendritic cells located in the sub-epithelium. The scheme of the vaginal

acquisition of HIV is shown in figure 2.2. HIV gp120 is essential for the virus entry in the $CD4^+$ cells[34]. The interaction between HIV gp120 and $CD4^+$ triggers a conformational change of gp120 and allowing a secondary interaction with chemockine receptor type 5 (CCR5), which is a protein on the surface of white blood cells[39]. Gp41 undergoes also a structural change and forming coiled-coils with the distal tips of gp41 introduced in the cell membrane. This critical step lead to the merging of the virus envelop with the cell membrane[40].

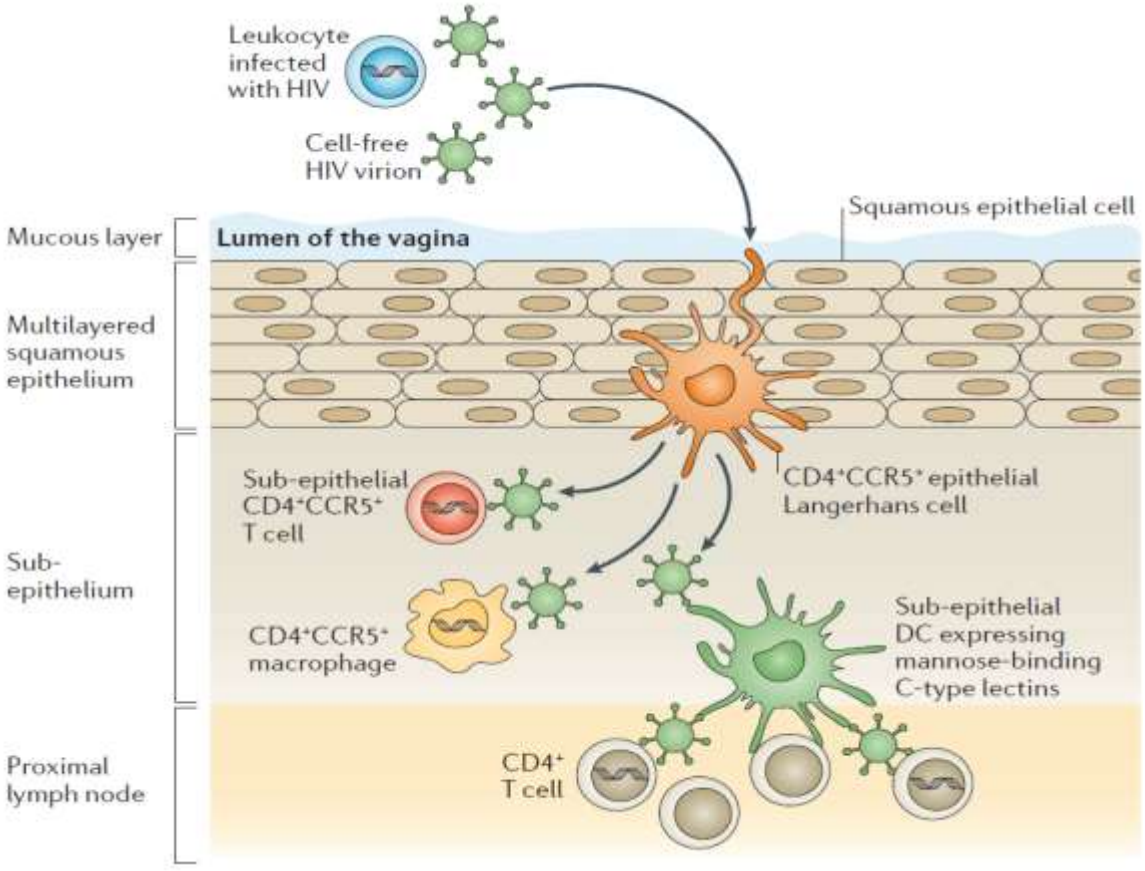

Figure 2- 2 Vaginal acquisition of HIV (Adopted from Michael M. Lederman et al. Nature 2006)

2.2.2 Current Topical Application against HIV/AIDS

HIV epidemic appears the worst outbreak of transmissible disease in modern human history[36] since its discovery in the early 1980. Until today, there is no vaccine against HIV in sight, which seems to be the ultimate and efficient solution to stop the spread of this HIV epidemic. Several efforts are investigated to delay or reduce the propagation of HIV especially topical microbicides. Those microbicides remain currently an efficient strategy to stop the exponential infection of women to HIV through vaginal route[36]. Anti-HIV microbicide are chemical or agent that reduce the sexual transmission of HIV. Those microbicides include entry inhibitors, detergents, agent that modified pH, polyanions, replications inhibitors, agent that bind glycans, or gp120, or gp41, or CD4 receptor[41]. In table 1, an extensive of t prospective anti-HIV microbicide are shown in table 2.2[41]. Those anti-HIV microbicides include but not limited to small molecule drugs, antibodies, peptides, aptamers and gene therapies[41].

Table 2- 2 Current prospective topical microbicide against HIV infection

Inhibitor	Description	Carriers
Virus entry inhibitors		
CCR5 antagonists		
RANTES[42] (natural chemokine) [a]	Blocks viral binding to CCR5	Non-phospholipid liposome (Novasomes 7474), secretion by recombinant Lactobacillus Jensenii[41]
C1C5 RANTES	CCR5 antagonist analog	Secretion by recombinant L. jensenii
PSC RANTES	Blocks viral binding to CCR5	Poly(lactide-co-glycolide) nanoparticles[41]
5P12 RANTES	Blocks viral binding to CCR5	Secretion by recombinant L. Jensenii, Glycosaminoglycan-based polymeric hydrogel[41]
BMS -663068	Target viral GP120	Vaginal tablet[41]
Broadly neutralizing antibodies		
b12	Target CD4 binding site	HEC-based gels[41]
VRC01	Target CD4 binding site	HEC-based gels[41]
HJ16	Target CD4 binding site	
447-52D	Targets CD4-induced face	
2G12	Targets glycan on gp120	
2F5	Targets membrane proximal region of gp41	HEC-based gels
4E10	Targets membrane proximal region of gp41	
Z1331	Targets membrane proximal region of gp41	
Carbohydrate-Binding agents		
CV-N	Blocks gp 120 interaction with	
Peptides		
Retrocyclins (RCs)	Blocks 6 helix bundle formation and binds to gp41	Polymeric (PVA, polyvinyl acetate) film[41]
M48U1	CD4 mimetic	Pluronic hydrogels (F127/HPMC and F127/F68/HPMC)[41]
RNA-based gene therapy strategies		
RNAi-based microbicides		
VRX496 (lentivector)	Antisense HIV env	Infusion[41]
RNA-based aptamer microbicides		
UCLA1	Binds to gp120	
UCLA005	Binds to gp120	
B40t77	Binds to gp120	
ODN 93 del	Inhibit viral entry and integration	
Aptamer-SiRNA/Chimeric microbicides		
CD4-AsiCs	Blocks viral entry via binding to CD4 and RNAi knockdown of viral host genes	HEC based gel

CCR5: C-C Chemokine Receptor 5; CV-N: Cyanovirin-N; EVA: Ethylene-Vinylacetate; gp: Glycoprotein; HEC: Hydroxyethyl Cellulose; IVR: Intravaginal Ring;MIV-150: (1S;2S)-N-(cis-6-fluoro-2-hydroxy-3-propionyl-phenyl)cyclopropyl]-N¢-(5-cyanopyrid-2-yl)urea; NNRTI: Non-Nucleoside RT Inhibitors; NRTI: Nucleoside RTInhibitor; NtRTI: Nucleotide RT Inhibitor; PVA: Polyvinyl Alcohol; RCs: Retrocyclins; RT: Reverse Transcriptase; RTI: Reverse Transcriptase Inhibitor; siRNA: Small-interfering RNA; TDF: Tenofovir Disoproxil Fumarate; TMC120: 4-[[4-[2,4,6-trimethylphenyl)amino]-2-pyrimidinyl]-amino]-benzonitrile.

RANTES (Regulated on Activation, Normal T cell Expressed and Secreted) also known as chemokine (C-C motif) ligand 5 (CCL5) are protein encoded by the CCL gene[43]. RANTES is produced by $CD8^+$ T cell and might play a fundamental role in HIV suppression[44]. C1C5 RANTES is a mutated analogue of RANTES and secreted by Lactobacillus Jensenii[45]. It is an antagonist of CCR5[45], a receptor know to play a key role during host cell HIV infection. PSC-RANTES [N-nonanoyl, des-Ser1[L-tioproline2, L-cyclohexylglycine3]-RANTES is CCR5 agonist[46]. R5 HIV1 is a HIV1, which bind to CCR5 receptor. PSC-RANTES competitively inhibit CCR5 receptor thereby, preventing R5 HIV1 to bind to the host cell.[46] 5P12 RANTES is a chemokine analogue. This chemokine inhibits CCR5 receptor and thereby preventing HIV infection[47].

(3-((4-Benzoyl-1-piperazinyl)(oxo)acetyl)-4-methoxy-7-(3-methyl-1*H*-1,2,4-triazol-1-yl)-1*H*-pyrrolo(2,3-*c*)pyridin-1-yl)methyl dihydrogen phosphate also called Fostemsavir (BMS-663068) acts as an entry inhibitor. This anti-HIV microbicide binds to the virus gp120 and thereby prevents the virus attachment to the host cell CD4 receptor[48].

B12, IgG1, VRC0na and HJ16 are a broadly neutralizing antibody used against HIV_1. The epitope recognized by this antibody overlaps with the CD4 receptor, which is the binding site of HIV gp120[49-50]. Thus, B12, IgG1 may be investigated for vaccine development against HIV.

The human antibody 447-52D was isolated from an HIV infected patient and exhibit a broad neutralizalization property against HIV.[51] The neutralizing antibody (447-52D) competes with CD4 receptor in binding with the viral glycoprotein gp120[52].

Human monoclonal antibody 2G12 is an antibody targeting HIV gp120. 2G12 distinctively neutralizes one epitope, a glycan on the HIV surface protein gp120 [53].

2F5, 4E10 and Z131 are broadly neutralizing human monoclonal antibodies (mAbs). Those mAbs target HIV transmembrane gp41 and thereby might prevent the infection to HIV[54].

UCLA1, UCLA005 are the shortened derivative of the B40. B40t77 is a truncated aptamer derivative of aptamer B40[55]. Those entries inhibitors are a family of RNA aptamer binding to HIV gp120 [56].

Tenofovir a Nucleoside Reverse Transcriptase Inhibitor

Tenofovir (TFV) is a nucleotide reverse transcriptase inhibitor (NtRTIs) with a molecular weight of 287 DA. It is approved for HIV treatment[57]. This HIV treatment is known antiretroviral treatment (ART). ART does not cure HIV but the anti HIV microbicide slows down the progression of the disease. TFV blocks HIV reverse transcriptase enzyme needed to copy HIV RNA into HIV complementary deoxyribonucleic acid (cDNA). Thus, this process blocks the replication of HIV.

Non nucleoside reverse transcriptase inhibitor (NNRTI) are retroviral microbicides used in the treatment of HIV/AIDS. NNRTIs inhibit HIV reverse transcriptase enzyme and thereby prevent its replication in the host cell.

An extensive list of anti-HIV microbicides used in a clinical setting with different clinical outcomes are reported in table 2.3

Table 2- 3 Preclinical and clinical HIV microbicide candidates

Candidates microbicide	Preclinical in vitro/in vivo efficacy	Clinical trials	Clinical outcomes
NtRTI/NRTI			
TFV gel (1% gel)	Partial protection from vaginal HIV infection in the BLT mouse model Durable protection from vaginal SHIV162p3 infection in macaques	CAPRISA 004 (Phase IIb)	A 39% lower risk of HIV acquisition Two seroconverters were superinfected with HIV subtype C[41]
TDF gel (1% gel)		VOICE (Phase IIb)	Ineffective in preventing HIV infection
		FACTS 001 (Phase III)	To test the effectiveness in preventing HIV and HSV-2[41]
		CAPRISA 008 (Phase III)	To test the effectiveness and viral resistance to TDF gel [41]
		CAPRISA 009 (Phase III)	To define the optimal treatment for women while using TDF gel[41]
TFV+ FTC(1+5% gel)	Fully protected macaques from a total of 20 exposures to vaginal		
TFV (IVR)	A controlled release of TFV from reservoir IVR provided adequate sheep vaginal concentrations for 90 days PK and safety profiles of TFV-releasing IVRs based on the pod design in macaques		
TDF (IVR)	Fully protected macaques from a total of 16 exposures to vaginal		
Stampidine	Favorable PK and safety profile (25 or 50 mg/Kg). No observable adverse effect Level (NOAEL) of 100 mg/kg. Antiviral efficacy in HU-PBL SCID mice and chronically FIV-infected domestic cats.	Phase I involving 30 therapy-naïve adult HIV-infected adult patients (5-25 mg/kg), capsules)	Clinically safe with no dose-limiting toxicity, Reduction in viral load[41].
WHI-07(2% gel microemulsion)	Favorable safety and efficacy profile for prevention of HIV and pregnancy. Protected cats from genital FIV transmission		

(Continues)

Table 2.3. Preclinical and clinical HIV microbicide candidates (continued)

Candidates microbicide	Preclinical in vitro/in vivo efficacy	Clinical trials	Clinical outcomes
NNRTIs			
Dapivirine (1% gel)		Fives gel formulations have been tested in five clinical trials	Dapivirine vaginal gels were safe, well tolerated and acceptable[41].
Dapivirine (1.25 mg film)		FAME 02: a Phase I PK and safety trial	
Dapivirine (NPs)	PEO-modified dapivirine-loaded NPs increased drug resistance at pig vaginal mucosa		
Dapivirine (IVR, 25 or 200 mg)		Four IVR formulations have been tested in four Phase I clinical Trials	Dapivirine reservoir and matrix IVRs were considered generally safe and well tolerated[41]
Dapivirine (IVR, 25 mg)		Phase III, ASPIRE	Designed to evaluate whether the dapivirine ring is safe and effective when used for 1 month at a time (up to 2 years)[41]
Dapivirine (IVR, 25 mg)		Phase III, ring study	Is investigating long-term safety, efficacy and acceptability of dapivirine ring use (up to 2 years)[41]
Dapivirine-maraviroc (IVR, 25 + 100 mg)		Phase I safety and PK	completed
Dapivirine-levonorgestrel (IVR)			For multi-purpose prevention of HIV and pregnancy[41]
MC 1220 (0.5 or1.5 % liposomal gel or microemulsion)	Partially protected macaques from vaginal SHIV-RT infection		
MC1220 (IVR, 400 mg)	Partially protected macaques from multiples RT-SHIV162P3, vaginal challenge.		
MIV-150 (gel)	Single or repeated application had limited activity in protecting macaque from vaginal SHIV-RT infection. Combination with zinc acetate provided complete protection in this model		
MIV-150 (IVR, 50 or 100 mg)	Silicone IVR marginally reduced infection frequency in macaques from vaginal SHIV-RT infection. EVA IVRs significantly protected macaques from SHIV-RT infection		
HI-443 (gel)	Prevented vaginal transmission of a drug-resistant clinical HIV isolate in Hu-PBL-SCID mouse model		

(*Continues*)

Table 2.3. Preclinical and clinical HIV microbicide candidates (continued)

Candidates microbicide	Preclinical in vitro/in vivo efficacy	Clinical trials	Clinical outcomes
CCR5 antagonists			
PSC-RANTES (1 mM))	Protected macaques from vaginal challenge with chimeric SHIV SF162[41]		
Maraviroc (0.3% gel)	Provided dose- and time-dependent protection against a single high-dose vaginal challenge with SHIV-162P3 in macaques[41].		
Maraviroc (3.3% gel)	Complete protection from vaginal SHIV-162P3 challenge in macaques		
UL29.2 siRNA	Vaginal instillation of siRNAs targeting HSV-2 protected mice from lethal infection[41]		
RNA-based aptamer			
UCLA005/UCLA005v11	Assessed their stability in vaginal lavages and susceptibility to vaginal nucleases[41]		
CD4 aptamer-siRNA chimeras			
CD4-AsiCs targeting CCR5, gag and vif	Knocked down HIV genes and inhibited HIV infection in tissue explants. Protected BLT mice from vaginal HIV infection[41]		
Dendrimers			
SPL7013 (3% gel)	Protective against vaginal challenge with SHIV89.6P in macaques[41].	Phase I: Assessed the safety, acceptability, retention of antiviral activity of vaginal 3% SPL7013 gel in healthy women	Antiviral activity was observed against HIV and HSV-2 *in vitro.* Altered vaginal microflora and genital AEs were apparent[41].
Broadly neutralizing Abs			
Ab VRC01	Partial protection from vaginal HIV infection in RAG-hu mouse model[41].		
Ab 3BNC117	Marked reduction in intravaginal infection in HIV-LucTG mice		
Ab b12	Neutralized mainly subtype B and C viruses[41].		

(continues)

Table 2.3. Preclinical and clinical HIV microbicide candidates (continued)

Candidates microbicide	Preclinical in vitro/in vivo efficacy	Clinical trials	Clinical outcomes
Ab 2E7	Neutralized 21 out of the 26 tested strains belonging to the A, A/G, B, B/C and C subtypes[41]		
Ab PG9	Neutralized 80% of HIV isolates[41]		
Ab PGT121	Neutralized 70% of circulating isolates		
Ab m43	Neutralized 34% of the HIV primary isolates from different clades[41]		
Nanobodies (JM4)	Neutralized over 95% of circulating HIV isolates [41]		
Engineered lactobacilli			
Human two-domain CD4	Decrease in virus infectivity in HeLa cells[41]		
Fusion inhibitor (FI-3	HIV and SHIV-162P3 neutralizing activity[41]		
C1C5 RANTES	Inhibited HIV infection in $CD4^+$ T cells and macrophages[41]		
Anti-ICAM-1 scFv	Blocked transmission of cell-associated HIV in the cervical epithelial model[41]		
Modified Cyanovirin-N	Colonized macaque vaginal environment during the SHIV challenge period Marked reduction in transmission of SHIV (SF162P3) after repeated vaginal challenges of macaques[41]		

Ab: Antibody; AE: Adverse Event; BLT: Humanized Bone Marrow/Liver/Thymus; CCR5: C-C Chemokine Receptor 5; FIV: feline immunodeficiency virus; FTC: Emtricitabine; HIV-LucTG mice: Homozygous for the Transgene and Luciferase to ROSA-Stop-Luc mice; Hu-PBL-SCID: Human-Peripheral Blood Lymphocytes-Severe Combined Immunodeficiency; ICAM: Intercellular Adhesion Molecule 1; IVR: Intravaginal Ring; MIV-150: (1*S*;2*S*)-*N*-(*cis*-6-fluoro-2-hydroxy-3-propionyl-phenyl)cyclopropyl]-*N′*-(5-cyanopyrid-2-yl)urea; NNRTI: Non-Nucleoside RT Inhibitors; NP: Nanoparticle; PEO: Poly(Ethylene Oxide); PK: Pharmacokinetics; RAG-hu: Humanized Rag2$^{-/-}$γc$^{-/-}$ Mouse Model; SHIV-RT: Simian Human Immunodeficiency Virus Reverse Transcriptase; siRNA: Small-interfering RNA; TDF: Tenofovir Disoproxil Fumarate; TFV: Tenofovir; WHI-07: 5-bromo-6-methoxy-5,6-dihydro-3'-azidothymidine-5'-(p-bromophenyl)-methoxyalaninyl phosphate.

2.2.3 Approved HIV/AIDS Microbicide

Several efforts are continually achieved to improve the life of people living with HIV. Up to date, FDA has approved several medications to treat HIV or at some extent slow down the rate

of progression of the disease. Those medications can improve the life of people living with HIV. Those anti-HIV/AIDS microbicides are either a single drug or a combination of many drugs. The combination of antiretroviral therapy (ART) offers several advantages because each anti-HIV microbicide block either the virus or the virus essential enzymes needed for its replication or transmission[58]. For instance, the combination of lopinavir (LPV) and ritonavir has a synergic effect by blocking the HIV protease enzyme. HIV protease is an essential enzyme responsible for processing the HIV's group specific antigen protein (GAG).d or GAG polyproteins which is essential in HIV's virion maturation[59]. A list of United States Food and Drugs Administration (US FDA) approved HIV microbicides[60] since the first case of HIV in US in the early 1981, are shown in table 2-4.

Table 2-4 United States Food and Drug Administration (FDA) approved HIV medicines

Drug class	Generic name (other names and acronyms)	Brand Name	FDA Approval date
Nucleoside Reverse Transcriptase Inhibitors (NRTIs)	abacavir (abacavir sulfate, ABC)	Ziagen	December 17, 1998
	didanosine	Videx	October 9, 1991
	emtricitabine (FTC)	Emtriva	July 2, 2003
	lamivudine (3TC)	Epivir	November 17, 1995
	stavudine (d4T)	Zerit	June 24, 1994
	tenofovir disoproxil fumarate (TDF)	Viread	October 26, 2001
	zidovudine (ZDV) or (azidothymidine, (AZT)	Retrovir	March 19, 1987

(Continues)

Table 2-4 United States Food and Drug Administration (FDA) approved HIV medicines **(continued)**

Drugs class	Generic name (other names and acronyms	Brand Name	FDA Approval date
	Non-Nucleoside Reverse Transcriptase Inhibitors (NNRTIs)		
NNRTIs interact with and inhibit reverse transcriptase enzyme.	efavirenz (EFV)	Sustiva	September 17, 1998
	etravirine (ETR)	Intelence	January 18, 2008
	nevirapine (extended-release nevirapine, NVP)	Viramune	June 21, 1996
		Viramune XR (extended release)	March 25, 2011
	rilpivirine (rilpivirine hydrochloride, RPV)	Edurant	May 20, 2011
Drugs class	Generic name (other names and acronyms)	Brand Name	FDA Approval date
	Protease Inhibitors (PIs)		
PIs block HIV protease, an enzyme HIV needs to make copies of itself.	atazanavir (atazanavir sulfate, ATV)	Reyataz	June 20, 2003[60]
	darunavir (darunavir ethanolate, DRV	Prezista	June 23, 2006[60]
	fosamprenavir (fosamprenavir calcium (FPV)	Lexiva	October 20, 2003[60]
	indinavir (indinavir sulfate, IDV)	Crixivan	March 13, 1996[60]
	nelfinavir (nelfinavir mesylate, NFV)	Viracept	March 14, 1997[60]
	ritonavir (RTV)	Norvir	March 1, 1996[60]

(Continues)

Table 2.4 United States Food and Drug Administration (FDA) approved HIV medicines **(continued)**

Drugs class	Generic name (other names and acronyms)	Brand Name	FDA Approval date
	saquinavir (saquinavir mesylate, SQV)	Invirase	December 6, 1995[60]
	tipranavir (TPV)	Aptivus	June 22, 2005[60]
Fusion Inhibitors			
Fusion inhibitors block HIV from entering the CD4 cells of the immune system.	enfuvirtide (T-20)	Fuzeon	March 13, 2003[60]
CCR5 Antagonists			
CCR5 antagonists block CCR5 coreceptors on the surface of certain immune cells that HIV needs to enter the cells.	maraviroc (MVC)	Selzentry	August 6, 2007[60]
Integrase Inhibitors			
Integrase inhibitors block HIV integrase, an enzyme HIV needs to make copies of itself	dolutegravir (DTG, dolutegravir sodium)	Tivicay	August 13, 2013
	raltegravir (raltegravir potassium, RAL)	Isentress	October 12, 2007
		Isentress HD	May 26, 2017
Pharmacokinetic Enhancers			
Pharmacokinetic enhancers are used in HIV treatment to increase the effectiveness of an HIV medicine included in an HIV regimen.	cobicistat (COBI)	Tybost	September 24, 2014

(continues)

Table 2.4 United States Food and Drug Administration (FDA) approved HIV medicines (continued)

Drug class	Generic name (other names and acronyms)	Brand Name	FDA Approval date
Combination HIV Medicines			
Combination HIV medicines contain two or more HIV medicines from one or more drug classes	abacavir/lamivudine (ABC / 3TC)	Epzicom	August 2, 2004
	abacavir, dolutegravir, and lamivudine (, ABC / DTG / 3TC)	Triumeq	August 22, 2014
	(abacavir sulfate / lamivudine / zidovudine, (ABC / 3TC / ZDV)	Trizivir	November 14, 2000
	(atazanavir sulfate / cobicistat, (ATV / COBI)	Evotaz	January 29, 2015
	(darunavir ethanolate / cobicistat, (DRV / COBI)	Prezcobix	January 29, 2015
Combination HIV medicines contain two or more HIV medicines from one or more drug classes.	(dolutegravir sodium / rilpivirine hydrochloride (DTG / RPV)	Juluca	November 21, 2017
	e (efavirenz / emtricitabine / tenofovir DF, (EFV / FTC / TDF)	Atripla	July 12, 2006
	(elvitegravir / cobicistat / emtricitabine / tenofovir alafenamide, (EVG / COBI / FTC / TAF	Genvoya	November 5, 2015
	elvitegravir/ cobicistat/ emtricitabine, / tenofovir disoproxil fumarate (QUAD, EVG / COBI / FTC / TDF)	Stribild	August 27, 2012

(continues)

Table 2.4 United States Food and Drug Administration (FDA) approved HIV medicines (continued)

Drug class	Generic name (other names and acronyms)	Brand Name	FDA Approval date
	emtricitabine, rilpivirine, and tenofovir alafenamide	Odefsey	March 1, 2016
	(emtricitabine / rilpivirine hydrochloride / tenofovir disoproxil fumarate (FTC / RPV / TDF)	Complera	August 10, 2011
	emtricitabine and tenofovir alafenamide	Descovy	April 4, 2016
	emtricitabine and tenofovir disoproxil fumarate	Truvada	August 2, 2004
	Lamivudine and zidovudine (3TC / ZDV)	Combivir	September 27, 1997
	lopinavir / ritonavir (LPV/RTV)	Kaletra	September 15, 2000

2.2.4 Pathophysiology of HIV

Human infection to HIV is through either unprotected sexual activity, or blood or mother to child[61]. Upon acquisition of HIV, the virus targets mainly mature T helper cells or T helper lymphocytes (T_h), macrophages, monocytes, astrocytes cells expressing the $CD4^+$ receptor on their surface. The replication of HIV inside T_h cells induces the depletion of those T_h cells, which play a key role in immune adaptive system. When $CD4^+$ T lymphocyte which is a subtype of white blood cells fall below 200 counts/mL of blood, the host latent phase progress to AIDS, a health state characterized by the development and exponential thrive of opportunistic diseases[61]. Opportunistic diseases include pneumocystis pneumonia, toxoplasma gondii encephalitis,

cryptosporidiosis, mycobacterieum tuberculosis, microsporidiosis, are infections that continue to cause morbidity and mortality in HIV/AIDS patients [62].

2.3 Chitosan/pentaphosphate Nanoparticle used for HIV microbicide delivery.

Chitosan is a linear polysaccharide composed of randomly distributed β (1-4) linked D-glucosamine and N-Acetyl D-glucosamine deriving from the deacetylation of chitin[63]. Chitosan is widely used in drug delivery system due to its biodegradable and biocompatible[63] properties. In acidic environment, chitosan crosslinks with the polyanion triphosphate, (hPAP substrate), to form a chitosan based nanoparticles (NPs). Chitosan polymer including sulfated chitooligopolysaccharide (SCOP) has shown some anti-HIV properties against HIV infection[64]. These intrinsic properties were similar to anti-HIV agents including, killing or disrupting the HIV virus membranes, or blocking HIV from entering the host cell[65]. It is shown that SCOP disrupts the binding of HIV GP120 to CD4 host cell receptor[64]. Thus, chitosan NPs can potentially be used as an anti HIV agent carrier for vaginal anti-HIV microbicide delivery. The presence of the cross linker TPP known as acid phosphatase substrate is further enhances the use of chitosan NPs as a phosphatase sensitive delivery system. In such design of phosphatase sensitive nanoparticle, it is anticipated that the ideal optimal formulation might release significantly the anti-HIV microbicide in the presence of hPAP during sexual activity relatively to the control. In addition, an ideal chitosan NPs formulation might contain high entrapment efficiency of the anti HIV microbicide. Up-to-date, there is no reported on the use of chitosan NPs a hPAP sensitive delivery system. The chemical structure of chitin, chitosan pentasodium triphosphaste is shown in table 2.4

Table 2- 5 Chemical structure of chitin, chitosan and pentasodium triphosphate

Chemical name	Chemical structure
Chitin	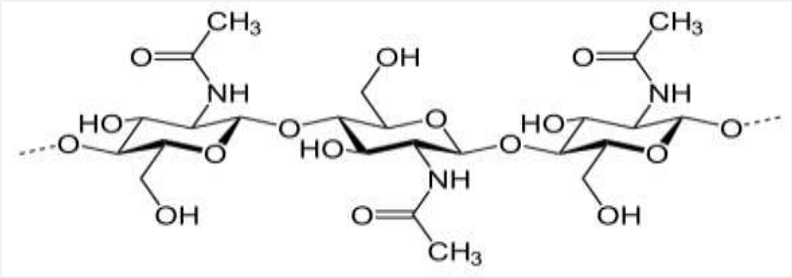
chitosan	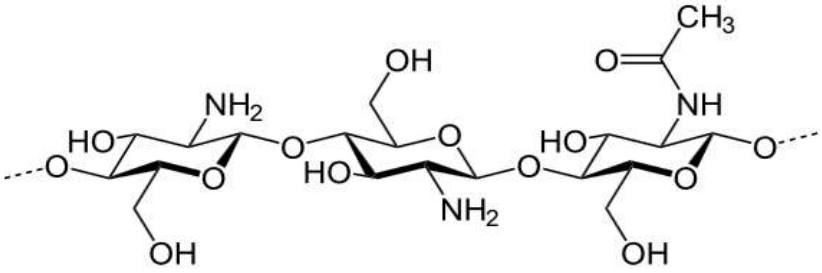
Pentasodim phosphate	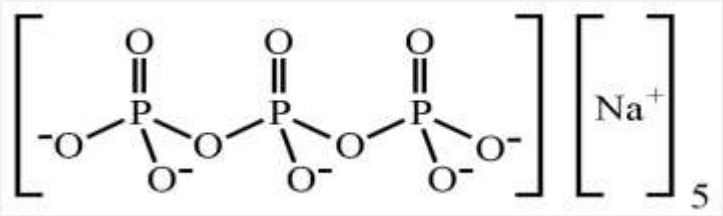

CHAPTER 3.

OPTIMAL CONCENTRATION OF 2,2,2-TRICHLOROACETIC ACID FOR PROTEIN PRECIPITATION BASED ON RESPONSE SURFACE METHODOLOGY

(Adapted from Ngo et al Journal of analytical and bioanalytical technique, 2014)

Citation: Ngo AN, Ezoulin MJM, Youm I, Youan BC (2014) Optimal Concentration of 2,2,2-Trichloroacetic Acid for Protein Precipitation Based on Response Surface Methodology. J Anal Bioanal Tech 5:198 doi: 10.4172/2155-9872.1000198

3.1 Rationale

For low protein concentrations containing biological samples, especially intended for proteomic studies, protein enrichment is a critical step to obtaining sufficient quantities. There are several methods for protein enrichment and purification [66-68]. However, each method has its own limitation. When lyophilization's method or filtration method is used to concentrate a protein, they may also concentrate non-proteinaceous elements[69]. The dialysis method may remove interfering elements, but it cannot concentrate proteins[68-69]. A recent method using a spin filter unit[70] allows the separation of the proteins from interfering elements such as salts, SDS, and lipids[68] . However, this method has its own limitations including subsequent sample loss (yield 44%) especially when less than 50 μg of the protein sample is analyzed[71].

The use of organic reagents for protein precipitation is common during sample preparation prior to proteome analysis[72-76]. These agents remove interfering elements such as similar polysaccharides or natural products (tannins, alkaloids, pigments)[69, 77-78]. Among these organic

reagents, 2,2,2-trichloroacetic acid (TCA) is the most widely used chemical for protein precipitation, and TCA-mediated protein precipitation is also independent of the physico-chemical properties of proteins[79-82]. However, the use of commonly final concentrations (10% w/v or 20% w/v) of TCA solution was not successful in precipitating low amounts of protein (0.02-0.03 mg) in an aqueous protein solution[69, 83]. Moreover, the use of higher concentrations of TCA can also degrade the quality of the sample [16, 17]. Thus, it is extremely important to identify the optimal concentration of TCA that precipitates both a low (<0.02 mg/mL) and a high amount of protein (2-20 mg/mL) in an aqueous solution while simultaneously allowing protein free supernatant analysis of any analyte interfering with the protein at higher concentration. The motivation for this study came for the need for better bioanalytical method for microbicide analysis in simulated human body fluid while avoiding the interference between the absorbency of both drug and proteins present in these biological fluids. In this study, it is hypothesized that response surface methodology, [84-88], can be used to identify the optimal concentration of TCA needed to solve this problem. To test this hypothesis, Bovine serum albumin (BSA), a well-characterized protein with a PI 5.6, is selected as a model protein[81]. BSA is a globular unglycosylated serum protein, and the most abundant serum protein [89] with a molecular weight of 65,000 Daltons. The general structure of serum albumin is an α-helix that acts as a protein transporter for steroids, fatty acids, and thyroids hormones[90-91]. Tenofovir, which is a nucleotide analogue reverse transcriptase inhibitor used for the treatment of HIV infections, is used as a model analyte [9]. This hypothesis is tested with supporting biochemical and spectral analysis (e.g. BCA assay), proteomic analysis (SDS PAGE), and visual analysis of protein pellets.

3.2 Material and Methods

3.2.1 Material

Trichloroacetic acid solution (6.1 N), and bovine serum albumin (BSA), were purchased from Sigma-Aldrich (St Louis, Missouri, USA). All percentages of w/v TCA mentioned below are the final concentrations of TCA in solution after the addition of a known volume of the above TCA solution (6.1 N). Caution: TCA can cause chemical burns and is harmful if inhaled. All the proteins solutions are made in deionized water, and the stock solution of BSA has a concentration of 2 mg/mL if not mentioned. Fresh human urine sample (total protein content = 20 ppm) is received from the University of Missouri Kansas City's student health and wellness in a sterile device.

3.2.2 Method of Protein Precipitation

First, 6.1 N TCA solution, is added to the microcentrifuge tube containing the aqueous solution of protein. Second, the mixture is vortexed for 30 seconds at high speed using a vortex-genie 2 model G-560 purchased from Scientific Industries, Inc. (Bohemia, New York, USA). Third, the microcentrifuge tubes are placed in VWR 18R refrigerated microcentrifuge (VWR, Radnor, PA) with a temperature of 4°C or in ice for 15 minutes. The protein solutions (typically, 880.6 – 1559.4 μL) are then pelleted down by centrifugation at 14, 000 rpm for 15 minutes. Finally, the pellets are separated carefully from the supernatant upon removal of each microcentrifuge tube from the refrigerated microcentrifuge.

3.2.3 Determination of the Absorbance of the Supernatant at 280 nm

For each absorbance measurement at 280 nm, the volume of the supernatant used is 1.3 mL, which is a mixture of the volume of the supernatant from each experiment (0.65 mL) and its identical replicated experiment (0.65 mL). The concentration of the protein left in the solution can be determined using the molar extinction coefficient of BSA. Deionized water is used as a blank in all readings of the absorbance. All UV measurements are carried out in triplicate on a Genesy

10 Bio Model UV-Vis spectrophotometer from Thermo Electron Corporation (Wisconsin, USA). The standard curve of the TCA absorbance (Y), made in deionized water at 280 nm, is Y = 0.01X (R2 = 0.9999), and X = % w/v TCA.

3.2.4 Bicinchoninic Acid (BCA) Method

The protein pellets are dissolved in buffer S1 for 15-20 minutes under continuous agitation with the above vortex-genie 2 model G-560 as shown in Scheme 1. The steps for the BCA assay are shown in Scheme 1, when the initial concentration of BSA is 2 mg/mL. Protein solution S (1 mL) is added directly to 1 mL of the BCA solution when the initial concentration of the BSA is in the range 0.008-0.04 mg/mL, considering the linearity working range used currently is 0-0.012 mg/mL. For human urine, after the protein precipitation step, the pellets are washed with deionized water, before addition of the buffer solution prior to solubilization. A critical step in the process requires that the volume of buffer S1 added to the pellet must equal to the initial volume of protein added to the microcentrifuge tube to ensure the same treatment, and to accurately estimate the amount of proteins precipitated. This is shown in equation (3-1):

$$\text{Percentage of proteins precipitated} = \frac{\text{amount of proteins precipitated}}{\text{total amount of proteins}} x100 \qquad (3\text{-}1)$$

The standard curve for protein absorbance (y) at 562 nm using BCA assay is y = 0.09557 x +0.0372 (R2 = 0.996), x = final concentration of protein in solution.

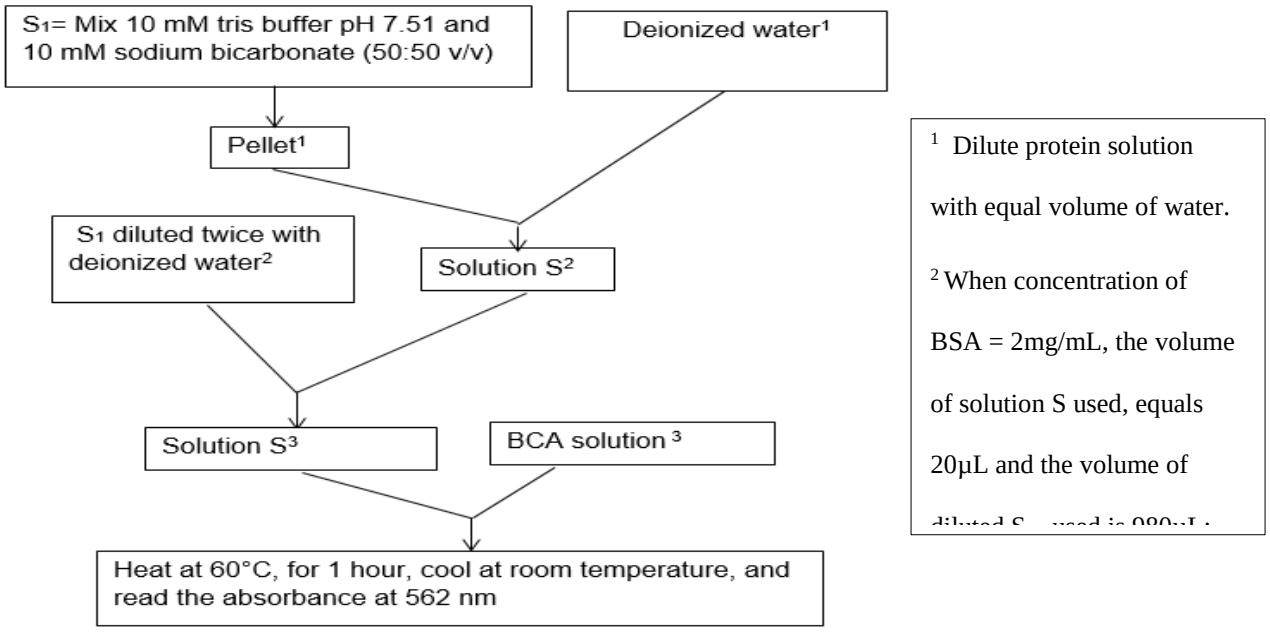

Figure 3- 1. BCA assay step

3.2.5 SDS-PAGE Method

Three hundred and fifty microliters from the remaining protein solution dissolved in the above buffer (buffer S1) is mixed with 0.350 mL of the sample buffer[92] and then heated at 98.5°C to denature the proteins prior to electrophoresis for 5 min. The denatured proteins are then run in a gradient of 4-12% sodium dodecyl sulfate-polyacrylamide gel (SDS-PAGE) for identification by electrophoresis[92] . A volume of 0.01 mL of the sample is loaded into the gel, and the proteins are stained with Brilliant blue R, which is purchased from Sigma-Aldrich (St Louis, Missouri, USA).

3.2.6 Optimum Concentration of TCA Using Central Composite Design

Central composite design (CCD), with five coded levels (Table 1), is used to elucidate the true optimal concentration of the TCA required for protein precipitation. The 13 experiments represent a CCD with 2^2 full factorial designs, four axial points, and a center point with 4 replications (Table 1). The mathematical model that derives from such a CCD is expressed as the following second-order polynomial equation:

$$y = \beta_0 + \sum \beta_i x_i + \sum \beta_{ii} x_i^2 + \sum \beta_{ij} x_i x_j \quad (3\text{-}2)$$

Where, *y* is the predicted response or dependent variable (absorbance of supernatant or percentage protein precipitated), β0 is the y intercept term, β*i* is the linear coefficient, β*ii* is the quadratic coefficient, β*ij* is the interactive coefficient, and *xi* and *xj* are the coded variables. Two independent variables (Table 3-1) are chosen based on preliminary screening studies, and the level of the two factors are chosen based on a steepest descent (ascent) method [93-94]. The protein concentration was 20 mg/mL in a mixture of human semen fluid simulant (HSFS) and human vaginal fluid simulant (HVFS). The volume ratio HSFS/ HVFS was 4/1 [95-96]. Table 3-1 shows the independent variables in physical units, with their associated coded values as well as the dependent variables. The second order model can be written in matrix notation as follows [97]

$$\hat{y} = \hat{\beta} + x'b + x'Bx \quad (3\text{-}3)$$

Where

$$x' = [\, x_1 \;\; x_2 \ldots x_k]; \quad x = \begin{bmatrix} x_1 \\ x_2 \\ \cdot \\ \cdot \\ \cdot \\ x_k \end{bmatrix}; \; b = \begin{bmatrix} \hat{\beta}_1 \\ \hat{\beta}_2 \\ \cdot \\ \cdot \\ \cdot \\ \hat{\beta}_k \end{bmatrix}; \text{and}$$

$$B = \begin{bmatrix} \hat{\beta}_{11}, & \hat{\beta}_{12}/2, & . & . & . & ,\hat{\beta}_{1k}/2 \\ & \hat{\beta}_{22} & & & & \hat{\beta}_{2k}/2 \\ & & . & & & \\ & & & . & & \\ & & & & . & \\ symetric & & & & & \hat{\beta}_{kk} \end{bmatrix}$$

x' is the transpose of x, Moreover, the eigenvalues λi, or characteristics roots of the matrix B, gives the nature of the response surface. The optimum point is maximum, minimum, or saddle point if λi are respectively positive, negative, or have different signs [98].

Table 3- 1 Independent variables and their level in central composite design and dependent variable

Independent variables			**Level**		
Coded values	-1.414	-1	0	+1	+1.414
X_1 = Volume of protein 2mg/mL solution (µL)	880.6	980.0	1220.0	1460.0	1559.4
X_2 = Volume of 6.1 N TCA solution (µL)	11.7	20	40	60	68.3
Dependent variables					
Y_1= Absorbance of the supernatant recorded at 280 nm					
Y_2 = Percentage of protein precipitated (%w/w)					

Application to production of protein-free supernatant for tenofovir analysis

Once the optimum concentration of TCA is found using the above CCD, the following method is used to analyze a model HIV microbicide, tenofovir TNF (0.01 mg/mL). TVF interferes

with simulated body fluid containing bovine serum albumin, BSA (20 mg/mL) solution. The optimal TCA concentration is compared to the commonly used concentration of TCA for protein precipitation (10, 20 % w/v). Briefly, 0.020 mL of a stock solution of TNF (0.7 mg/mL) is added into three different microcentrifuge tubes containing 1.324 mL, 1.240 mL and 1.030 mL of BSA solution (20 mg/mL), respectively. Next 0.056 mL, 0.140 mL and 0.350 mL of TCA solution 6.1 N are added into the (BSA + TNF) mixture so that the final concentration of TCA are respectively 4% w/v, 10% w/v and 20% w/v. The final concentration of TNF is 0.01 mg/mL in each final mixture. Finally, the protein is precipitated as described above and the absorbance of the supernatant is recorded by optical scanning between 240-290 nm. Finally, the absorbance of the supernatant is compared to the absorbance of aqueous solutions of TCA (4, 10 and 20 % w/v). The standard curve of the aqueous solutions of TCA and TNF absorbance (Y) recorded at 260 nm, is respectively Y (TCA) = 0.1702X – 0.0066 (R2=0.9997), and X = % w/v of TCA concentration; Y(TNF) = 0.0461x + 0.0045 (R2=1), x=TNF concentration (μg mL^{-1}).

As suggested by ICH guideline (Q2B), validation of analytical procedures, the limit of detection (LOD) and limit of quantitation (LOQ) can be determined as follow:

$$LOD = 3.3\,\sigma/S \tag{3-4}$$

$$LOQ = 10\,\sigma/S \tag{3-5}$$

Where, σ is the standard deviation of the blank and S is the slope of the calibration curve of the analyte. The estimate of σ is carried out by measuring the absorbance of the supernatant (n = 5) after precipitation of the protein without TNF (analyte of interest). The absorbances of the blanks are 0.671 ± 0.019 (σ = 0.019) and 1.605 ± 0.047 (σ = 0.047) for 4%w/v and 10% w/v TCA when deionized water is used to setup the baseline, respectively. Using the above blank to setup

the baseline, the standard curves are Y = 0.045X - 0.0086, (R2 = 0.9976), (S = 0.045) and, Y = 0.0383X - 0.0181 (R2 = 0.9952) (S = 0.0383), respectively. when the protein is precipitated with 4% w/v TCA and 10% w/v TCA, where, Y and X are the absorbance recorded at 260 nm and the concentration (0.002-0.020 mg/mL) of TNF, respectively.

3.2.7 Statistical Analysis

The statistical analysis is performed using JMP® software version 10 (SAS Institute, Cary, NC). Polynomial equations of the response values of absorbance of the supernatant at 280 nm (Y1), and the percentage of precipitated protein (Y2), are derived from the total result of 13 runs in the above CCD design. Analysis of variance (ANOVA) is performed to ensure the model fit. Experimental variables that significantly affect these responses are identified through a Pareto chart. A theoretical optimum condition is obtained by setting the maximum desirability of maximum protein precipitation yield. A student t-test is used for the checkpoint analysis, and a P-value below 0.05 is considered statistically significant and warrants the rejection of the null hypothesis.

3.3 Results

3.3.1 Result of CCD

Table 2 shows the results of the absorbance of the supernatant and the percentage of the proteins precipitated using BCA assay obtained from the 13 experiments along with the final concentration % w/v TCA in solution.

Table 3- 2 Central composite design showing independent variables with measured responses

Experiment	Level of Controlled variables in Coded Form		Absorbance of the supernatant at 280 nm	percentage of protein precipitated (w/w)	%w/v TCA	
	X_1	X_2	Y1	Y2		
1	-1	-1	0.033	84.1	2.00	
2	-1	+1	0.062	81.67	5.77	
3	+1	-1	0.067	66.15	1.35	
4	+1	+1	0.049	92.67	3.95	
5	-1.414	0	0.049	85.43	4.35	
6	+1.414	0	0.037	89.74	2.50	
7	0	-1.414	0.725	61.34	0.95	
8	0	+1.414	0.065	82.16	5.30	
9	0	0	0.049	80.2	3.18	
10	0	0	0.054	82.11	3.18	1
11	0	0	0.052	82.01	3.18	
12	0	0	0.046	75.14	3.18	
13	0	0	0.049	83.10	3.18	

The second order polynomial model as a result of the central composite design model are:

$$Y_1 = 0.050 - 0.001X_1 - 0.115X_2 - 0.012\,X_1X_2 - 0.045X_1^2 + 0.131X_2^2 \quad (3\text{-}6)$$

$$Y_2 = 80.51 - 0.107\,X_1 + 6.692X_2 + 7.237X_1X_2 + 3.906X_1^2 - 4.011X_2^2 \quad (3\text{-}7)$$

Where Y_1 is the absorbance of the supernatant; Y_2 is the percentage of protein precipitated; and X_1 and X_2 are the coded independent variables. Based on the above Eq. (3- 6) and Eq. (3-7), the vector b and the matrix B values are shown below:

$$b(Y1) = \begin{bmatrix} -0.001 \\ -0.115 \end{bmatrix}, \qquad B(\mathrm{Y1}) = \begin{bmatrix} -0.045 & -0.006 \\ -0.006 & 0.131 \end{bmatrix} \quad (3\text{-}8)$$

$$b(Y2) = \begin{bmatrix} -0.107 \\ 6.692 \end{bmatrix}, \qquad B(\mathrm{Y2}) = \begin{bmatrix} 3.906 & 3.619 \\ 3.619 & -4.011 \end{bmatrix} \quad (3\text{-}9)$$

The matrix B(Y_1) has two real eigenvalues of opposite signs, indicating that the optimal solution is a saddle point (λ_i)= (-0.045, 0.131). The matrix B (Y_2) also has two real eigenvalues of opposite signs, indicating that the optimal solution is also a saddle point: (λ_i)= (-5.416, 5.311)

Table 3-3 shows the ANOVA results to check the significance of the model parameters for both mathematical models that derived from the experimental design.

Table 3- 3 Results of ANOVA analysis for the statistical model parameters for the absorbance of the supernatant (Y_1), and the percentage of the protein precipitated (Y_2).

Response	Source	DF[a]	SS[b]	MS[c]	F-ratio[d]	R^2
Y_1	Model	5	0.253	0.051	2.125	60.28
	Error	7	0.167	0.023	Prob> F	
	Total	12	0.420		0.177	
Y_2	Model	5	818.630	163.730	16.446	92.15
	Error	7	69.690	9.960	Prob>F	
	Total	12	888.32		0.001*	

a degree of freedom
b Sum of Square
c Mean sum of square
d Model MS/ error MS

Table 3-4 shows the lack-of-fit test to check the mathematical models adequacy. In other words, this test allows assessment if both equation models for Y1 and Y2 can adequately predict the absorbance of the supernatant and the percentage of protein precipitated, respectively.

The ANOVA results for the regression coefficients show that the regression coefficients for the model Y2 are significant considering 95% F distribution. The lack-of-fit test also shows that the model Y2 adequately fit the data and can predict the percentage of protein precipitated (Table 3-

4). The protein absorbency recorded at 280 nm is reproducible, but the model Y1 cannot be used to adequately predict the final absorbance of the supernatant based on the lack-of-fit test[99] (Table 4). Moreover, the response surface and the contour plots, which derived from the CCD, are used to characterize the shape of the surface and can locate the optimum using computer software[97](Figure 3-1).

Table 3- 4 Lack-of-fit test analysis to check the model adequacy predicting the absorbance of the supernatant (Y_1), and the percentage of protein precipitated (Y_2).

Response	Source	DF[a]	SS[b]	MS[c]	F-ratio[d]
Y_1	Lack-of-fit	3	0.167	0.055	5857.55
	Pure error	4	0.000	0.023	Prob> F
	Total error	7	0.167		<.0001*
Y_2	Lack-of-fit	3	29.240	9.745	0.964
	Pure error	4	40.450	10.112	Prob>F
	Total error	7	69.687		0.491

a degree of freedom

b Sum of Square

c Mean sum of square

d Model MS/ error MS

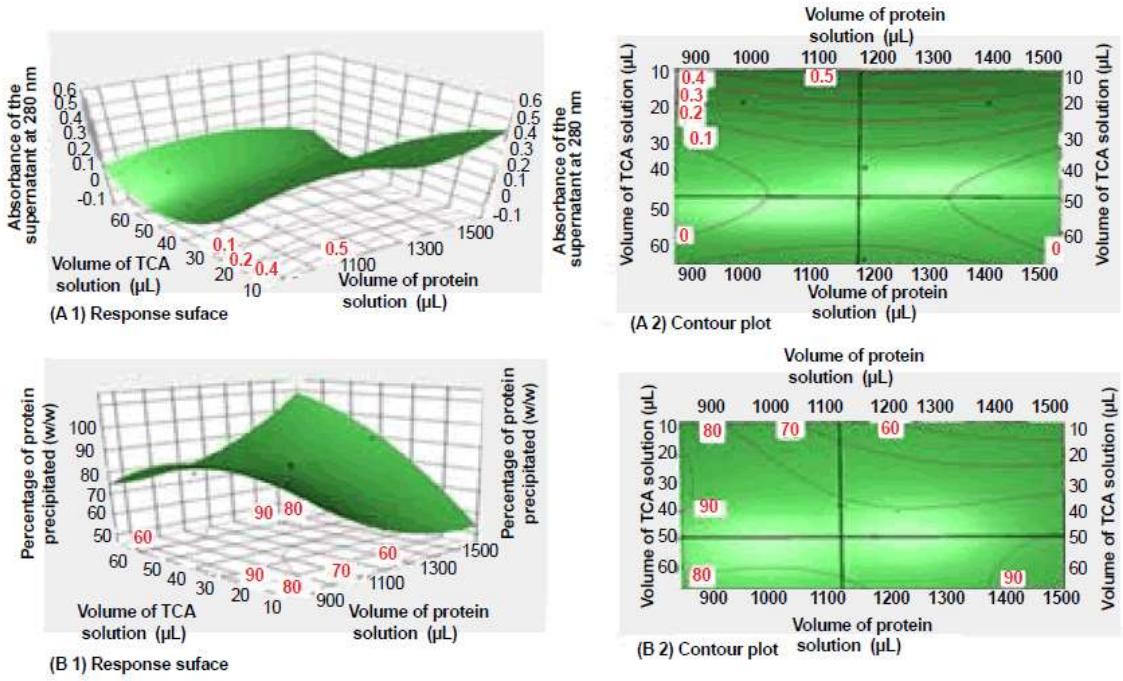

Figure 3- 2 Three-dimensional responses surface (A1), and contour plot (A2) showing the supernatant absorbance data (A) and those of the percentage of protein precipitated (B 1 and B2) as a function of volume of protein solution and volume of TCA solution. The intersections of the two orthogonal lines, in figures (A2), and (B2) are the saddle point.

3.3.2 Checkpoints analysis for the prediction of model Y2

The second order statistical model (Y2) is checked in triplicate with two random points with respective (X1, X2) values of (−0.5, −0.5) and (+0.5, +0.5), in addition to the theoretically optimal point (+0.6, +1) shown in (Table 5). Bias for the fitted model (Y2) is computed using the following equation Eq. (3- 9):

$$Bias\% = \frac{Predicted\ value - observed\ value}{observed\ value} x100 \quad (3\text{-}10)$$

The results of the checkpoints analyses show that the predicted and measured values of the percentage proteins precipitated are statistically insignificant considering a 95% student's t-

distribution. The predicted percentage of protein precipitated (Y_2), and the measured Y_2 values, are statistically insignificant if the p-value (p) is greater than 0.05 using the student's t-test. For checkpoint #1, the result is t = -1.78, degree of freedom (df) = 2, and p = 0.11. For checkpoint #2, t = -2.21, df = 2, and p = 0.08. For checkpoint #3, t = 2.26, df = 2, and p = 0.92. Thus, the model Y_2 can accurately predict the Y_2 values for a given volume of aqueous solution of BSA solution, and a given the volume of TCA solution 6.1N within the experimental design space. The Y_2 values depend mainly on the volume of TCA and the interaction between both the volume of the protein solution and the volume of TCA (Figure 3-2).

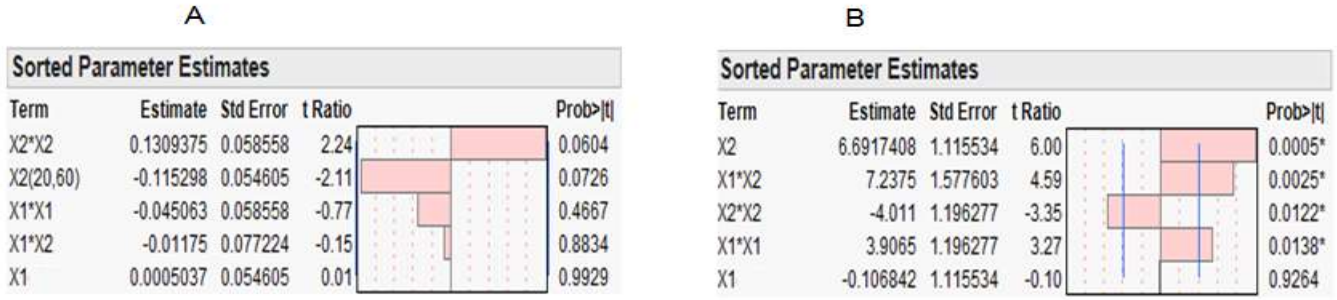

Figure 3- 3 Pareto chart showing the effect of the independent variables (X_1, volume of protein solution; X_2, volume of TCA solution), on the absorbance of the supernatant recorded at 280 nm and the percentage of protein precipitated using BCA assay. Sorted parameter estimates and their corresponding t-ratio are shown on the horizontal-axis. Bars extending beyond the vertical line indicate values reaching statistical significance ($\alpha = 0.05$).

Based on the prediction profiler (Figure 3-4), the optimal percentage w/v of TCA in solution required to precipitate the maximum amount of protein in aqueous solution is 4.22% w/v TCA (rounded to 4% w/v). Using 4% w/v TCA, the percentage protein precipitated is 87.96 ± 1.55% w/w (n = 5).

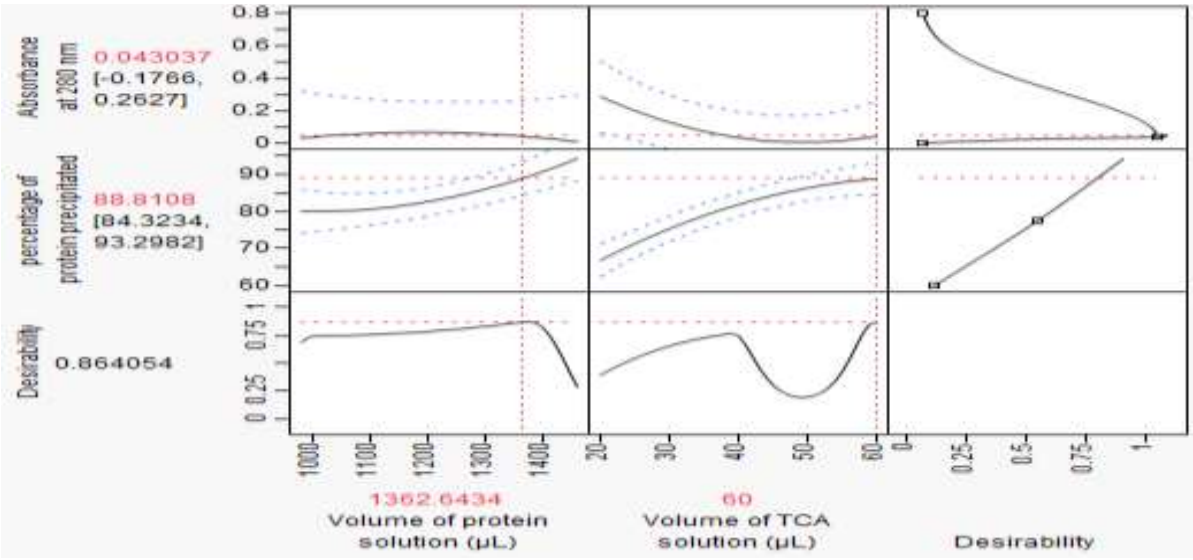

Figure 3- 4 Prediction profiler and desirability showing the effect of the volume of protein solution and the volume of TCA solution on the absorbance of the supernatant measured at 280 nm and the percentage of protein precipitated using BCA assay.

3.3.2 SDS PAGE Analysis

Figure 3-5 shows the intensity of the coomassie-stained protein band on the SDS gel for protein recovered in pellets after the precipitation phase. The intensities of the band are in agreement with the percentage of protein precipitate measured by the BCA assay. The orders of the lane are the points of the experimental design 1-9 (Table 3-2). Lanes 10-11 show the band intensity for commonly used concentrations of TCA for protein precipitation; respectively 10% w/v TCA and 20% w/v TCA.

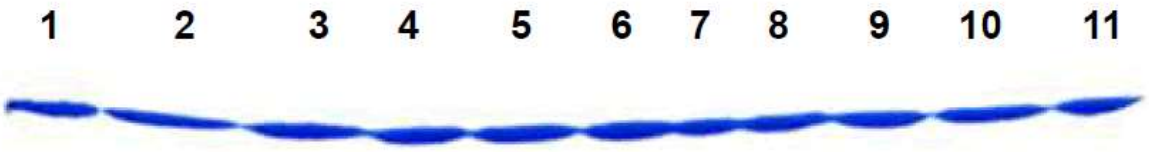

Figure 3- 5. SDS-PAGE analysis of BSA precipitation by TCA. Lane: 1, 2.00% w/v TCA; 2, 5.78% w/v TCA; 3, 1.35 %w/v; 4, 3.95%w/v TCA; 5, 4.35%w/v TCA; 6, 2.50% w/v TCA; 7, 0.95%w/v TCA; 8, 5.30%w/v TCA; 9, 3.18% TCA; 10, 10.00 %w/v TCA; 11, 20.00% w/v TCA.

3.3.3 Effect of TCA concentration on the percentage precipitated protein for lower concentration of proteins solution

Figure 3-5 shows the percentage of protein precipitate when the initial concentration of protein is within the range 0.008-0.040 mg/mL. The volume of protein solution used equals to 1 mL, and the optimal concentration 4% TCA found from the experimental design is used to precipitate the proteins.

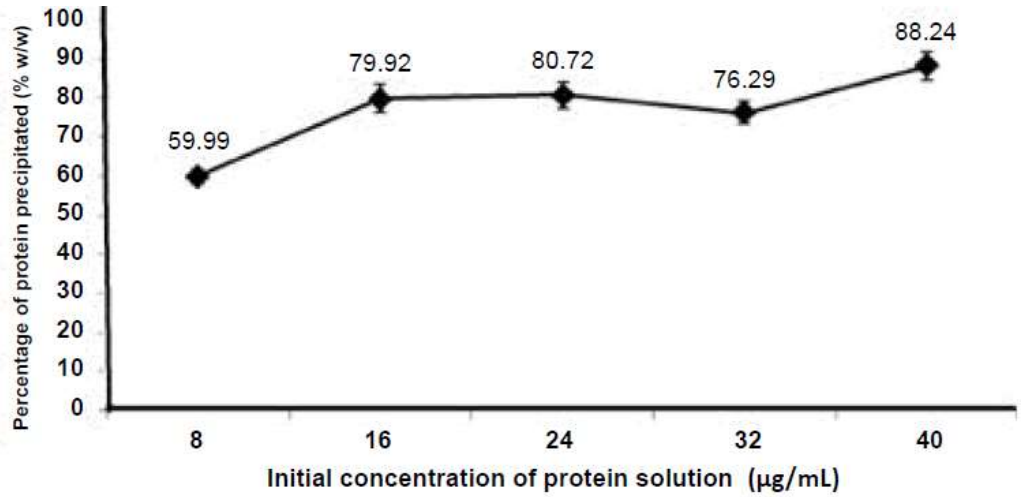

Figure 3- 6 Percentage of protein that precipitated at initial concentration less than 40µg/mL based on BCA assay. In this study, the final concentration of TCA is kept constant and equals to 4%w/v for a total sample volume of 1 mL. Error basr represent the standard deviation.

Figure 3.6 shows the precipitate of proteins based on the final concentration of TCA solution used and the initial concentration of protein in solution. When the initial concentration of proteins is very low, between 0.024 mg (total sample volume = 1 mL), there is no precipitation of protein when the final concentrations of TCA used are 10% w/v (Figure S2 shown in Supplementary file) and 20% w/v TCA (Figure S3 shown in Supplementary file), respectively. However, the precipitation of protein is observed when the final concentration of TCA is 4% w/v TCA.

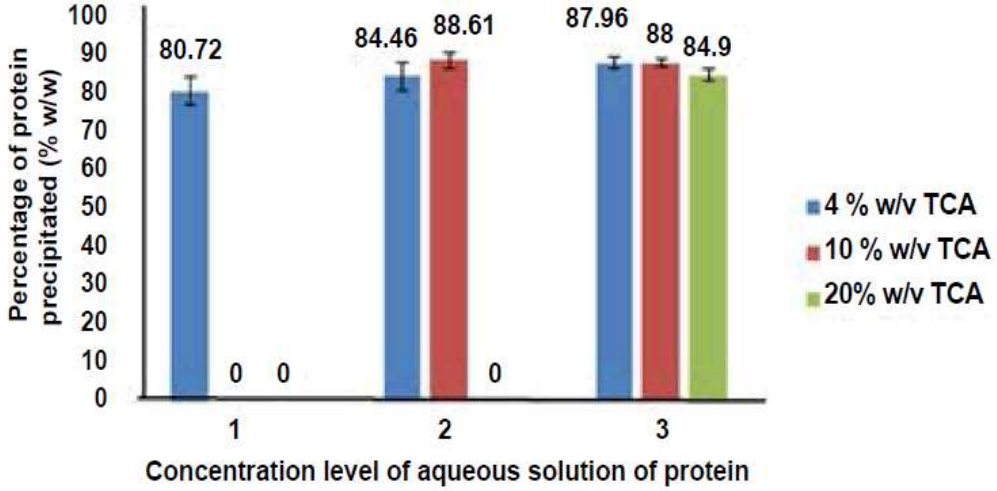

Figure 3- 7 Effect the concentration of TCA solution on the outcome of protein precipitation for different concentration of protein solution. The three types of concentrations of protein solution are respectively 24µg/mL for (level 1); 100µg/mL for (level 2) and 2000µg/mL for (level 3).

3.3.4 Application to supernatant "clarification" for tenofovir analysis

Figure 3-7B shows that the optimal concentration can be used to dramatically reduce the interference between BSA (20 mg/mL) and TNF while the commonly used concentration (20% TCA) (Figure 7A) is unable to reduce the interference.

The LOD and LOQ obtained using 4% w/v TCA are respectively, 0.0014 mg/mL and 0.0042 mg/mL. The LOD and LOQ also obtained using 10% w/v TCA are 0.0041 mg/mL and

0.0123 mg/mL respectively. Using 20% TCA, due to strong absorbance of the media, the absorbance of TNF cannot even be recorded as shown in Figure 7A.

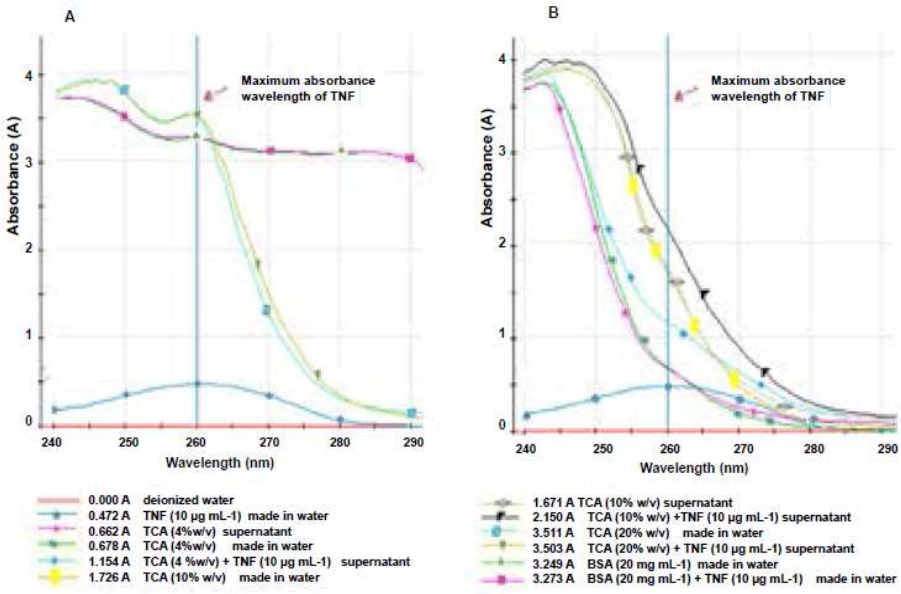

Figure 3- 8 Interference between TNF and bovine serum albumin (BSA) and reduction of the interference by protein precipitation with the optimal concentration 4%w/v, in comparison with the 10-20% w/v concentration of TCA commonly used for protein precipitation.

3.3.4 Application to the Precipitation of Protein in Human Urine

Figure 3-8 shows the effectiveness of 4% w/v TCA for protein precipitation in fresh human urine containing low amount of protein. It clearly appears that 100% w/w of proteins are pelleted using 4%TCA, whereas the percentage is ~50% w/w using 20% TCA.

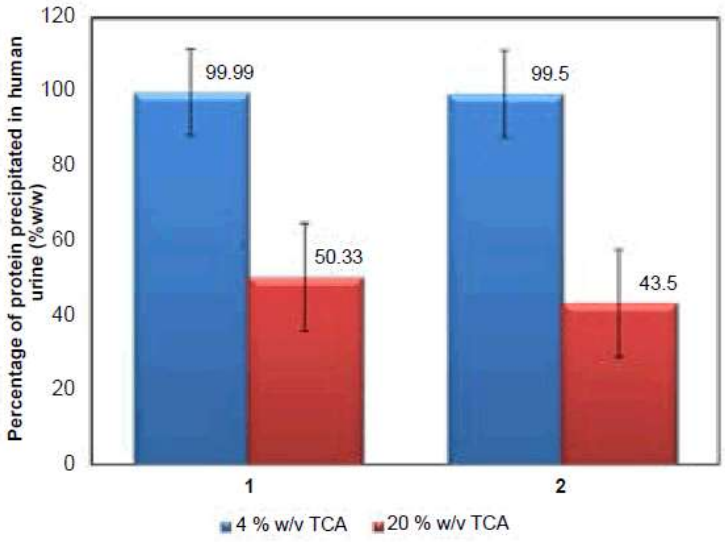

Figure 3- 9 Percentage of protein precipitated in human urine using 4% w/v TCA solution 6.1 N. 1: first collection of urine; 2: second collection of urine form the same donor. The volume of fresh human urine was kept constant and equal to1 mL. Error bars represent the standard deviation.

3.4 Discussion

In this study, the optimal concentration of TCA required for maximal precipitation of both high (2-20 mg/mL) and low amounts of protein in aqueous solution (0.008-0.04 mg/mL) is determined using response surface methodology (RSM) with supporting biochemical, proteomic analysis. The thorough RSM analysis clearly shows in Figure 3-1 that the stationary point of TCA-mediated protein precipitation is a saddle point. The precipitation of protein by TCA is specifically due to two properties, the acidity of TCA and the trichloro moiety that bear that molecule. Molten globule' or 'A-state(s)' (a "thermodynamic state, clearly different both from the native state and the denatured state of the protein), is a type of partially folded protein state [100]. The 'A-state' of protein is prone to stickily aggregate [81]. It is demonstrated that the precipitation of protein by TCA is governed by the formation of the sticky aggregation-like 'A-state' [81].

The percentage of proteins that precipitate varies from 76.29 to 92.67% w/w when the BSA concentration is in the range of 0.016-2 mg/ mL. Figure 3-5 and Table 3-2 show the percentage of protein precipitated for high and low amounts of aqueous solution of proteins, respectively. The precipitation of protein by TCA is separated into two phases based on TCA concentration. When, the TCA concentration is less than 2% w/v, the protein precipitation is incomplete. In the second phase, as long as the concentration of TCA is greater than or equal to 2% w/v, more than 80% w/w of the protein is precipitated Table 3-2. However, some traces of proteins are left in solution as shown by the absorbance recorded at 280 nm Table 3-2, which is slightly above TCA absorbance alone. When the concentrations of TCA are 10% w/v and 20% w/v, respectively, 88.0% w/w and 84.9% w/w of the proteins in relatively higher concentrations (2 mg/mL) are precipitated. It is clear that the amount of protein precipitated is equally high (in comparison to that obtained with lower TCA concentration, Figure 3-6 but the increase of the concentration of TCA away from 4%, w/v does negatively affect the outcome of the protein precipitation in many ways. For instance, the addition of TCA to relatively lower concentrations of protein solutions (less than or equal to 0.024 mg/mL and 0.1 mg/mL) in 1mL of BSA aqueous solution, so that the final concentrations of TCA are respectively 10% w/v and 20% w/v in the mixture, does not result in precipitation of protein (Figure 3-6). In previous studies, it was reported that the addition of 20% w/v TCA to urine containing a low concentration of protein did not result in protein precipitation [83]. Moreover, it was reported that the amount of the total protein must be observed beyond 0.020-0.030 mg to observe the obvious precipitation of the protein[79] . However, this study shows that there are indeed obvious precipitations of protein when the total amount of protein is 0.016-0.020 mg for a total volume of 1 mL using 2-4% w/v TCA solution Figure 3-5 . It was reported in another study that when the final concentration of TCA is greater than or equal to 50-60% w/v, most of the protein

remains in solution after the addition of TCA [81-82]. The limit of detection of the BCA assay is 0.0005 mg/mL. Thus, as low as 0.002 mg/mL, BSA is detected by the BCA assay, when the concentration of TCA used is within the range 2-4% TCA w/v, but it remained to be confirmed based on the limit of the current method based on visual inspection of pellets. There is a possibility of loss of the significant proportion of the pellets during the removing of the supernatant; especially when they are invisible to the naked eye at a relatively lower concentration of protein (<0.012 mg/mL). Thus, it is clear that higher concentration of TCA (far away from the stationary point of TCA mediated protein precipitation) is the ultimate reason why a low amount of protein in aqueous solution usually fails to precipitate in aqueous solution after the addition of TCA (Figure 3-6). The physicochemical explanation to the fact that higher TCA concentration fails to precipitate at a low protein concentration might be ascribed to TCA-specific physicochemical properties (density, surface tension, and polarizability). For example, the relatively high density of TCA (1630 mg/mL) may hinder relatively smaller pellet deposition at higher TCA concentrations for lower protein concentrations. Moreover, the use of higher TCA concentrations (typically 30% w/v) is not only the waste of TCA, but also it negatively affects the quality of the sample with low recovery[81-82]. However, when the protein concentration is around the optimum point, it maintained its 'A-state'[81]. For example, cardiotoxin analogue III (CTX III), a protein with pI's 9.38 with a well-known all-β-sheet protein conformation, maintained its native 'A-state' structure when treated with a TCA concentration below 3% w/v, while it is completely in its unfolded state when treated with 45% w/v TCA [81]. A recent study has shown that the maximum amount of precipitated protein is obtained when the concentration of TCA is between 5-40% w/v [82]. However, in that study, the use of 15-45% w/v TCA was suggested for the precipitation of proteins[82]. A close comparison of the intensity of the coomassie-stained protein band on the SDS gels of this previous study clearly

suggests that the maximum amount of protein precipitated is already reached with 5% w/v TCA. Thus, the result of these previous studies clearly supports our current experimental design outcome that the optimal concentration of TCA for the precipitation of protein is 4% w/v based on BCA assay. Moreover, consistent with previous studies, there is no difference among the intensities of the coomassie-stained protein band on the SDS gels (Figure 3-4). Using 0.008 mg/mL of BSA solution, 59.99% w/w of the protein is precipitated with 4% w/v TCA. However, the percentage of precipitated protein might improve if a more advanced method, with higher resolution for the visualization of pellets, can be used to separate the pellet from the supernatant. All the above method of precipitation of protein was done in deionized water or in simulated diluted biological fluid. We have tried to validate the effectiveness of 4% TCA for precipitation of protein in fresh human urine (within 2 hour after collection) in a sterile device with no dilution, where the concentration of protein was 20 ppm based on microalbumin assay. As shown in Figures 8 both 20% TCA and 4% TCA are effective in the precipitation of protein in fresh human urine containing as low as 20 ppm. The amount of protein precipitated was almost 100% w/w with 4% TCA whereas the amount of protein precipitated using 20% TCA was only 50% w/w based on BCA assay. The plausible explanation could be the synergic action of both TCA and the presence of acid and organic reagent such as acetone in human urine [36]. A previous study compared the effectiveness of gold nanoparticle to TCA for the enrichment of low protein concentrations containing biological samples [18]. That study also demonstrated that TCA (20% w/v) was inefficient in enrichment for low amount of protein containing biological sample. These analyses were based on visual analysis of protein pellets. For a total protein of 8 μg, it was quite impossible to see any eventual pellet with the naked eye, whereas gold nanoparticle might have helped increase the size of the complex protein-gold nanoparticle. However based on the BCA assay in this study, 4% w/v TCA is efficient

for the precipitation of low protein concentration made in deionized water (Figure 3-5) up to 8 ppm for a total volume of 1 ml, but it was quite impossible to see the pellet deposition because of the limitation of the naked eye. Moreover, in the screening study, this optimal concentration 4% w/v can precipitate low protein concentration containing fresh human urine for a total volume of 10 mL. This outcome is consistent with the result of the experimental design data. As shown in Figure 3-2, the terms that significantly affect the precipitation of protein are the volume of TCA (X2) and the interaction between the independent variables (X1X2). Finally, 4% w/v was efficient for the precipitation of protein up to 20 ppm (V=1 mL) both made in deionized water or in real fresh human urine. TCA(20% w/v) is unable to precipitate low protein concentration below 100 ppm made in deionized water, but amazingly it works for 20 ppm protein concentration in real fresh human urine. The discrepancy observed remained to be elucidated in future studies. Proteomics analysis have shown that human urine contains a total of 67 protein forms of 47 unique proteins were identified, including transporters, adhesion molecules, complement, chaperones, receptors, enzymes, serpins, cell signaling proteins and matrix proteins [101]. These facts suggest the potential application of this optimal condition to wide variety of protein enrichment scenarios. This method is successfully applied for (TFV), a model microbicide, and analysis in a mixture of BSA solution (20 mg/mL). As shown in Figure 3-7A, it is impossible to quantify TFV (final concentration 0.01 mg/mL) when either present into BSA solution (20 mg/mL) or present in the supernatant free protein when protein is precipitated with 20% w/v TCA using the above UV spectrophotometric. However, as shown in Figure 3-7B, the absorbance of the supernatant free protein using 4% w/v TCA is similar to the absorbance of 4% TCA made in water which consistent with the result of the CCD further confirming complete protein removal from the media. The final absorbance of the supernatant is that of the residual 4% w/v TCA initially introduced for the

purpose of protein precipitation. The LOD and LOQ obtained using 4% w/v TCA are significantly lower than those obtained using 10% w/v TCA. This suggests that the method for determination of TFV using 4% w/w TCA is more sensitive than that using 10% w/v TCA [102-103]. Moreover, the extent of tenofovir binding is not concentration-dependent and less than 1% and 7.2% bound in human plasma and serum, respectively [104]. This fact would enable better estimate of this drug or similar drug level in such biological matrixes after protein precipitation.

3.5 Conclusions

This study demonstrates for the first time that response surface methodology can be used to identify the stationary point of TCA-mediated protein precipitation. The optimal concentration of TCA (a saddle point) required to precipitate both low (<0.02 mg/mL) and concentrated aqueous protein solutions (2-20 mg/mL) and urine sample is a 4% w/v TCA. This finding is important because (1) low amount (2-5 times less) of TCA are required, (2) the use of optimal TCA concentration is fast and cost effective (3). This optimal concentration exhibits unprecedented and tremendous advantageous either for protein enrichment or for the analysis of xenobiotic such as tenofovir in supernatant free protein.

CHAPTER 4

SODIUM ACETATE COATED TENOFOVIR-LOADED CHITOSAN NANOPARTICLES FOR IMPROVED PHYSICO-CHEMICAL PROPERTIES
(Adapted from Ngo et al Pharmaceutical research, 2015)

4.1 Rationale

Sodium acetate (SA) is approved by European food control authorities and is an edible salt that is added to food as a seasoning. It has a wide range of applications. Firstly, it is used as antibacterial additive and preservative agent in food compounds; it is an inhibitor of gram-negative bacteria, and fungi that grow in food[105 106-107]. Secondly, oysters shelf-life can be extended through dipping in SA [108]. SA is generally prepared by mixing an aqueous solution of sodium carbonate or hydroxide with an aqueous solution of acetic acid. The recovery of SA, in this aqueous solution, is generally either by crystallization or evaporation using techniques such as spray drying[109]. Despite its widespread use in food industry, up-to-day, little is known about the coating property of SA for pharmaceutical nanoformulations. Chitosan is a polysaccharide obtained from the deacetylation of chitin and have been used as a nanocarrier for novel drug delivery system because of its biodegradable and biocompatible properties[63] . Among chitosan based nanocarriers, chitosan crosslinked with polyanion triphosphate (TPP) based nanoparticles (NPs) have been widely used for the nanoencapsulation of HIV/AIDS microbicide such as tenofovir (TFV) [9, 15]. The solubility in water, logP and oral bioavailability of TFV are 13.4 mg/mL, −1.1, and, 25–39%, respectively. TFV is a BCS class III drug[110]. The phosphoric acid group of TFV has two Pak values of 2 and 6.8, respectively [111]. Below pH=5, its two basic amino groups are protonated and thus positively charged and its phosphonic acid group has a charge of−2 above pH=7 [112] . However, the nano-encapsulation process using chitosan-TPP ionic gelation, and a highly water-soluble drug such as

TFV, has several limitations. Firstly, the encapsulation efficiency (EE %) of such drugs is typically very low. For instance, Meng and al. encapsulated only 5.83% of TFV in chitosan NPs [9]. Secondly, chitosan NPs exhibits an initial burst release [113] leading to a failure to sustain release, and to protect drugs. Thirdly, the freeze drying process is not effective for chitosan based NPs in absence of cryoprotectant. This leads to the aggregation of NPs[114]. It is hypothesized that in situ formation of SA, can be used to uniformly coat chitosan NPs and dramatically increase the physico-chemical properties (e.g., improvement of the freeze drying process, EE %, non-aggregation of NPs without the use of cryoprotectant, physical stability, and sustained drug release profile). This hypothesis is tested with supporting physico-chemical characterization of the NPs (e.g., particle mean diameters (PMD), EE%, zeta potential (ζ), Fourier transform infrared spectroscopy (FTIR), powder X-ray diffractometry (XRD), and transmission electron microscopy (TEM)), and in vitro cell culture for cytotoxicity assessment (e.g., assessment of cell membrane integrity, mitochondrial activity, assessment of nitric oxide (NO) or cytokines production). In addition, two non-aqueous titrations (using either perchloric acid or lithium methoxide) and the melting point assessment of the pure salt (SA used as a control, and freshly prepared in this study by the freeze-drying technique) provide an additional proof to confirm the nature of the salt coating chitosan NPs.

4.2 Material and Methods

4.2.1 Material

Chitosan (high molecular weight, source: crab shells, % deacetylation degree > 75%, viscosity = 800–2000 cps), sodium diacetate (SD), lipopolysaccharide (LPS), sodium acetate anhydrous (SAA), sodium acetate trihydrate (SAT), lithium methoxide (LM) in methanol (1 M), methanol, acetonitrile, acetic anhydride, perchloric acid (PA), crystal violet, calcium chloride dihydrate,

Dulbecco's phosphate buffered saline (DPBS), Dulbecco's modified eagle medium (DMEM), neutral red (NR), acetic anhydride and, potassium hydroxide are purchased from Sigma Aldrich (St. Louis, MO, USA). Fisher Scientific (Pittsburgh, PA, USA) supplies sodium triphosphate pentabasic (Na5TPP), hydrochloridric acid, sodium hydroxide, ethanol, and glacial acetic acid reagents. The murine macrophage RAW 264.7 (TIB-71) and fetal bovine serum (FBS) are purchased from the American Type Culture Collection (ATCC) (Manassas, VA, USA). Tenofovir (TFV) is purchased from Pichemicals (Zhang Jiang Hi Tech Park, Shanghai, China). Griess reagents is supplied by Promega (Madison, WI, USA). All chemicals used in the study are of analytical grade and used as received without further purification. Sodium acetate (SA), the pure salt used as control is currently prepared in situ by sublimation, in this study, using the freeze drying technique after half neutralization of glacial acetic acid with sodium hydroxide.

4.2.2 Method of Preparation of Chitosan-TPP Nanoparticles

Chitosan-TPP NPs are prepared according to ionic gelation method[9] with a modification of the process. Firstly, chitosan is dissolved for 24 h in 2% V/V aqueous solution of glacial acetic acid (pH~2.3) so that the final concentration of chitosan is 2 mg/ml. Secondly, volume (V) ~2.2 ml of sodium hydroxide (2 M) is added to 20 ml of the aqueous chitosan solution to raise the pH of the solution from ~2.3–2.94 to 4.76 which is the pKa value of acetic acid to produce enough acetate ion while keeping the pH of the solution acidic, a crucial condition to keep both protonated the amino groups of chitosan polymer, and soluble chitosan polymer. Thirdly, 2 mg, 4 mg and 6 mg of TFV powder are added to 3 different beakers containing, TPP aqueous solution (V=4 ml, 2 mg/ml) along with a blank formulation (0 mg of TFV) to form the mixture TPP-TFV aqueous solution. The pH is adjusted to 5.7±0.2 with a few drop of hydrochloric acid (2 M) to minimize

hydroxide ion amount in TPP aqueous solution. Then, the mixture TPP-TFV aqueous solution (V=4 ml), with a total amount of TFV=2 mg, 4 mg, and 6 mg is added dropwisely into three chitosan solutions (pH= 4.76, V=20 ml) and named formulation F1, F2 and F3, respectively, along with the blank formulation as shown in Table 4-1. Thus, chitosan NPs are formed instantaneously by ionic gelation. At this stage of the process, the uncoated NPs are formed. Fourthly, after 2–6 h of continuous stirring, the colloidal dispersion, is directly frozen at −20°C for 12 h, without centrifugation to avoid the loss of TFV in the supernatant and subsequently freeze-dried using the freeze dryer Freezone model (Labconco Corporation, Kansas City, Missouri, USA) without any addition of cryoprotectants. The coated NPs are obtained after the freeze-drying process. The schematic representation of the process of preparing coated chitosan NPs with SA is shown in Figure 4-1.

Table 4- 1Physical Mixtures and Formulation Variables

Physical mixture	Blank	P1	P2	P3
Chitosan amount (mg)	40	40	40	40
Sodium pentaphosphate amount (mg)	8	8	8	8
Tenofovir amount (mg)	0	2	4	6
Formulation	Blank	F1	F2	F3
Volume of chitosan aqueous solution in 2% v/v acetic acid (2mg/mL, pH=4.76)[1] (mL)	20	20	20	20
Volume of aqueous solution of triphosphate (2mg/mL, pH= 5.60-5.99)[2] (mL)	4	4	4	4
Amount of tenofovir add into triphosphate aquesous solution (mg)	0	2	4	6

1. pH raised with (2M, ~2.2 mL) of sodium hydroxide aqueous solution;
2. pH decreased with (2M, few drops) of hydrochloridric acid aqueous solution

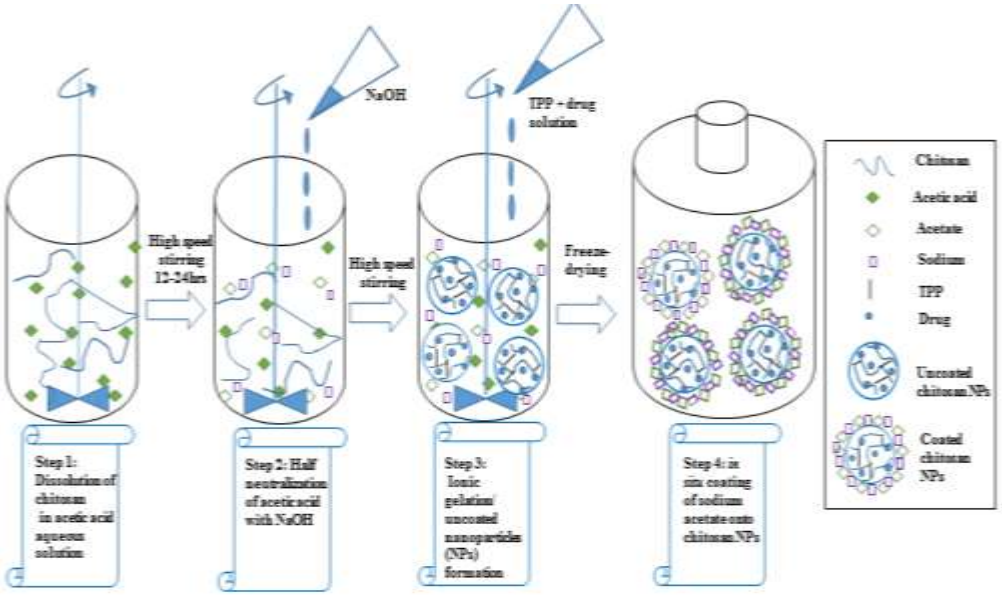

Figure 4- 1 Schematic representation of the process of coating chitosan nanoparticles with sodium acetate salt.

4.2.3 Particle Size and Zeta Potential Analysis

Uncoated chitosan NPs are suspended by sonication (Qsonica LLC, Newtown, CT, USA) after centrifugation in deionized water. SA coated chitosan NPs are straightforwardly dispersed in deionized water. Particle size expressed as particle mean diameters (PMD), and polydispersity index (PDI) are measured through dynamic light scattering (Zetasizer Nano ZS, Malvern Instruments Ltd, Worcestershire, UK) at the temperature of 25°C. Samples with PDI<0.05, are considered monodispersed according to the National Institute of Standards[9]. The zeta potential (ζ) of both uncoated and coated NPs suspended in deionized water is determined by the zeta potential analysis mode of the instrument. Nanosphere™ size standard (59±2.5 nm) and zeta potential standard (68± 6.8 mV) are used to calibrate the instrument before the size and ζ analysis.

4.2.4 Encapsulation Efficiency (EE %) Determinations

4.2.4.1 EE% Determination of Uncoated Chitosan NPs

The final amount of TFV entrapped into the uncoated chitosan NPs after centrifugation is calculated from the difference between the total amount of TFV initially used and the amount of drug found in the supernatant after encapsulation process. The free drug amount in the supernatant is measured using UV spectrophotometer (Spectronic Genesys 10 Bio, Thermo Electron Corporation, WI, USA) at a wavelength of 260 nm. The drug EE% is calculated as follows:

$$EE\% = \frac{Total\ amount\ of\ TFV - free\ TFV}{Total\ amount\ of\ TFV} * 100 \quad (4.1)$$

The standard curve of TFV absorbance (Y), used is Y=0.0448X (R2=0.9994), where X=concentration of TFV (µg/mL).

4.2.4.2 EE% Determination of Coated Chitosan NPs

The amount of TFV entrapped in the core-shell NPs after freeze-drying, is measured at 260 nm using the above UV spectrophotometer. Briefly,1 mg/ml of different formulations (F1, F2, and F3), along with the appropriate blank are dissolved in 2 M HCl up to 23 h at room temperature and followed by 1 h of sonication to accelerate the dissolution of chitosan NPs using the sonicator (Qsonica LLC, Newtown, CT, USA). Then, the dissolved NPs solutions are centrifuged (14, 000 rpm, 10°C) for 20 min using refrigerated microcentrifuge (VWR, Radnor, PA) to remove any eventual traces of undissolved debris of chitosan NPs. Finally, the total amount of TFV entrapped,

is recorded at 260 nm along with the appropriate blank, used to setup the baseline. The drug EE% is calculated as follows:

$$EE\% = \frac{Total\ amount\ of\ TFV\ entrapped}{Total\ amount\ of\ TFV} * 100 \qquad 4.2$$

The same standard curve of TFV Equation. (4.1) is used to assess the total amount of drug in the NPs because, the media does not shift the calibration curve based on preliminary screening.

4.2.5 Fourier Transform Infrared (FTIR) Spectroscopy

The FTIR is used to confirm the chemical nature of the salt coating chitosan NPs after freeze-drying. Powdered samples are deposited on the crystal for analysis at room temperature. The spectra are recorded on an Agilent Cary 630 FTIR spectrometer with a software microlab version 4 (Agilent Technologies, Santa Clara, CA, USA) in a wavenumber range of 500–4000 cm^{-1}, and at a resolution of 4 cm^{-1}.

4.2.6 Powder X-ray Diffractometry (XRD)

XRD is carried out to assess the crystallinity of the NPs coated with SA. The powder XRD scans are performed using a MiniFlex automated X-ray diffractometer (Rigaku, The Woodlands, TX) at room temperature. Ni-filtered Cu Kalpha radiation is used at 30 kV and 15 mA. The diffraction angle is covered from 2θ = 5°C to 2θ=60 °C with a step size of 0.05 ° /step, and a count time of 2.5 s/step (effectively 1.2 ° / min for approximately 46 min/scan). The diffraction patterns are processed using Jade 8+ software (Materials Data, Inc., Livermore, CA). In general, for crystal

structure determination, the relatives intensities of the diffracted beams which are directed by the position of atoms can be estimated using the following equations [115]:

$$I = |F|^2 p\left(\frac{1+\cos^2 2\theta)}{\sin^2 \theta \cos \theta}\right) \quad (4.3)$$

where, F is defined as follows,

$$F = \sum_i^N f_n e^{2\pi i(hu_n+kv_n+lw_n)} \quad (4.4)$$

where, I= relative intensities of the diffracted beams, F=structure factor for hkl reflection in terms of atom position in 3 dimensions with defined coordinates (u, v, w), θ=Bragg angle, and p= multiplicity factor, f_n = atomic scattering factor of atom n, h,, l are values from the miller index of the plane of atoms producing the peak.

Non-Aqueous Titration of Acetate Ion in the Salt with Perchloric Acid (PA)

PA solution (0.015 M) in glacial acetic acid is used as a titrant to determine the molar mass of the salt coating chitosan NPs. Three different samples, sodium acetate anhydrous (SAA), sodium acetate trihydrate (SAT) and sodium diacetate (SD) with a known molar mass (M) are used as controls to validate the molar mass of SA. Crystal violet (dye) (0.0005%w/v, 100 µl), dissolved in acetonitrile, is used to determine the equivalence point. Briefly, approximately 10 mg of the appropriate salt is dissolved in 20 ml of acetonitrile, followed by addition of 100 µl of the dye, under continuous stirring. Then, the amount of the acetate in salt is titrated with PA until the color of the solution changes from purple to green [115]. The molar mass of the salt is calculated using the following equation assuming the purity of the salt is ~100%:

$$M = \frac{m}{C_a V_a} \quad (4.5)$$

where, M= molar mass found of the salt, m=mass (g) of the salt, Ca= concentration of PA (0015 M), and Va=volume of PA added to reach the equivalence point. The molar mass M is corrected and termed molar mass corrected (Mc) to find the true molar mass of the different salt using as a reference the known molar mass of SAA. The following equation allows us to find Mc:

$$M_c = M * \frac{\text{expected molar mass of SAA}}{\text{average molar mass found of SAA}} \quad (4.6)$$

Non Aqueous Titration of Acetic Acid Content in the Salt with Lithium Methoxide (LM) in Methanol

LM solution (0.015 M) in methanol, used as a titrant, is used to titrate the acetic acid content if any of the new salt SA dissolved in methanol [116]. Glacial acetic acid in methanol (0.006 M, 20 ml), SAA~10 mg, SD~10 mg, dissolved in methanol are used as controls. Briefly, the appropriate salt (~10 mg, 20 ml) dissolved in methanol or glacial acetic acid solution (0.006 M, 20ml) diluted in methanol, is titrated with LM using a pH-meter. The titration curve, pH = f (Vb) of the change in pH values, due to the addition of the LM is plotted against the volume Vb; (Vb = volume of LM added). Microsoft Excel 2013 is used to fit the non-aqueous titration curve.

4.2.7 Method of Determination of Melting Point (MP)

The melting point (MP) of SA salt is measured to determine its purity. Commercial available SAA, SAT, and SD are used as controls. Briefly, the appropriate salt is packed into a Kimble Chase capillary melting point tube made of borosilicate glass, 1.5-1.8 x 90 mm, purchased from (Fisher Scientific, USA). The tube is gradually heated in a MEL-TEMP capillary melting point apparatus (Sigma Aldrich, USA) and the temperature is measured with a Fluke 51 II digital

thermometer containing a thermocouple probe (Fluke, USA) as a range from the appearance of the first drop of liquid to a complete melt of the salt.

4.2.8 Morphological Analysis

The surface morphology of both uncoated and coated chitosan NPs is visualized with the transmission electronic microscopy (TEM). To get the specimens, the drops of coated or uncoated NPs suspension are placed on a copper grid with a carbon support film and air-dried. The NPs are viewed under a scanning transmission electron microscope CM12 (FEI, Hillsboro, OR, USA) at 80 kV accelerating voltage. Digital images are acquired with an ORIUSTM SC 1000 11 Megapixel CCD camera (Gatan, Pleasanton, CA, USA).

4.2.9 In Vitro Drug Release Study

The respective amount of 25.00 mg,12.50 mg and 8.33 mg of the formulation F1, F2 and F3 suspended in 4 ml of Tri–HCl buffer (9.1 mM, pH=7.51) or citrate buffer (1 M, pH=4.2). These environments simulate the pH condition of the mixture of human seminal fluid and human vaginal fluid (HVF), and that of HVF alone, respectively[15]. These nano-suspensions are placed into a cellulose ester membrane dialysis bag (Spectra/Por®, Float-A-LyzerG2, MWCO 3.5–5 KD, Spectrum Laboratories Inc. Rancho Dominguze, CA, USA). The dialysis bag is then dipped into a tube of 50 ml total capacity containing 24 ml of the appropriate buffer. The whole system is incubated in a thermostatically controlled shaking (50 rpm) water bath (BS-06, Lab Companion, Seoul, Korea) at 37°C. At set time intervals (0, 3, 6, 9, 12, 24…120 h), 1 ml of the buffer solution outside the dialysis bag is removed and replaced by fresh buffer solution to maintain a sink condition. The concentration of the drug released from the NPs in the outer tube solution is determined by a UV spectrophotometer at 260 nm as indicated in the EE% determination section.

Each experiment is run in triplicate. In addition, the release curve is fitted with Korsmeyer-Peppas model[117] to elucidate the release mechanism of TFV from the NPs, using the following equation;

$$\frac{M_t}{M_\infty} = at^n \quad (4.7)$$

where, $\frac{M_t}{M_\infty}$ represents the fractional drug release, *a* is a constant combining structural and geometric features of the drug dosage form, and n typify the release mechanism (e.g. fickian diffusion (n=0.5); anomalous diffusion (0.5<n<1.0; case II transport (n=1) and super case II transport (n>1).

4.2.10 Macrophage RAW 264.7 Culture

These cells are grown and maintained in a monolayer culture, in 75 cm^2 culture flasks (Techno Plastic Product, Switzerland), at 37°C in a humidified atmosphere of 5% carbon dioxide (CO_2) and 95% air.

4.2.10.1 Exposure protocol

The NPs are freshly suspended in DMEM/FBS 5% at 1000 µg/ml, dispersed by sonication (VWR, model 150 D; VWR International, West Chester, PA, USA) for 10 minutes, sterilized for 30 minutes under UV light [118], and diluted 1:1, 1:10, 1:100 and 1:1000. Macrophages RAW 264.7 (2×10^5 cells/100 µL/well) are seeded in 96-well culture plates (growth surface: 0.34cm^2) and incubated for 48 hours. Then, the cells are subjected for 24 hours to the NPs at 1, 10, 100 and 1000 µg/ml corresponding to 0.3, 3, 30 and 300 µg/cm^2, respectively. Wells containing cells without NPs are used as the negative controls. As a positive control, the macrophages are treated with lipopolysaccharide (LPS) (10 µg/mL), a well-known activator, to stimulate an inflammation [119].

4.2.11. Assessment of Cell Membrane Integrity

The cell membrane integrity is measured using the specific accumulation of the vital dye neutral red (NR) in lysosomes [120]. After exposure to the NPs, the cells are washed twice with Dubelcco's phosphate buffer saline (DPBS), and then 100 µL of fresh medium containing 50 µg/mL NR is added to each well and incubated for 3 hours. Then, the cells are washed twice with DPBS, and the dye is extracted with 1% acetic acid/50% ethanol (v/v). The plate is shaken for 15 minutes in the dark to solubilize all the NR crystals prior to the fluorescence intensity measurement (530-560 nm excitation, 590 nm emission) using a DTX 800 multimode microplate reader (Beckman Coulter, Brea, Ca, USA).

4.2.12 Assessment of Mitochondrial Activity

The mitochondrial activity is examined using a resazurin assay (Sigma-Aldrich, St. Louis, MO, USA) [121]. After exposure to the NPs, the cells are washed twice with DPBS, fresh medium is added, and then 10 µl of resazurin (0.1 mg/mL in DPBS) is added to each well. The assay plate is shaken for 30-60 seconds and incubated for 3 hours. Afterwards, the plate is shaken for 30-60 seconds prior to determining the fluorescence intensity (530-560 nm excitation, 590 nm emission) using the above microplate reader.

4.2.13 Assessment of Intracellular Nitrogen Species: Nitric Oxide (NO)

NO Production in Culture Supernatant, a Measure Of Inducible NO Synthase (iNOS) activity, is examined via nitrite accumulation measurement, the stable end product of the autoxidation of NO in aqueous solution[120]. After the indicated exposure period to the NPs, cell supernatants are collected and centrifuged at 1,000 x g for 10 minutes to remove cellular debris and particulate materials. Then, 50 µL of the supernatant is placed into a new plate and mixed with the Griess reagents according to the manufacturer's instructions. Absorbance is measured at 540

nm using the microplate reader and nitrite concentration is calculated using the sodium nitrite standard curve.

4.2.14 Multiplex Immunoassay Analysis of Cytokines Secretion

After macrophages RAW 264.7 exposure to the NPs, cell free supernatants are harvested and analyzed for cytokines using a high-sensitivity multiplexed bead-based immunoassay (Milliplex MAP Mouse Cytokine/Chemokine Magnetic Bead Panel, Millipore Corp., Billerica, MA; and Luminex MAGPIX instrument, Luminex Corp., Austin, TX, USA). Supernatants from untreated cells (negative control) and LPS-treated cells (positive control) are evaluated. Four cytokines, [e.g. interleukins (IL), including IL-1α, IL-1β, IL-6 and IL-7] levels are measured according to the manufacturer's protocol. Briefly, premixed magnetic beads conjugated to antibodies for all 4 analytes are mixed with equal volumes of supernatants (25 μL) in 96-well plates. Plates are protected from light and are incubated on a microplate shaker overnight at 4°C. Then, magnetic beads are washed twice with 200 μL of wash buffer, and detection antibodies are added to each well. The mixtures are incubated at room temperature for 1 hour. Streptavidin-phycoerythrin conjugate compound is added to each well, and the mixtures are incubated for 30 min at room temperature. The magnetic beads are washed and resuspended in wash buffer for 5 min, and plates are assayed on the Magpix system with xPONENT software. The median fluorescence intensity is analyzed using a 5-parameter logistic method from a standard curve of each respective analyte to determine the concentration of the cytokines in supernatants. These assays are run in duplicate.

4.2.15 Statistical Analysis

All values are expressed as mean ± standard deviations. One-way analysis of variance (ANOVA) in combination with all pairs Tukey’s HSD (Honestly Significant Difference) post- test

are used to find means of data that are significantly different from each other. All statistical analysis is carried out using JMP software version 10, (SAS Institute, Cary, North Carolina, USA). A P-value below 0.05 is considered statistically significant and allows the rejection of the null hypothesis.

4.3 Results

4.3.1 Particle Mean Diameters (PMD), Zeta Potential (Z) And Polydispersity (PDI) Analysis

The PMD for the uncoated or coated blank and the three different formulations before and after freeze drying respectively, (F1, F2 and F3) and the ζ and PDI are shown in Table 4-2. The PDI of the NPs is overall conserved before and after freeze drying (Table 4-2) suggesting that the coating salt prevents aggregation of the NPs. However, the PMD in general increases slightly due to the additonal thickness of the shell, (SA) on the core chitosan NPs as shown in Table 4-2. Figure 4-2 shows the uncoated NPs PMD distributon (Figure 4-2, A1, B1, C1, and D1), before freeze-drying and coated NPs PMD distribution after freeze- drying (Figure 4- 2, A2, B2, C2 and D2), respectively. Unlike the zeta potential (ζ) of the uncoated chitosan NPs, which is ~ above + 25 mV (Table 4-2), ζ of coated/freeze-dried NPs (~ neutral) is consistent with that of the pure salt further confirming coating by SA (ζ =-4.87±0.64 mV).

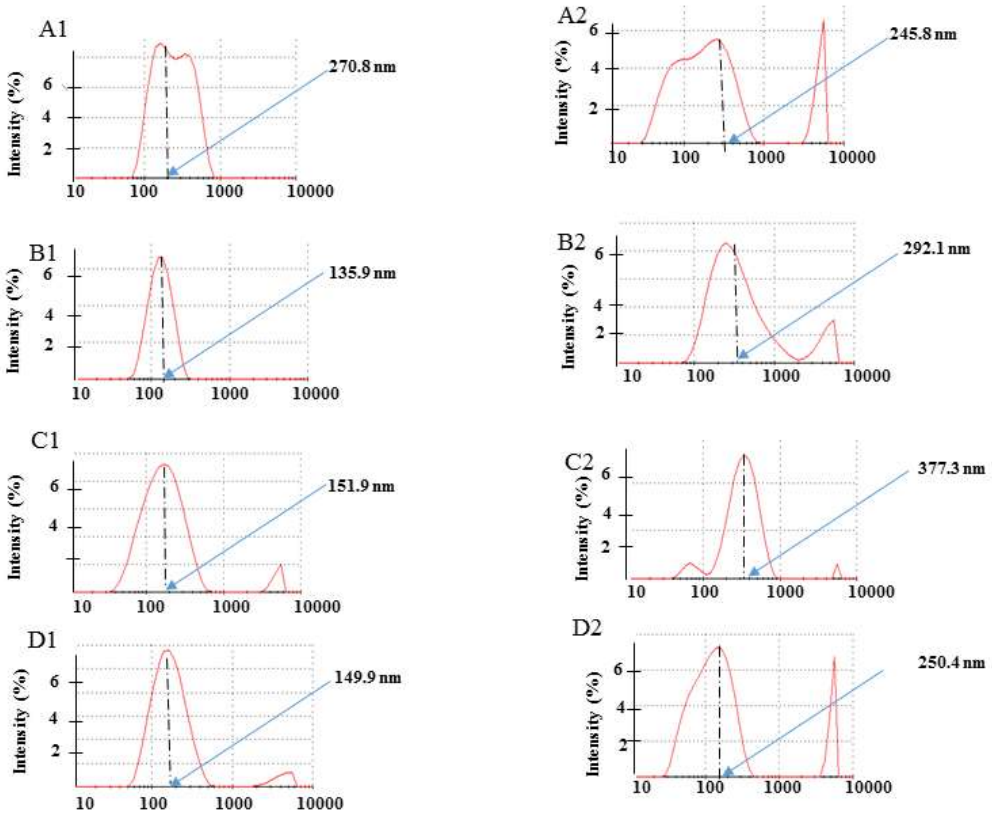

Figure 4- 2 Particle size distributions by intensity of uncoated chitosan NPs (a1, b1, c1, and d1) and coated chitosan with SA (a2, b2, c2, and d2) for blank, F1, F2 and F3 formulation, respectively.

Table 4- 2 Particle Mean Diameters(PMD), Zeta Potential (ζ), Polydispersity Index (PDI), and Percent Encapsulation Efficiency (EE %) for Different Formulations

Formulation	Blank	F1	F2	F3
Size NPs Uncoated d. (nm) [a]	348.33±74.64	135.67±1.86	150.67±1.2	155.93±4.34
Size NPS coated d. (nm) [b]	165.2±70.01	261.23±118	379.53±130.26	171.53±70.01
EE% [a]	n/a	11.74±0.71	5.52±0.34	6.12±0.1
EE% [b]	n/a	89.27±0.77	92.74±4.00	86.34±4.53
Zeta potential (ev)[a]	28.47±2.07	25.97±1.07	27.53±2.05	24.3±2.05
Zeta potential (ev)[b]	3.06±1.95	0.08±0.86	2.23±0.68	1.22±0.88
PDI[a]	0.47±0.05	0.30±0.05	0.34±0.07	0.32±0.04
PDI [b]	0.30±0.05	0.24±0.02	0.37±0.14	0.43±0.08

[a] Data for uncoated chitosanf NPs
[b] Data for coated chitosan NPs

4.3.2 Encapsulation Efficiency (EE%) Determination

The EE % of TFV for different formulations uncoated and coated before and after freeze drying are shown in Table 4-2, respectively. The EE% of uncoated NPs are indeed very low (EE% =5.5–11.7%) due mostly to drug loss by mass transfer towards the supernatant during the centrifugation process , whereas those coated with SA, after freeze drying using the new process developed in this study are indeed high (EE%~86.3–92.7%) and improved by ~8–17 fold.

4.3.3 Morphological analysis

Figure 4-3 shows the visualization of the uncoated NPs (A, B) and coated NPs (C, D) before and after freeze drying respectively. The salt coating chitosan NPs (Fig. 3, D, E, and F)

is clearly visible after freeze drying. The coating of SA onto chitosan NPs give a coreshell structure in which the shell is SA and the core is TFV loaded chitosan NPs or chitosan blank NPs as shown in Figure 4-3(D, E, and F).

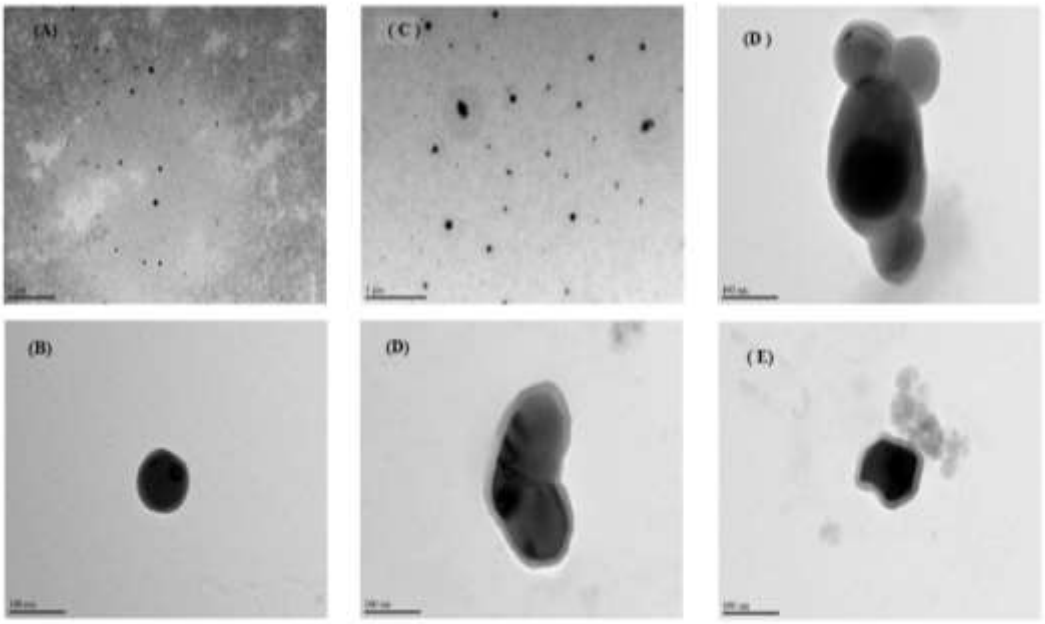

Figure 4- 3 Transmission electron micrographs (TEM) of uncoated chitosan NPs (A, B) for the blank formulation synthesized before freeze drying and coated chitosan NPs (C, D) after freeze drying, respectively. TEM of two different samples of these coated chitosan NPs after 24 h incubation at 37°C (Tris HCl buffer pH 7.51 (E, F). Scale bar represents 100 nm for (B, D, E, F) and 1000 nm for (A, C), respectively.

4.3.4 Determination of the Melting Point (MP)

The MP of the different salt of acetic acid are shown in Table 4-3. The melting point of SA (salt prepared using this new method) is identical to the melting point of SAA (supplied by company) suggesting that both SAA and SA are made almost of the same main element which are acetate *anion* and sodium *cation.*

Table 4- 3 Melting point of the different salt and molar mass of the different salt of acetic acid

Sample	Sodium acetate anhydrous (SAA)	Sodium Acetate (SA)	Sodium acetate trihydrate (SAT)	Sodium diacetate (SD)
Melting point (ºC)	332.5-338	333-338	329-333	325-333
M = Molar mass found (g/mol)	75.57±2.95	74.05±0.39	121.65±1.81	134.81±12.21
Mc = molar mass corrected (g/mol)	82.03±3.2	80.38±0.42	132.05±1.96	146.34±13.26
Expected molar mass	82.03	n/a	136.08	142.09

4.3.5 Non-aqueous titration of acetate with perchloric acid (PA)

To further elucidate and confirm the nature of the salt coating the NPs additional analyses are done. SAA, SAT, and SD, are used as controls to find the molar mass (M) of the salt (SA) coated (chitosan NPs using PA as a titrant. Molar mass corrected (M_C) and M and of the different salt after titration with PA are shown in Table4.3. Mc (SAA) ~82.03 g/mol is identical to Mc (SA) ~80.38 g/mol, whereas Mc (SA) is statistically different to both Mc (SAT) and Mc (SD) based on ANOVA test. This result suggests that the composition of SA in term of acetate *anion* and sodium *cation* is similar to that of SAA and not SD (sodium diacetate) although, SA is prepared from half neutralization of acetic acid with sodium hydroxide followed by freeze-drying.

4.3.6 Non aqueous titration of acetic acid content in the salt with lithium methoxide (LM)

Figure 4-4 shows the titration curve of different salts and acetic acid glacial in methanol with LM used a titrant. The titration curve of both SAA and SA with LM overlaps suggesting that the two salt are the similar in term of acetate ion. There is no inflexion point, whereas the titration curve of both acetic acid in methanol, and SD has an inflexion point. This suggests SD contains indeed acetic acid whereas both SAA and SA do not contain acetic acid.

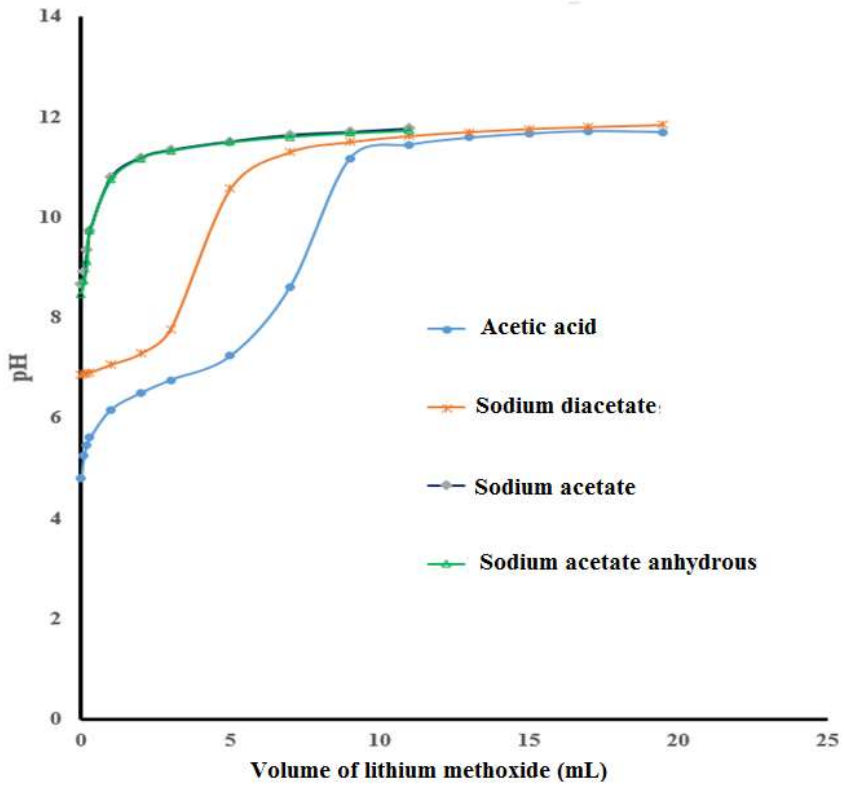

Figure 4- 4 Titration curve of different acetic acid salt with lithium methoxide in Methanol.

4.3.7 In vitro drug release profile

Figure 4-5 shows the release profile of TFV from different nanoformulations. Table 4-4 gives the value of "n" that charaterized the release mecanism of the TFV from the NPs. Sustained release of the drug occurs over a period of 5 days. The drug release mechanism is anomalous transport based on Korsmeyer Peppa model.

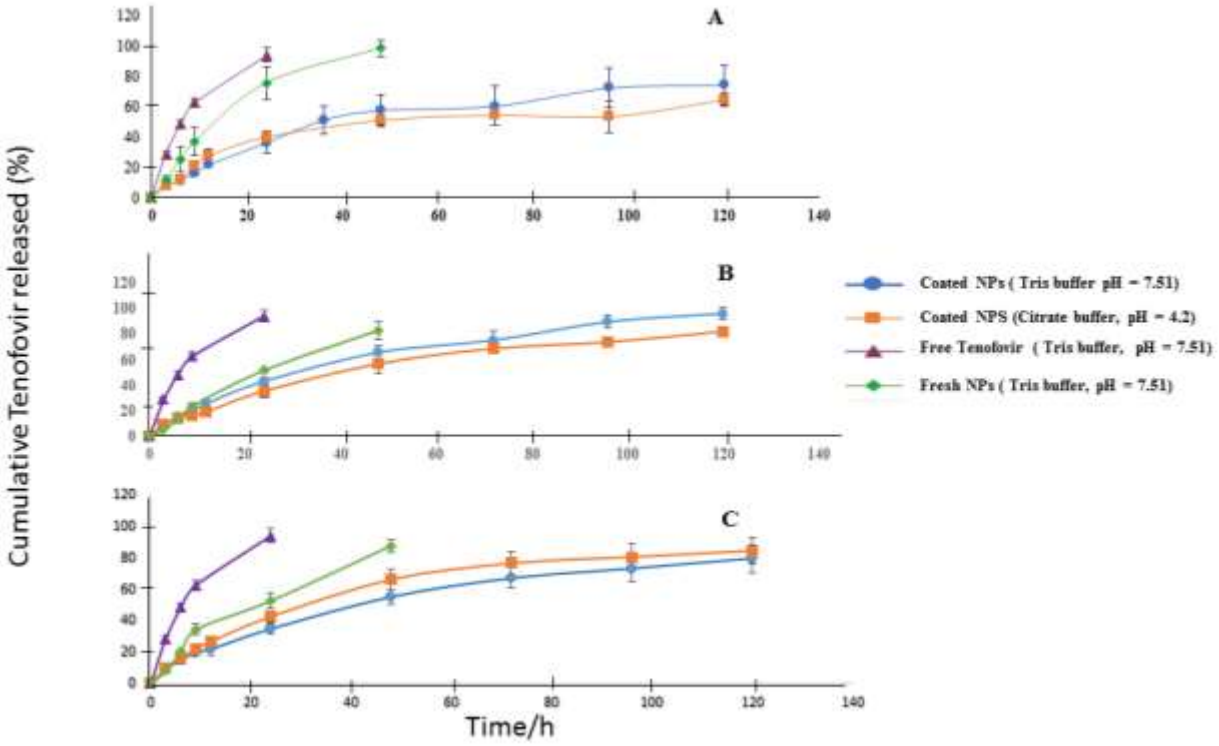

Figure 4- 5 In vitro drug release study A=formulation F1, B=formulation F2 and C=formulation F3. Release of coated NPs in Tris–HCl buffer pH=7.51 (solid line blue, dot marker), and in citrate buffer pH=4.2 (solid line orange, square marker), respectively. Release of tenofovir (TFV) from uncoated NPs (solid line green, fill diamond marker) and release of native TFV solution (solid line purple, fill triangle marker), respectively. Data are expressed as mean ± SD (n =3).

Table 4- 4 Value of "n" for the different coated nano-formualtions using the Korsemeyer-Peppas model

Formulation	Citrate buffer ph 4.2	Tris Hcl buffer pH 7.51
F1	n = 0.86 (R^2 =0.970)	n = 0.78 (R^2 =0.991)
F2	n = 0.61 (R^2 =0.974)	n = 0.79 (R^2 =0.998)
F3	n = 0.71 (R^2 = 0.999)	n = 0.63 (R^2 = 0.994)

R^2 represents the fit of the model, n indicates the likely release mechanism.

4.3.8 FTIR Spectral Analysis

Figure 4-6 shows the FTIR result of the individual component (A = TFV, B = TPP, C = chitosan) used for the preparation of TFV loaded chitosan NPs as well as the three physical mixtures (D = P1, E = P2, F = P3). Indeed, P1, P2, and P3 are the physical mixtures of the three main ingredients, namely TFV , TPP and chitosan, respectively. In Figure 4-6, the FTIR spectra of P1, P2, and P3 show the presence of the individual component TFV, TPP and chitosan respectively. The FTIR spectrum of G = SAA is identical of the FTIR spectrum of H = SA. The FTIR spectrums of coated NPs I ="blank",J = F1, K= F2, and L= F3 are identical to the spectrum of the pure salt SA after lyophilization. Thus, these futher confirm the deposition of SA on the surface of chitosan NPs. The two bands Figure 4-6 (G-L) on the FTIR spectrum at 1572.89 cm^{-1} and 1411.55 cm^{-1} derived from the resonance of electron within the carboxylate ion. $–COO^-$ of SA. This observation is expected because these bonds are transitional between single and double bonds [122]. The antisymmetric stretch and symmetric stretch of single bond C-O is found at 1042.48 cm^{-1} and 921.37 cm^{-1} respectively [122]. The bands at 3000.04 cm^{-1} and 2940.67 cm^{-1} are also the

antisymmetric stretching vibration of CH_3, and overtone transition from the ground state to the second excited state of the CH_3 symmetric distortion, respectively. These results well characterize SA coating because antisymmetric characteristic IR absorption stretch frequency of both carboxylate (COO^-) and single bond CO present is SA chemical structure are usually higher than to that of symmetric stretch.

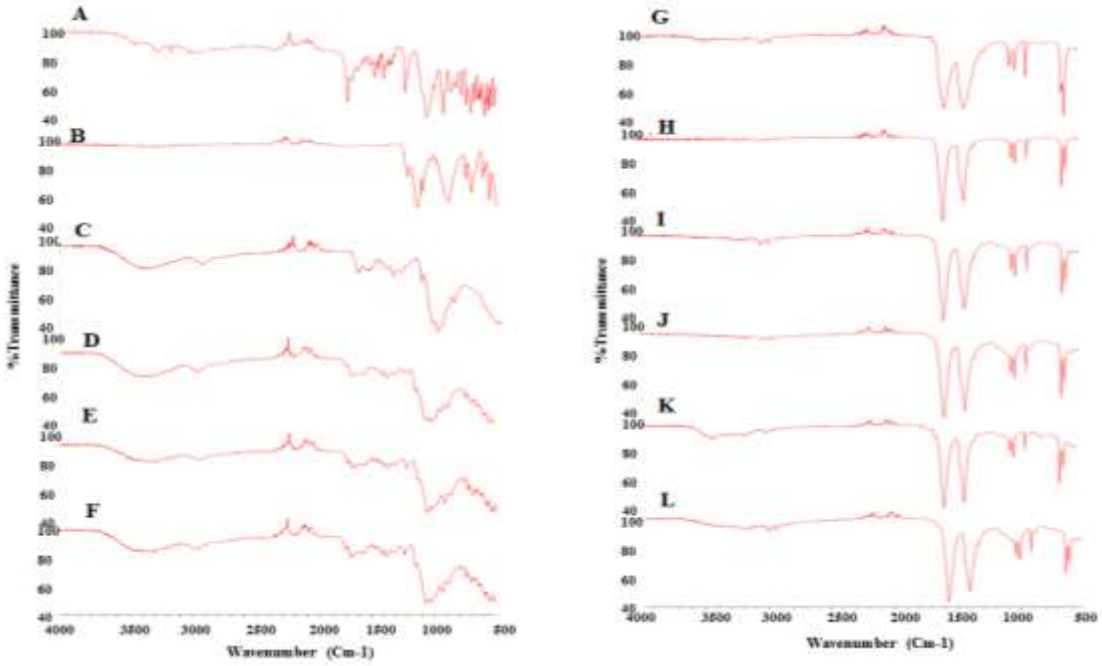

Figure 4- 6 FTIR spectra of native tenofovir (A), sodium triphosphate pentabasic (B), chitosan (C), physical mixture P1 (D), physical mixture P2 (E), physical mixture P3(F), sodium acetate anhydrous (SAA) (G), pure sodium acetate coating chitosan NPs (SA) (H), blank formulation (I), formulation F1 (J), formulation F2 (K) and formulation F3 (L), respectively.

4.3.9 X-ray Powder Diffractometric (XRD)

Figure 4-7 shows the XRD pattern of the individual component (A = TFV, B = TPP, C = chitosan) used for the preparation of TFV loaded chitosan NPs as well as the three physical mixtures (D = P1, E = P2, F = P3). P1, P2, and P3 respectively. The physical mixtures P1, P2, and P3 (Figure 4-7 D, E, and F) show peaks for the individual components, chitosan, TFV, and TPP, but they do not show peak for SA. This is to be expected for a dry physical mixture of components. The XRD pattern of coated NPs I ="blank", J = F1, K = F2, and L = F3 are identical to the pattern of H = SA after lyophilization. This confirms further the coating of the salt SA on the surface of chitosan NPs.

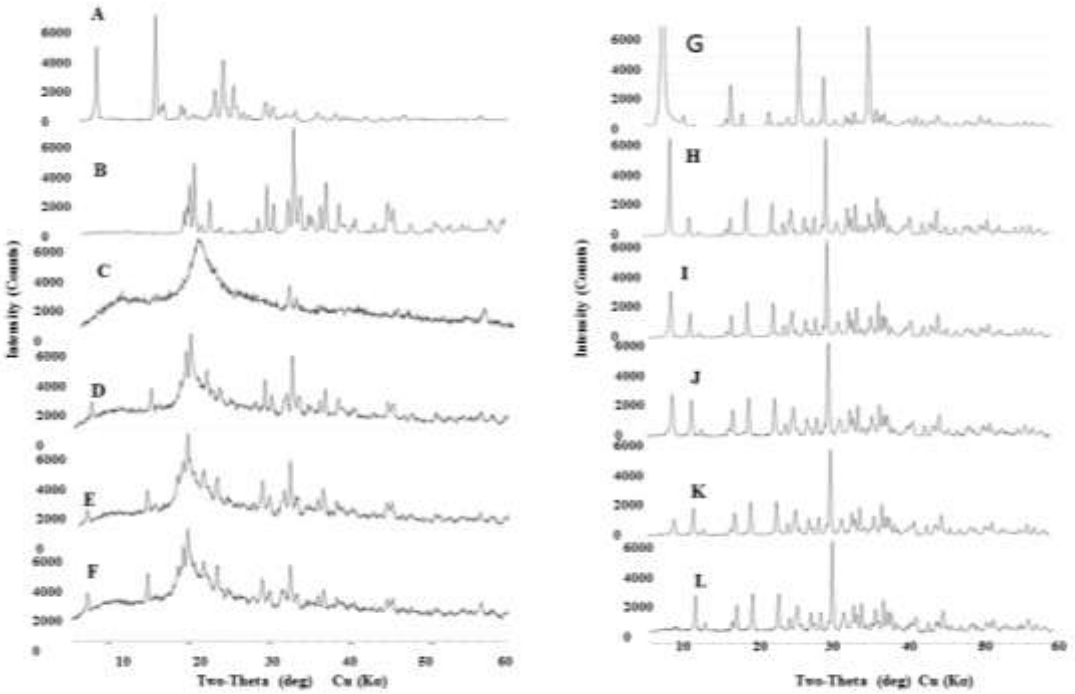

Figure 4- 7 XRD pattern of native tenofovir (A), sodium triphosphate pentabasic (B), chitosan (C), physical mixture P1 (D), physical mixture P2 (E), physical mixture P3 (F), sodium acetate anhydrous (SAA) (G), pure sodium acetate coating chitosan NPs (SA) (H), blank formulation (I), formulation F1 (J), formulation F2 (K) and formulation F3 (L), respectively.

4.3.10 Nanoformulation Cytotoxicity Assessment

4.3.10.1Assessment of Cell Membrane Integrity

Figure 8A shows the result of the membrane integrity of the cell. The NPs are investigated for their effect on plasma membrane integrity using the NR assay, which enables to distinguish between viable, damaged, or dead cells. The specific accumulation of NR in lysosomes is dependent of an intact plasma membrane and functioning lysosomes. As shown, in Figure 8A, the four nanoformulations (F0, F1, F2, and F3) do not compromise the cell membrane integrity of the macrophages, as no significant disruption of NR cell uptake is noted, based on both ANOVA test and all pairs Tukey's HSD test. In contrast, upon exposure to the positive control (LPS), a dramatic loss of cell membrane integrity is observed (~ 81%, $p<0.001$).

4.3.10.2 Assessment of Mitochondrial Activity

Figure 8B shows the mitochondrial activity of the cell. Resazurin assay is used to evaluate the mitochondrial activity. As illustrated in Figure B, following 24 hours exposure, the four nanoformulations (F0, F1, F2, and F3) do not cause any impairment of mitochondrial activity in the macrophages based on both ANOVA test and all pairs Tukey's HSD test. In contrast, the positive control (LPS) induces a dramatic decrease of mitochondrial activity by ~98 % ($P<0.001$).

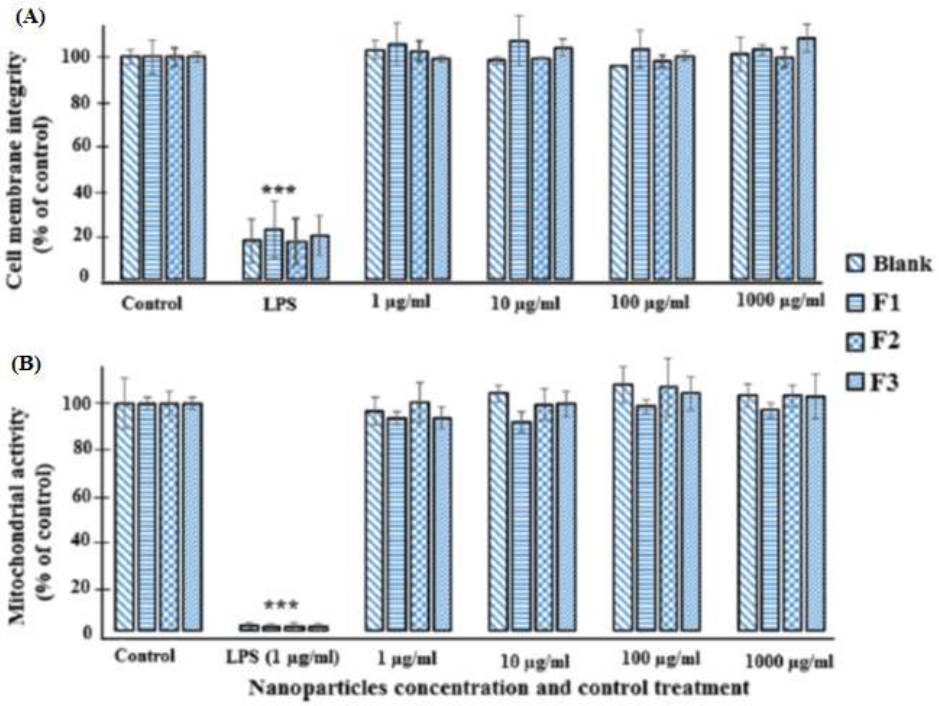

Figure 4- 8 (A) Percent Raw cell membrane integrity (% control) treated with the different NPs formulations Blank (pattern fill, downward diagonal), F1 (pattern fill, dark horizontal), F2 (pattern fill, sphere), and F3 (pattern fill, dark upward diagonal) respectively (n=3).*P<0.05 vs media, **P<0.01 vs media, ***P<0.001 vs media. (B) Percent Raw cell mitochondrial activity (% control) treated with different NPs formulations Blank (pattern fill, downward diagonal), F1 (pattern fill, dark horizontal), F2 (pattern fill, sphere), and F3 (pattern fill, dark upward diagonal), respectively, (n=3).*P<0.05 vsmedia, **P<0.01 vs media, ***P<0.001 vs media control. Error bars represent the standard deviation.

4.3.11 Assessment of NO Production

Figure 4-9 shows the nitric oxide released from the cell. The NPs are tested for their potential action in inducing cellular NO production, which is considered as a sensitive biomarker for pro-inflammatory response associated to macrophage activation. The secretion of NO by RAW 264.7 cells in the supernatant culture medium is quantified, by measuring nitrites accumulation. As shown in Figure 4-9, in the absence of a stimulator the basal levels of nitrites in RAW 264.7 cells

are 7.4-8.27 µM. In response to 24 hours stimulation by LPS, inducible NO Synthase (iNOS) is strongly induced in the macrophages as evidenced by the significant accumulation of nitrites in cell culture supernatant 22.54- 25.50 µM (Figure 4-9) compared to controls (untreated cells) *(P< 0.001).* For the four nanoformulations (F0, F1, F2, and F3), there are no significant effect on nitrite production compared to the basal level (Figure 4-9).

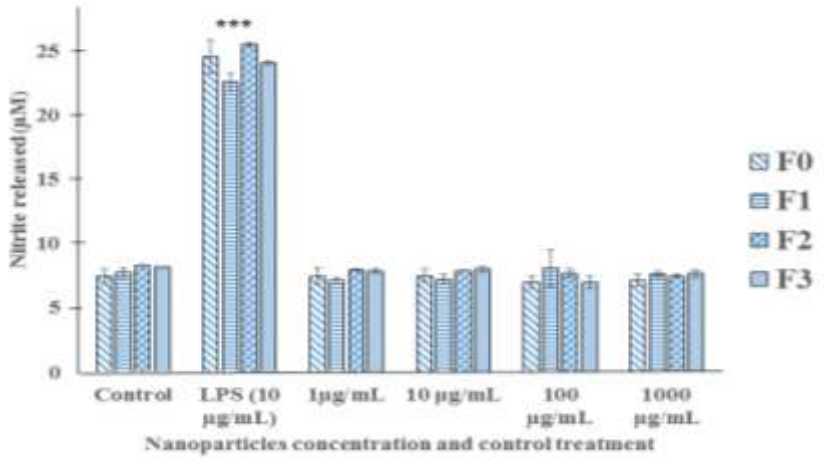

Figure 4- 9 Percent nitrite oxide release from raw when exposed to the different NPs formulation B Blank (pattern fill, downward diagonal), F1 (pattern fill, dark horizontal), F2 (pattern fill, sphere), and F3 (pattern fill, dark upward diagonal), respectively (n=3).*P<0.05 vs media, **P<0.01 vs media, ***P<0.001 vs media control. Error bars represent the standard deviation.

4.3.12 Multiplex Immunoassay Analysis of Cytokines Secretion

The release of selected cytokines is shown in Figure 4-10. The results indicate that in the absence of a stimulator (untreated cells) the basal level of cytokines IL-1α, IL-1β, IL-6 and IL-7 is the range of 0.70-5.28 pg/mL (Figure 4-10). As expected, LPS-stimulated macrophage highly produces cytokines *(P< 0.001)* compared to untreated cells as follows: IL-1α (12 fold), IL-1β (15 fold), IL-6 ($8x10^4$ fold), IL-7 (1.5 fold) as shown in (Figure 4-10). For the four nanoformulations (F0, F1, F2, and F3), there are no significant production of cytokines compared to the basal level.

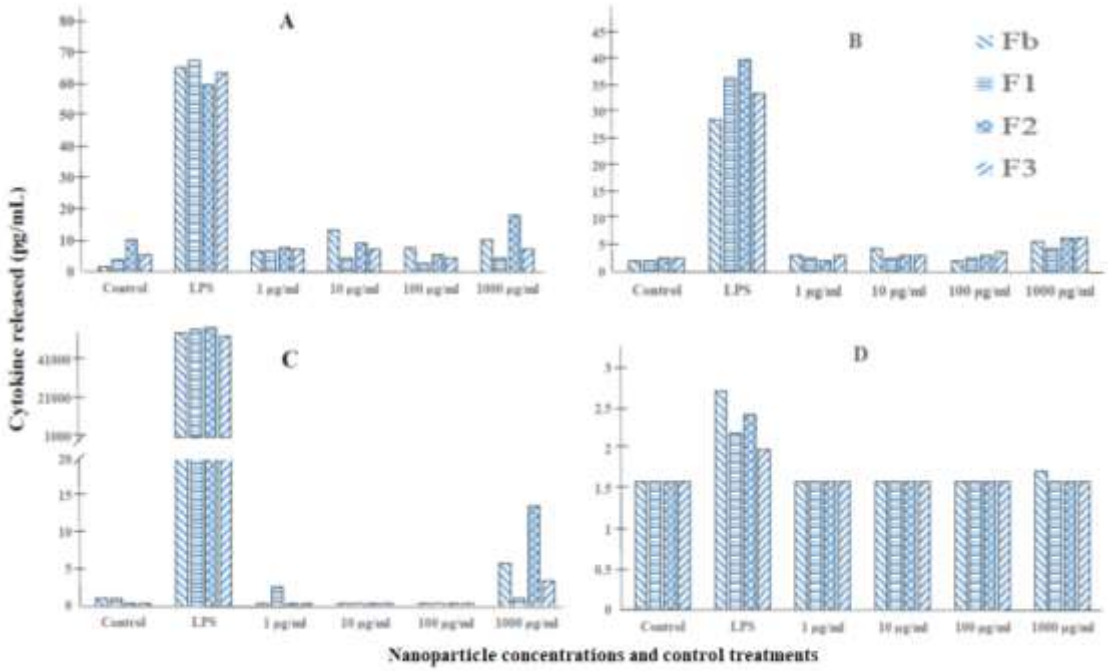

Figure 4- 10 Percent cytokine/interleukin (IL) (A, B, C and D) release respectively for IL-1α, IL-1β, IL-6 andIL-7 frommacrophage after exposure to the differentNPs formulations B Blank (pattern fill, downward diagonal), F1 (pattern fill, dark horizontal), F2 (pattern fill, sphere), and F3 (pattern fill, dark upward diagonal), respectively,(n=2).

4.4 Discussion

In this study, sodium acetate (SA) is successfully used to coat chitosan NPs for improved physico-chemical properties. After a thorough, and initial screening, the following unique and novel process is developped to *in situ* coat chitosan NPs with SA to overcome limitations of classical ionic gelation method in four steps. Each step of this preparation process of SA *in situ* coated chitosan NPs is indeed crucial for both the formation of chitosan NPs, and its successful coating by SA.

In the first step, the effective dissolution of chitosan and protonation of its amino groups occurs only in acidic environment (e.g. 2% v/v acetic acid aqueous solution, (pH~2.3-2.94, V =

20 mL, “see method section”) [123]. Therefore, SAA salt aqueous solution with a basic pH cannot not be used as an alternative solution to dissolve chitosan polymer.

The second step requires dropwise addition of sodium hydroxide aqueous solution to raise the pH of the chitosan aqueous solution to 4.76 which is the pKa value of acetic acid [124]. This enables a selective deprotonation of half glacial acetic acid and produces half acetate ion according to Henderson Hasselbach equation while [125] concomitantly increasing sufficiently the amount of sodium *cation* in the medium. The pKa value of amino acid groups of chitosan is ~6.3 [126]. Based on Henderson Hasselbalch equation, at pH= 4.76 the amino groups of chitosan polymer is still highly protonated.

The third step requires the decrease of the pH of the aqueous solution of TPP in the range of 5.5-5.99. This pH decrease avoids competitive binding between hydroxide ion (OH^-) and TPP, formed instantaneously after dissolution of Na_5TPP in deionized water(pH>9) [127] to protonated amino groups of chitosan, and also keeping full ionization of TPP for efficient ionic gelation. Triphosphoric acid, the acid form of the polyanion TPP can undergo as many as 5 dissociations, and therefore has 5 pKa values (pKa1= 1; pKa=2.2; pKa3 = 2.3; pKa4 = 3.7 and pKa = 8.5) [128]. That means, at pH = pKa4 +2 = 5.7, TPP is almost fully ionized based on Henderson Hasselbalch equation [129] and may crosslink with protonated amino group of chitosan polymer through electrostatic attraction. At this step of the process, the TPP aqueous solution or mixture with the drug (TFV) is also added dropwise into chitosan aqueous solution. The color of the solution changes from colorless to milky (Tyndall effect) indicating the instantaneously formation of the uncoated chitosan NPs through ionic gelation [130]. The EE % of TFV in uncoated chitosan NPs is indeed low before freeze-drying (Table 4-2). In fact, the highly water-soluble drug escapes the NPs compartment during the centrifugation favoring its concentration in the supernatant phase.

This limitation of the drug encapsulation is overcome by avoiding the centrifugation step [9] and by freezing the TFV loaded chitosan NPs suspension at (-20ºC,), as described in the above method section.

The fourth step is the *in situ* coating on the surface of chitosan NPs by SA during the freeze drying process. Indeed, on the phase temperature-composition diagram, the eutectic point of the binary systems comprised of water and acetic acid, is reached at -26.7ºC with 59% w/w acetic acid [131]. The triple point of water occurs at the pressure 6.12 mBar and at the temperature of 0.01ºC [132] and that of acetic acid occurs at the pressure of 12.7 mbar and a the temperature of 16.68ºC, respectively[133]. Thus, at the used freeze drying operating condition (pressure ~ 0.06 mBar, and temperature -48ºC) with ~2.1 % w/w acetic acid, below both the eutectic and triple points, any mixture of ice and acetic acid is solid [131] and are co-sublimated during the lyophilization process. There is a uniform and dense deposition of SA salt on the surface of the NPs (Figure. 4-3 D, E, and F). The *in situ* formation of SA is due to the electrostatic attraction between the negatively charged acetate *anion* from deprotonated acetic acid and the positively charged of sodium *cation* generated mostly from sodium hydroxide (2M). In fact, this electrostatic attraction between acetate and sodium ions follows Debye-Hűckel theory which states that, in a solution(e.g. before freezing the NPs suspension), near a given ion, counter ions are likely to be found and vice versa [134]. Thus acetate and sodium ions are found close to each other around chitosan NPs in the nanosuspension . In addition it is well documented that SA has a hydrotropic behavior in aqueous solution with CH_3, the hydrophobic part, oriented at the solution vapor interface and COO^-, the hydrophilic part, pointed toward the aqueous phase [135]. Upon freeze drying, the SA salt is spontaneously formed *in situ* through electrostatic attraction between acetate and sodium on the surface of chitosan NPs. This coating of SA onto chitosan NPs may be attributed to the dual intrinsic surface active and

efflorescent behaviours of SA. In fact water and acetic are sublimated during the freeze drying and SA migrates onto the porous chitosan NPs to form a coating. The dynamic of adsorption of SA onto chitosan NPs may also be enhanced by both the vacuum (low pressure and temperature) created during the freeze drying. There may be also the "shielding" attraction effect between uncoated chitosan NPs ($\zeta\sim > +$ 25 mv) and SA ($\zeta = -$ 4.87 ±0.64 mV). This new core-shell nanosystem has a core made of TFV loaded chitosan NPs, and the shell made of SA. There is a very visible, distinctive, uniform, and unique coating layer of SA on the surface of chitosan NPs (Figure 4- 3 D, E, and F.).

There are different crystal structure of monobasic acetic acid salt. For instance, sodium diacetate (SD) crystalizes in the cubic system (space group = Ia3)[136], whereas sodium acetate trihydrate (SAT) crystalizes in the monoclinic system (space group = $C^{2/C}$) [137]. . The relative intensities (I) of the two salts (SAA, SA) appear at the same double Bragg's angle (2Ɵ) as shown in (Figure 4-7 G and H). The angular positions of both SAA (Figure 4-7 G) and SA (Figure 4-7 H) of the diffracted beams which defined the shape and size of the unit cell are almost the same as shown in Figure 4-7 [138]. Thus, both SA and SAA are qualitatively identical as shown in Figure 4-7. The XRD results are also consistent with the FTIR and the TEM results strongly confirming the coating of the chitosan NPs with SA. Future crystallographic study will be performed to determine the space group and lattice parameters of SA.

These results are in agreement with the melting point data, used to assess the purity of the new salt. The melting point range of SA is almost identical to the melting point range of SAA (Table 4-3). These results are also consistent with the titration of SA with both PA and LM used as titrants (Table 4-3). Mc (SAA) is identical to Mc (SA). In addition, the titration curve of both SAA and SA almost overlaps (Figure 4-4). This suggests that the salt coating chitosan NPs is

indeed SA. The titration curve which does not have an inflexion point (Figure4- 4), suggesting that the salt does not contain any acetic acid.

Collectively, the FTIR, XRD, TEM, ζ, MP, and non-aqueous titration data indicate that, the shell coating chitosan NPs is indeed SA salt.

The SA salt coating chitosan NPs exhibits at least four potential advantages.

Firstly, it dramatically increases the EE% of TFV by 8-17 fold (Table 4-2). Indeed, there is less drug loss in the supernatant because, both the centrifugation for collection and washing of NPs steps are avoided respectively after the ionic gelation prior freeze-drying [9]. But, rather, the aqueous solution of acetic acid is leveraged for the efficient encapsulation of TFV. Indeed the *in situ* coating with SA, on the surface of chitosan NPs allows the efficient entrapment of TFV in the core chitosan NPs. In fact, chitosan NPs suspension is immediately frozen after the step 3 (Figure 4-1). The removal of both water and acetic acid by sublimation using the freeze drying technique prevents TFV to escape that time chitosan NPs. Concomitantly, during the freeze-drying, the intrinsic surface active and efflorescent properties of SA constraint TFV to remain and be mainly entrapped in the core chitosan NPs during the self-assembly of the core shell NPs as explained above.

In (Figure 4-6 J, K, and L), the FTIR spectrum for the three formulations shows only the spectrum of SA but not those of TFV. Therefore, TFV is mainly entrapped in the core of NPs. This result is also consistent with the XRD pattern (Figure 4-7 J, K, and L) showing only the pattern of SA. These results are consistent with the morphology analysis showing SA coating TFV loaded chitosan NPs (Figure 4-3 D, E and F).

Secondly, the coating prevents the aggregation of chitosan NPs [Figure 4- 3, Figure 4-11 B and Table 4-2 (PMD, PDI)], whereas there is a formation of a *"cake"* of the "blank" and the

three formulations (F1, F2, and F3) using the commonly ionic gelation process after freeze-drying (Figure 4-11 A) without any use of cryoprotectant in both processes.

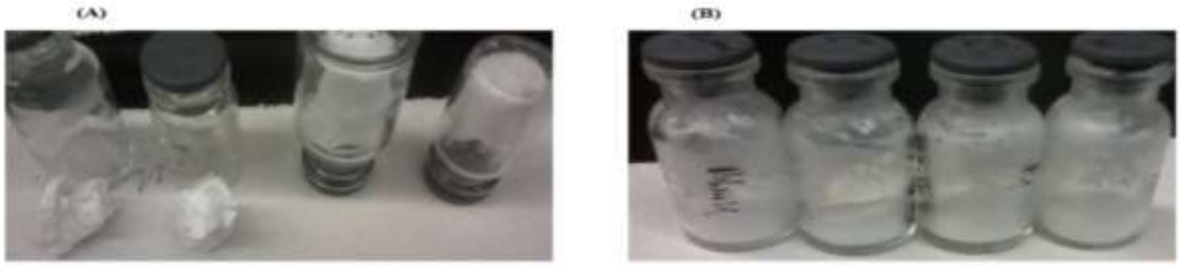

Figure 4- 11 Aggregation of chitosan NPs for "blank ", F1, F2, F3 formulation using the classical ionic gelation process after freeze drying respectively without use of cryoprotectant (A). It is noteworhty that SA coated chitosan NPs prevents their aggregation during freeze-drying process without also use of cryprotectant (B). (GIF 302 kb)

The non-aggregation of the core-shell NPs may be attribute to both the hydrotropic and efflorescent properties of SA, and the decrease of the surface tension between coated chitosan NPs which could be correlated to the decrease of the ζ by 9-20 fold compared to uncoated chitosan NPs formed a the step 3 of this specific process (Table 4-2). The PDI of the NPs is overall conserved after freeze-drying as shown in Table 4-2.

Using potassium hydroxide as an alternative base to neutralize acetic acid, there is also no "caking" of chitosan NPs after freeze-drying. Future study will be done in depth to clarify whether or not this process apply to different salts of carboxylic acid [109].

Thirdly, it exhibits sustained release of TFV as shown in Figure 4-5, thus avoiding burst release compared to the uncoated NPs.

It is counter intuitive that, there is a sustained release profile of free TFV solution extending over a period of 20–24 h. It is noteworthy that similar release profile was obtained with other drug solutions such as diclofenac solution (MW 296 Da) using a cellulose membrane (MWCO 12 kDa). In that study, the release period of solution of diclofenac was also extended over 24 h[139]. These observations may be attributed to the release rate limiting effect resulting from the interference of the dialysis bag membrane, which may slow down the drug diffusion towards the outer phase thus prolonging the time to reach drug concentration equilibrium on either side of the membrane. However, in the same condition and considering the dialysis membrane retardation effect, it clearly appears that the coated NPs exhibited a more sustained release kinetics compared to those of native drug solution and uncoated chitosan NPs for the same amount of drug in the media (~110 μg).

Based on Korsmeyer Peppa model, [117] the release mechanism is an anomalous transport with $0.61 \leq n \leq 0.86$, for the three different formulations (F1, F2 and F3) as shown in Table4-4. Therefore, the release of TFV from the chitosan NPS (core) followed a combination of both a fickian-controlled drug release and a swelling-controlled drug release [140] under continuous erosion of SA (shell structure). This erosion is relatively slow and time dependent. SA layer is still visible after 24 hours of incubation in the release media at 37ºC (Fig 4-3 E and F). The thickness of the coating layer can be controlled by acting on the initial concentration of glacial acetic acid aqueous solution and NaOH solutions. Thus, this finding can be potentially used to control and sustain or delay release of bioactive agent in the biological matrix.

Fourthly, it stabilizes the colloidal dispersion in aqueous media. Indeed, it is quite impossible to disperse any portion of the freeze dried un-coated chitosan-TPP "cake".
in deionized water whereas, the SA coated NPs can easily be dispersed in deionized water with no additional surfactant. The possible dispersion of the coated NPs might be explained by the surface

active and hydrotropic properties of SA [135] whereas the non-possible dispersion of the B cake might be explained by the very poor aqueous solubility properties of chitosan at pH 6 or above [141].

Based on International Organization for Standardization (ISO) ISO 10993-5 for cell viability, with 100 % viability assigned to the control, products with cell viability higher than 80% are not cytotoxic. Cytotoxicity level is classified as weak within 80%–60% ; moderate within 60%–40% and strong below 40% respectively [142]. Thus, under the current experimental conditions, LPS induces a strong cytotoxicity including, cell membrane damage (viability~19%) (Figure4-8A), and mitochondrial deficiency (viability~2%) (Figure 4-8B), associated high production of pro-inflammatory mediator NO (Figure 4-9) and cytokines IL-1α, IL-1β, IL-6 (Figure 4 -10). In contrast, SA coating chitosan NPs appears to be non-cytotoxic to the macrophages as the core-shell NPs do not impair the cell membrane integrity (viability ~100%) (Figure 4- 8A). In addition, the mitochondrial activity is maintained intact (viability ~ 100%) (Figure 4-8B). Moreover, the NPs do not neither induce a proinflammatory response associated to macrophage activation as reflected by a low level of both NO (Figure 4-9), and low level of cytokines production (Figure 4-10), which are comparable to the basal level. It is noteworthy that IL-7 has been reported to facilitate HIV transmission through sexual intercourse [143] Thus, this finding suggest that the NPs may not promote HIV infection which could support their potential as a drug delivery template for topical/vaginal microbicide.

4.5 Conclusion

This study demonstrated for the first time that sodium acetate (SA) can be used to uniformely coat *in situ* chitosan NPs during ionic gelation for improved physicochemical properties. The coated NPs exhibits higher encapsulation efficiency (86-93%) of water soluble drug such tenofovir. The release of TFV is sustained and the release mecanism is anomalous transport. This unique coating strikingly prevents the chitosan NPs aggregation during the freeze drying process. These NPs are non cytotoxic to the macrophage cell line.

The potential application of these findings are countless; this unique, edible, and highly reproducible coating salt may be potentially useful for, (i) masking the unpleasant taste, (ii) increasing the shelf-life by protecting against moisture, light and microbial growth (preservative), (iii) preventing enzymatic degradation or maintaining activity of proteomics and genomics derived bioactive agents(iv) controlling, sustaining or delaying release of bioactive agent in biological matrix, (v) improving solubility of poorly water soluble drug. Future study will be done to assess those properties.

CHAPTER 5.

IN-VITRO ASSESSMENT OF HUMAN ACID PHOSPHATASE TRIGGERING TENOFOVIR RELEASE FROM CHITOSAN/TPP NANOPARTICLES

5.1 Rationale

Vaginal route is a major route of infection to HIV (2), and studies from a population of monkeys showed that pre-exposure propyilaxis (PrEP), using topical tenofovir gel, had an effective protection 70 -100%[7]. Beside using topical gel as anti HIV/AIDS microbicide, polymeric nanoparticles are a promising topical delivery system, typically chitosan-based nanoparticle (Chitosan NPs) because chitosan NP is a mucoadhesive property in nature [9,8]. Chitosan is a polysaccharide copolymer and randomly distrbuted of D-glucosamine and N-acetyl-D-glucosamine[144]. In acdic environment, the amino moiety of chitosan protonates and crosslinks with the polyanion triphosphate (TPP) through intermolecular and intramolecular crosslinking leading to a formation a chitosan based nanoparticle (NPs). Chitosan NPs is widely used as a carrier[145], for topical drug delivery due its intrinsic mucoadhesive properties [9].

TPP, the crosslinker of this carrier, is itself a substrate of human prostatic acid phosphatase (hPAP) [11]. Cellular human acid phosphatase (chPAP) and secreted human prostatic acid phosphatase (shPAP), (100kDa glycoprotein holding two subunits of approximately 50 kDa each), are the two forms of hPAP. [18].The amount of human prostatic acid phosphatase produced by the epithelial cell of the prostate gland varied from 195 U/mL to 1428 U/mL of first portion semen ejaculated and from 57 U/mL to 241 U/mL in the second portion semen ejaculated[21]. Such amount of enzyme could be used to trigger the release of microbicides upon ejaculation into the vaginal tract and thereby controling the release of these HIV's microbicides loaded Chitosan-TPP nanoparticles. However, the intramolecular and intermolecular crosslinling during the formation

of chitosan NPs can lead to chemical steric hindrance. Therefore it is paramount important to pinpoint the hPAP responsive chitosan NPs resulting in significant release of the anti HIV/AIDS microbicide.

Tenofovir (TFV) is a reverse transcriptase enzyme inhibitor and is used for the treatment of HIV/AIDS[15]. TFV is used as a model anti HIV/AIDS microbicide and is a biopharmacetic classification system (BCS) class 3 drug due its high aqueous solubility and low permeability[145].

We hypothesize that hPAP responsive chitosan NPs can be engineered by optimizing chitosan NPs formulation independent variables. This hypothesis is tested with physico-chemical characterization of chitosan NPs (e.g. percent encapsulation efficiency (%EE), particle mean diameter (PMD), percent drug release) fourier transform infra-red (FTIR), powder X-ray diffraction analysis (pXRD), and transmission electron microscopic (TEM). The optimal formulation, which releases significant amount of TFV in the presence of hPAP, cytoxocity assessment on vaginal epithelial VK2/E6E7 is assessed by MTS assay. The unknown hPAP michaelis menten constant (kM) and velocity Vmax on TPP used as substrate are determined.

5.2 Material and Methods

5.2.1 Material

Chitosan, high molecular weight, deacetylated degree>75% , L-ascorbic acid (AsA), potassium antimonyl tartrate trihydrate (AT),ammonium molybdate tetrahydrate (AM), acetic acid reagent sodium acetate, and tris[hydroxymethyl]aminomethane (tris) are purchased from Sigma Aldrich (St. Louis, Missouri, USA). Pentasodium triphosphate (TPP), Sodium phosphate dibasic, hydrochloridric acid and glacial acetic acid reagent are purchased from Fisher Scientific (Fair Lawn, New Jersey, USA). Human Prostatic Acid Phosphatase hPAP (E.C.3.1.3.2) are purchased from Lee Bio solution (St Louis, Missouri, USA). Tenofovir (TFV) is purchased from Pichemicals

(Zhang Jiang HiTech Park, Shangai, China). All chemicals used in the study were of analytical grade and used as received without further purification.

5.2.2 Preparation of Chitosan-TPP Nanoparticles

Chitosan NPs is prepared according to our previous publication [145]. Briefly, chitosan is dissolved in 20 mL of glacial acetic acid aqueous solution for 24 hours. Then, the pH is raised to 4.76 with 2 M NaOH aqueous solution. Secondly, 4 mL of a mixture of different concentration of pentasodium phosphate (TPP) and 5 mg of TFV is added dropwised into chitosan aqueous solution under continuous magnetic stirring. The pH of TPP/TFV mixture is adjusted to approximately 5.3-6.0 with few drops of 2M HCl. Chitosan NPs is spontaneously formed through intramolecular and intermolecular interactions[145]. After 4 hours of continuous stirring, the nanosuspension is straightforward frozen using liquid nitrogen and subsequently freeze-dried using freeze dried using the freeze dryer Freezone model (Labconco Corporation, Kansas City, Missouri, USA). Five different formulations are designed as shown in the table 5-1 below along with their respective blank formulations (B, no TFV).

Table 5- 1 Formulation independent variables and physical mixtures

Physical										
	P1		P2		P3		P4		P5	
Chitosan amount (mg)	30		30		70		70		50	
Sodium triphosphate pentenbasic amount (mg)	14		6		14		14		10	
Tenofovir (mg)	5		5		5		5		5	
Formulation										
	B1	F1	B2	F2	B3	F3	B4	F4	B5	F5
Chitosan concentration (mg/mL) (20 mL, pH = 4.76) [a]	1.5	1.5	1.5	1.5	3.5	3.5	3.5	3.5	2.5	2.5
Acetic acid concentration (% v/v)	1.3	1.3	2.3	2.3	1.3	1.3	2.3	2.3	1.8	1.8
Pentaphosphate (TPP) concentration (mg/mL) (V= 4mL, p	3.5	3.5	1.5	1.5	1.5	1.5	3.5	3.5	2.5	2.5
Tenofovir amount (mg)	0	5	0	5	0	5		5		5
[a] pH raised to 4.76 with sodium hydroxide aqueous solution (2M)										
[b] pH decreased with few drops of hydrochloridric acid aqueous solution (2M)										

5.2.3 Particle size and zeta potential measurement

Fresh Chitosan NPs are dispersed by sonication (Qsonica LLC, Newtown, CT, USA) after ionic gelation process and centrifugation in deionized water. chitosan NPs after freeze drying are straight forwardly dispersed in deionized water. Particle size expressed as particle mean diameters (PMD), and polydispersity index (PDI) are measured through dynamic light scattering (Zetasizer Nano ZS, Malvern Instruments Ltd, Worcestershire, UK) at the temperature of 25°C. Samples with PDI<0.05, are considered monodispersed according to the National Institute of Standards [145]. The zeta potential (ζ)of chitosan NPs before and after freeze drying suspended in deionized water is determined by the zeta potential analysis mode of the instrument. Nanosphere™ size standard

(59±2.5 nm) and zeta potential standard (68±6.8 mV) are used to calibrate the instrument before the size and ζ analysis.

5.2.4 Encapsulation Efficiency (EE %) Determinations

EE% Determination of Chitosan NPs before freeze drying. The final amount of TFV entrapped into fresh engineered chitosan NPs after centrifugation is calculated from the difference between the total amount of TFV initially used and the amount of drug found in the supernatant after encapsulation process. The free drug amount in the supernatant is determined using UV spectrophotometer (Spectronic Genesys 10 Bio, Thermo Electron Corporation, WI, USA) at a wavelengthof 260 nm. The drug EE% is calculated as follow:

$$EE\ \% = \frac{Total\ amount\ of\ TFV - free\ amount of\ TFV}{Total\ amount\ of\ TFV} * 100 \quad (5\text{-}1)$$

The amount of TFV encapsulated in freeze-dried chitosan NPs after freeze-drying, is measured at 260 nm using the above UV spectrophotometer. Briefly,1 mg/ml of different formulations(F1, F2, F3, F4 and F5), along with the appropriate blank are dissolved in 2 M HCl up to 23 h at room temperature and followed by 1 h of sonication to accelerate the dissolution of chitosan NPs using the sonicator (Qsonica LLC, Newtown, CT, USA)[145]. Then, the chitosan/TPP solutions are centrifuged (14, 000 rpm, 10°C) for 20 min using refrigerated microcentrifuge (VWR, Radnor, PA). Finally, the total amount of TFV is recorded at 260 nm along with the appropriate blank, used to setup the baseline. The drug EE % is calculated as follows:

$$EE\ \% = \frac{Amount\ of\ encapsulated\ TFV}{Total\ amount\ of\ TFV} * 100 \quad (5\text{-}2)$$

5.2.5 Raman Infrared (FTIR) Spectroscopy

The Raman infrared spectroscopy is used to obtain the infra-red spectra of chitosan NPs. Powdered samples are deposited on the crystal for analysis at room temperature. The spectra are obtained from 4000 to 400 cm^{-1} on a Digilab model FTS-14C Fourier transform spectrometer equipped with a Ge/CsI beamsplitter and a TGS detector at a resolution of 4 cm^{-1}.

Powder X-ray Diffractometry (PXRD)

The PXRD is performed to characterize the physical properties of chitosan NPs. The powder XRD scans are completed using a MiniFlex automated X-ray diffractometer (Rigaku, TheWoodlands, TX) at room temperature. Ni-filtered Cu Kalpha radiation is used at 30 kV and 15 mA. The diffraction angle is covered from $2\theta=5°$ to $2\theta=60°$ with a step size of 0.05 ° /step, and a count time of 2.5 s/step (effectively 1.1 ° /min for approximately 46 min/scan).

Transmission Electron Microscopy (TEM)

Chitosan NPs exhibiting significance drug released under the influence of human Prostatic acid phosphatase (hPAP) morphology is visualized with TEM. To get the specimens, the drops of chitosan NPs suspension are placed on a copper grid with a carbon support film and air-dried. The NPs are viewed under a scanning transmission electron microscope CM12 (FEI, Hillsboro, OR, USA) at 80 kV accelerating voltage. Digital images are acquired with an ORIUSTM SC 1000 11 Megapixel CCD camera (Gatan, Pleasanton, CA, USA).

Phosphate Assays

Principle

Under acidic medium, orthophosphate ion (PO_4^{3-}) formed a complex with ammonium molybdate. This antimony phosphomolydate complex is reduced with ascorbic acid to form a blue

complex which absorbed light at 860 nm [146-147]. In this process, Antimony tartrate is used as a catalyst[148]. The absorbance is proportional to the concentration of orthophosphate in the sample. The reduction to the blue color is achieved by addition of 0.2 mL of 1% w/v ascorbic acid[11]. Four different calibration curves are plotted to determine the amount of orhophosphate released for each different pH value due to the pH dependency of the rate of the bue color development. A series of 6 different concentrations (4.73 µg/mL, 9.46 µg/mL, 18.93µg/mL, 28.29µg/mL, 37.86 µg/mL and 47.32µg/mL) of Sodium phosphate dibasic (2mL) dissolved in buffer at the appropriate pH value (3.72, 4.85, 5.85 and 7.51) were used to plot the calibration curve. An appropriate blank is used along each experiment, and after the full color development, 1 hour for pH 3.72; 2 hours for pH 4.85 and 18 hours for pH 5.85, in 2.72 M acetate buffer the absorbance is read at 860 nm. For pH 7.51 in 9.1mM Tris-HCl buffer, the absorbance was read in 1 h after full color development. The addition of 0.2 mL of hPAP to the Tris-HCl buffer does not change the pH whereas, the addition of acid ascorbic changed the pH to an acidic pH. Thereby the acidic pH allowed the development of the blue color.

At pH 3.72; pH 4.85; pH5.85 and pH 7.51, the standard curves are $y = 0.096 x$ ($R^2 = 0.995$); $y = 0.053x$ ($R^2 = 0.997$); $y = 0.032x$ ($R^2 = 0.997$) and $y = 0.0061x - 0.0055$ ($R^2 = 0.994$), respectively

Where y = absorbance and x = concentration of orthophosphate

Orthophosphate reduction by AsA resulting from the hydrolysis of TPP by hPAP is monitored over a time period of 1 h (pH 3.72, pH 7.51), 2 h (pH 4.85), 18 h (pH 5.85)..The amount of orthophosphate is determined using each corresponding above calibration.

5.2.6 Human prostatic acid phosphatase Activity Assay

A set of 5 different concentrations of TPP (used as hPAP substrate) aqueous solution (2 mL), respectively, 14.71 µg/mL, 29.43µg/mL, 44.14µg/mL, 58.86µg/mL, 73.57µg/mL, are dissolved in a 15 mL tube containing the above acetate or Tris-HCl buffer solution. Then, TPP are incubated at 37 °C , in a water bath (Circulating water bath, thermo electron corporation, Marietta, Ohio), with the hPAP enzyme (2µg/mL, 0.2mL, hPAP is initially dissolved in deionized water). After 10 min of incubation [149] at 37ºC, the reaction is quenched by the addition Of 0.5mL of 1.5% w/v ammonium molybdate [11] and 0.1mL of 3%w/v antimony tartrate. The reaction rate (velocity) is the amount of orthophosphate concentration per unit time (min^{-1}) resulting from TPP hydrolysis by hPAP. The linear Lineweaver-Burk plot is used for the determination of Km and Vmax [150]. as follows:

$$1/v = (Km /Vmax) *1/[S] + 1/Vmax \quad (5\text{-}3)$$

Where, v is the reaction rate (velocity) and [S] is the initial substrate (TPP) concentration. The slope of this plot is (Km /Vmax) and the y-intercept is 1/Vmax.

5.2.7 *In Vitro* Drug Release Study

The amount of 1.5 00 mg, of each corresponding the formulation is suspended in 0.5 ml of Tris–HCl buffer (9.1 mM, pH=7.51). Then 0.5 ml of hPAP (100 U/mL) is added to the nanosuspension. For each control, the equivalent formulation is added to 1 ml of the above Tris-HCL without addition of hPAP. These environments mimic the pH condition of the mixture of human seminal fluid and human vaginal fluid (HVF), and that of HVF alone, respectively [145]. These nano suspensions are placed into a cellulose ester membrane dialysis bag (Spectra/Por® Float-A-Lyzer G2, MWCO 8–10 k`D, Spectrum Laboratories Inc. (Rancho Dominguze, CA, USA). The dialysis bag is then dipped into a tube of 50 ml total capacity containing 10 ml of Tris

H-Cl buffer. The whole system is incubated in a thermostatically controlled shaking (50 rpm) water bath (BS-06, Lab Companion,Seoul, Korea) at 37°C. At a set time intervals (0, 1, 2, 3, 6, 9, 24, 48, 72 h), 1 ml of the buffer solution outside the dialysis bag is removed and replaced by fresh buffer solution to maintain a sink condition. The concentration of the drug released from the NPs in the outer tube solution is determined by a US spectrophotometer at 260 nm as indicated in the EE% determination section. Each experiment is run in triplicate. In addition, the release curve is fitted with Korsmeyer-Peppas model [117] to elucidate the release mechanism of TFV from the NPs, using the following equation;

$$\frac{M_t}{M_\infty} = at^n \quad (5\text{-}4)$$

where, $\frac{M_t}{M_\infty}$ represents the fractional drug release, "a" is a constant combining structural and geometric features of the drug dosage form, and n characterizes the release mechanism (e.g., fickian diffusion (n=0.5); anomalous diffusion (0.5<n<1.0; case II transport (n=1) and super case II transport (n>1). For the determination of n, only the portion of $\frac{M_t}{M_\infty}$ <6, should be used[117].

The dissolution profile of each formulation under the influence of hPAP and its corresponding control are compared using the difference factor (f_1) and the similarity factor (f_2) expressed below [151]:

$$f_1 = \left(\frac{\sum_{t=1}^{n}|R_t - T_t|}{\sum_{t=1}^{n} R_t}\right) * 100 \quad (5\text{-}5)$$

$$f_2 = 50 * \log_{10}\left[\frac{100}{\sqrt{1+\frac{\sum_{t=1}^{n}(R_t - T_t)^2}{n}}}\right] \quad (5\text{-}6)$$

Where, n is the number of time points, R_t is the mean dissolution value for the reference product (e.g. TFV release from chitosan NPs without the influence of hPAP) and T_t is the mean

dissolution value for the test product (e.g. TFV release from chitosan NPs under the influence of chitosan NPs). In general, a f_1 value less than 15 and a f_2 value greater than 50 indicate sameness or equivalence in release profile [151].

5.2.8 VK2/E6E7 Culture

These cells are grown and maintained in a monolayer culture, in 75 cm2 culture flasks (Techno Plastic Product, Switzerland), at 37°C in a humidified atmosphere of 5% carbon dioxide (CO2) and 95% air. The complete growth media is made of Keratinocyte-Serum Free medium with 0.1 ng/mL human recombinant EGF, 0.05 mg/mL bovine pituitary extract and additional calcium chloride (0.4 mM, final concentration)

Exposure Protocol

The NPs are freshly suspended in the above complete growth culture media at 1000 μg/ml, dispersed by sonication (VWR, model 150 D; VWR International, West Chester, PA, USA) for 10 min, sterilized for 30 min under UV light [145], and diluted 1:1,1:10, 1:100 and 1:1000. The vaginal epithelial cell VK2/E6E7 (2×10^5 cells/100 μL/well) are seeded in 96-well culture plates (growth surface: 0.34 cm2) and incubated for 48 h. Then, the cells are subjected for 24 h to the NPs at 1, 10, 100 and 1000 μg/ml corresponding to 0.3, 3, 30 and 300 μg/cm2, respectively. Wells containing cells without NPs are used as the negative controls. As a positive control, the Cells treated with lipopolysaccharide (LPS, 10 μg/ml) are used as the positive control. LPS is a well-known activator of toll-like receptors, to stimulate an inflammation

5.2.9 MTS Assay

Cell proliferation level is determined by MTS assay. Viable cells bio-reduce MTS compound mix with PMS (cellTiter 96® AQ_{ueous}) into formazan[152]. After exposure to NPs/blank formulations, the old media containing cells is discarded, replaced with 100 µL of fresh media, and equilibrated for 30 min at 37ºC. Then, 20µL cellTiter 96® AQ_{ueous} (Promega, Madison, WI, USA) is added to each well and incubated for 1 hour. The absorbance is read at 450 nm using a DTX 880 multimode microplate reader (Beckman Coulter, Brea, CA, USA).

$$Viability\ (\%) = \frac{aborbance\ (test)}{absorbance\ (control)} x100 \qquad (5\text{-}7)$$

Where absorbance (test) and absorbance (control) denote the amount of formazan

5.2.10 Statistical Analysis

All values were expressed as mean ± standard deviations. One way analysis of variance (ANOVA) in combination with Tukey ‘s HSD (Honestly Significant Difference) post- test were used to find means of data that are significantly different from each other. All statistical analysis was carried out using JMP10, SAS Institute, Cary, North Carolina, USA)., and each experiment was triplicated.

5.3 Results

5.3.1 Particle Size, Zeta Potential, %EE and PDI

Figure 5-1 shows the particle size distribution of the optimal formulation. In general, the size of the freeze dried chitosan NPs ranges 129.1-249.4 nm except for the formulation F3 and B3 where there is a dramatic change of the freeze dried chitosan NPs. All the nanoformualtions exhibit an increase in drug %EE and decrease in zeta potential. The particle size, %EE, zeta potential and PDI are shown in table 5-2.

Table 5- 2 Particle size distribution, zeta potential, polydispersity index and percent encapsulation efficiency of nanoparticle

	Formulation									
	B1	F1	B2	F2	B3	F3	B4	F4	B5	F5
Size (nm) [a]	161.7±1.6	130.8±0.9	187.2±2.8	173.7±0.6	233.7±15.3	225.2±7.6	173.3±8.6	164.8±1.6	142.4±3.3	150.3±5.8
Size (nm) [b]	204.3±29.6	149.9.7±0.2	152.5±28.3	190.4±3.0	7250.3±1268.5	8924.7±799.8	144.5±56.7	249.4±44	129.1±27	158.2±49.4
%EE [a]	-	6.8±0.7	-	5.1±2.1	-	5.5±2.3	-	4.2±1.9	-	5.9±0.5
%EE[b]	-	93.7±4.4	-	90.6±1.1	-	92.4±1.6	-	89.3±1.5	-	86.3±2
Z (mV) [a]	21.3±0.5	22.2±0.3	30.5±0.8	31.1±0.3	35.2±0.7	36.0±1.1	30.6±1.4	30.8±2.2	32.6±2.3	30.8±0.8
Z (mV)[b]	4.2±0.5	4.4±0.2	9.3±0.5	11.0±1.9	11.2±8	23.3±8.5	6.8±1.1	8.0±1.2	6.9±2.6	11.7±2.2
PDI [a]	0.2	0.2	0.4	0.4	0.6	0.4	0.4	0.4	0.4	0.4
PDI [b]	0.3	0.3	0.3	0.3	1.0	1.0	0.3	0.3	0.3	0.3

[a] data before freeze drying
[b] data after freeze drying

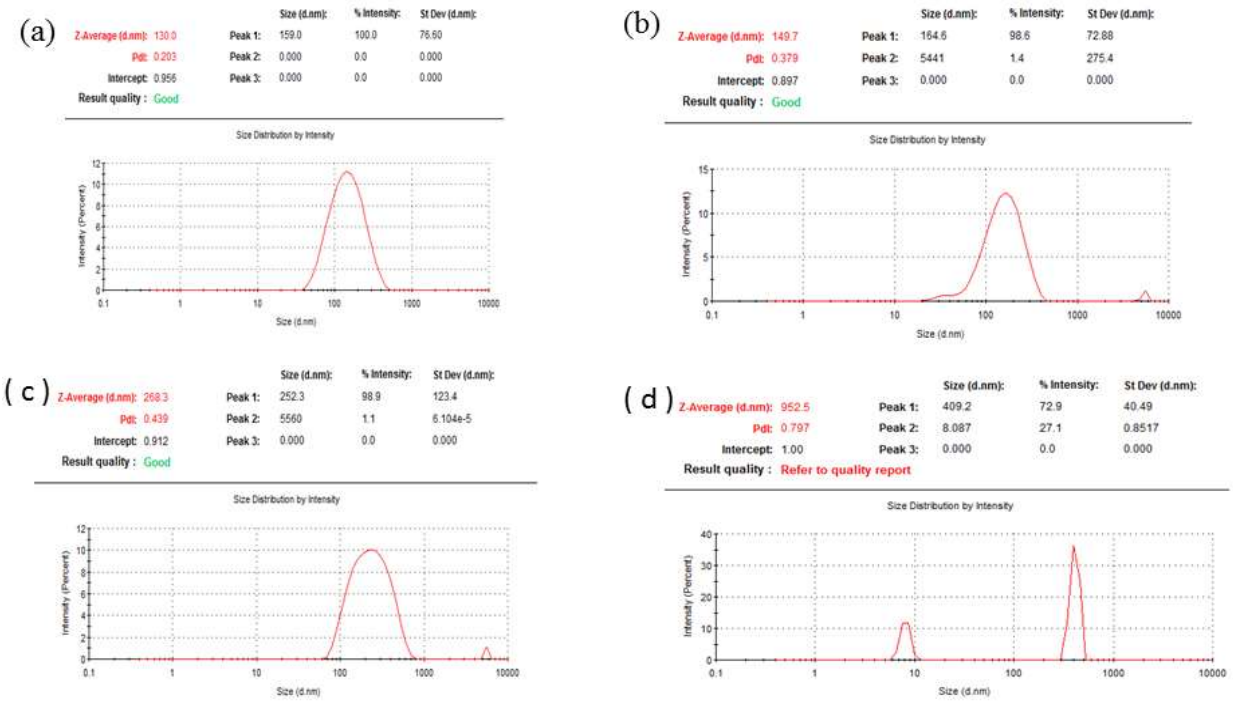

Figure 5 - 1 Particle size distribution of chitosan NPs (Formulation F1) prior freeze drying (a) and after freeze drying with no incubation at 37ºC (b), freeze dried chitosan NPs incubated at 37ºC for 6 h without addition of human prostatic acid phosphatase (hPAP) (c) and freeze dried chitosan chitosan NPs incubated with hPAP for 6h at 37ºC, respectively.

5.3.2 Fourier Transform Infra red analysis

Figure 5-2 shows the FTIR spectrum of th different formulation. Unlike the physical mixture, all the formulations F1-F5 exhibit identical IR spectrum, and show the formation of SA *in situ* formed during the preparation process of chitosan NPs. The composition of P1-P5 and F1-F5 are given in **table 5-1.**

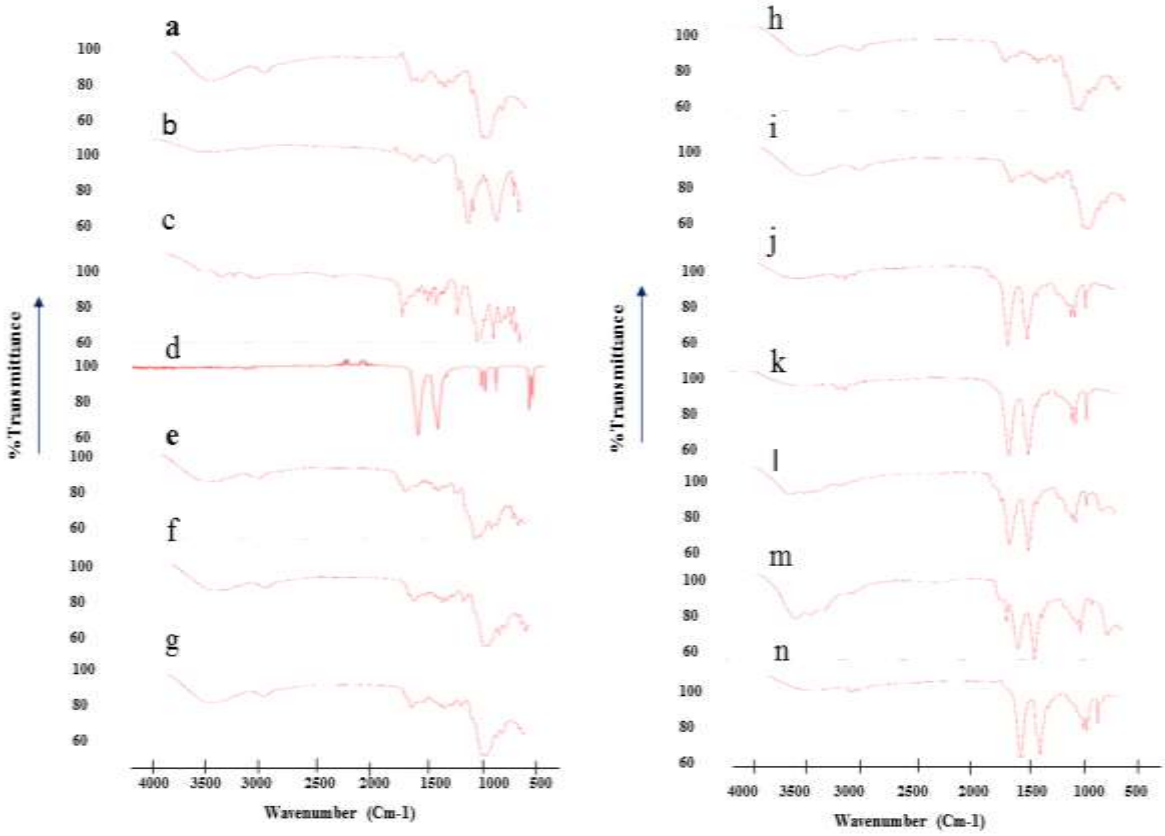

Figure 5 - 2 IR analysis of chitosan (a), sodium triphosphate pentabasic (b), tenofovir (c), sodium acetate (d), physical mixture p1 (e), physical mixture p2 (f), physical mixture p3 (g), physical mixture p4 (h), physical mixture p5 (i), formulation F1 (j), formulation F2 (k), formulation F3 (l), formulation4 (m) and formulation F5 (n), respectively

5.3.3 Powder X-Ray Analysis

Figure 5-3 shows the p-XRD spectrums of all the formulation. These formualtions show that there is also formation of SA with a characteistic pic of SA at 2 theta equal 30ºC as shown in Figure 5-3 d, i-n.

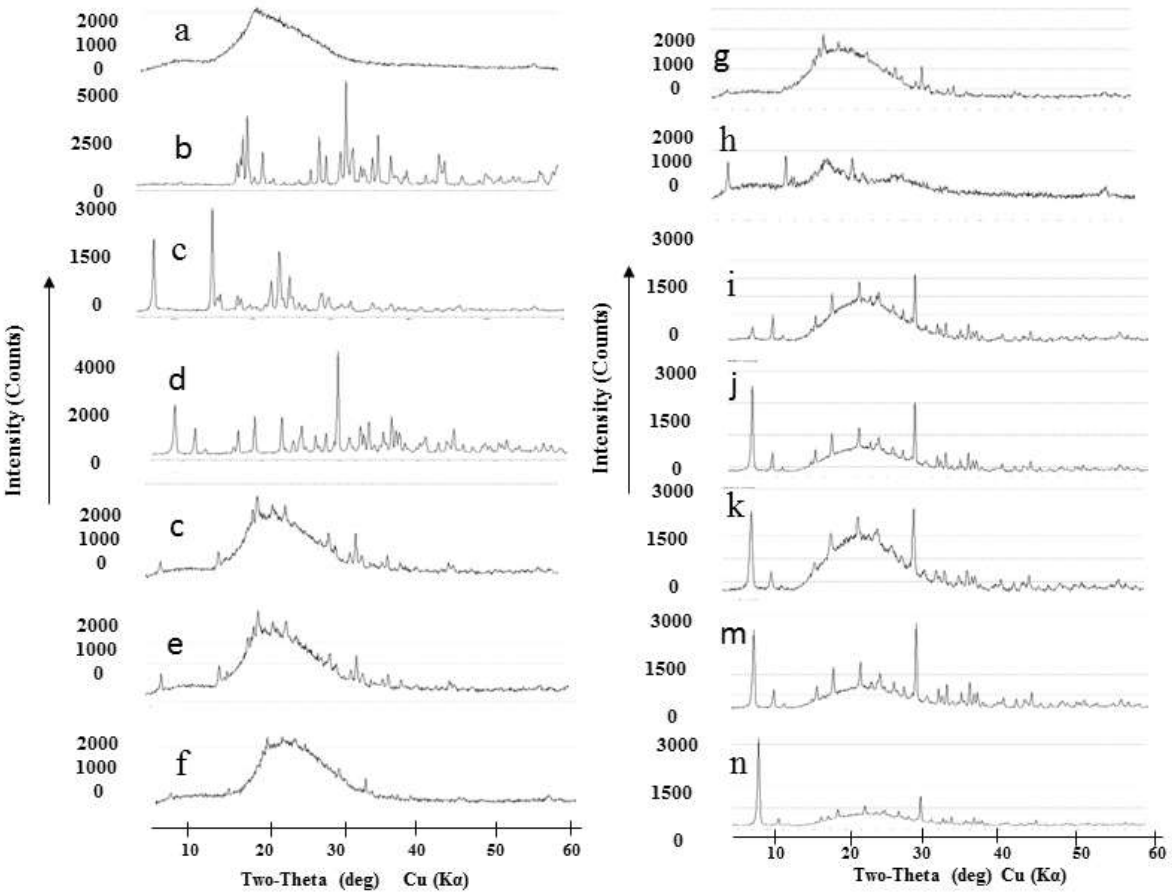

Figure 5 - 3 Pxrd pattern of chitosan (a), sodium triphosphate pentabasic (b), tenofovir (c), sodium acetate (d), physical mixture p1 (e), physical mixture p2 (f), physical mixture p3 (g), physical mixture p4 (h), physical mixture p5 (i), formulation F1 (j), formulation F2 (k), formulation F3 (l), formulation F4 (m) and formulation F5 (n), respectively.

5.3.4 Morphology Analysis

Figure 5-4 shows the morphological analysis of the optimal formulation F1. The shape of chitosan NPs are shepherical (figure 5-4 a-c). However the addition of hPAP on chitosan NPs shows a formulation with different shape as shown in figure 5-4 d.

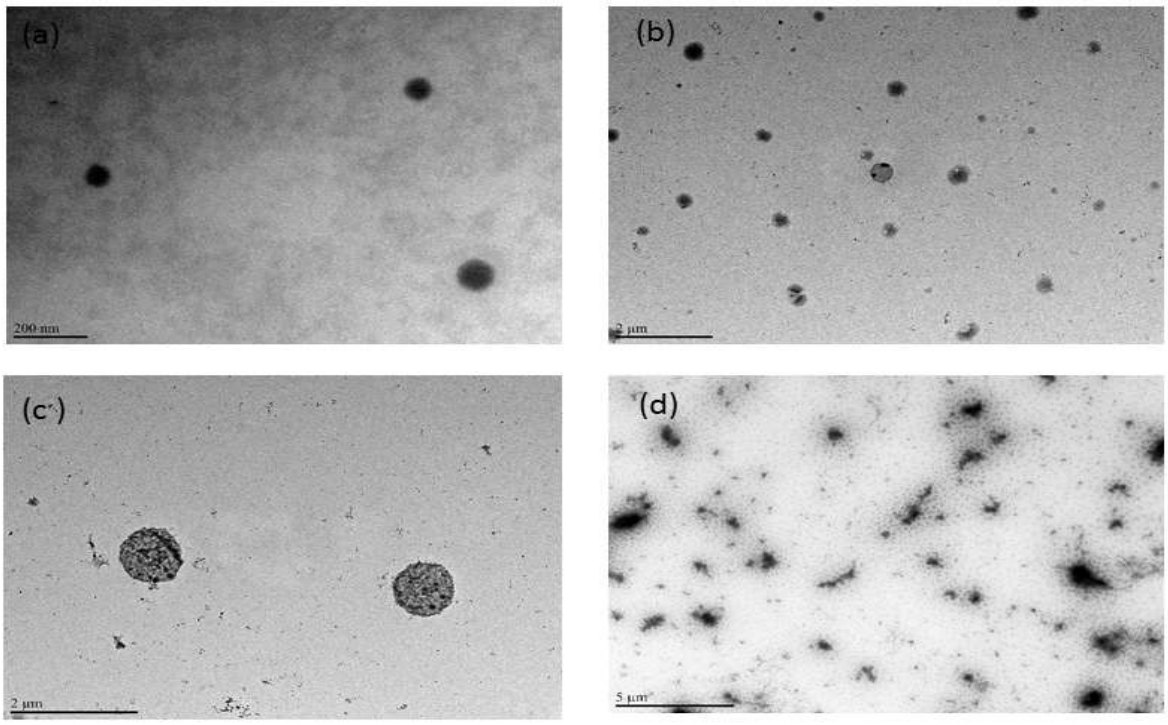

Figure 5 - 4Transmission electron micrographs (TEM) of chitosan NPs prior freezed drying(a) for formulation (F1) synthesized before freeze drying, F1 formulation without addition of human prostatic acid phosphatase (hPAP) nor incubation at 37ºC (b), F1 formulation incubated at 37ºC without addition of hPAP(c), and F1 formulation incubated at 37ºC with addition of hPAP (d) respectively. Scale bar represents 200 nm for (a) and 2000 nm for (b, c), and 5000 nm for (d) , respectively.

5.3.5 Michaelis constant Km and rate maximal Vmax

Figure 5-5 shows the velocity of hPAP vs pH. The maximal velocity is reached at pH 5.86. The michaelis menten constant at ph 3.72, 4.85, 5.85 and 7.51 are 0.012±0.012 mM, 0.385±0.065 mM, 0.506±0.198 mM, and 0.019 ±0.008 mM, respectively.

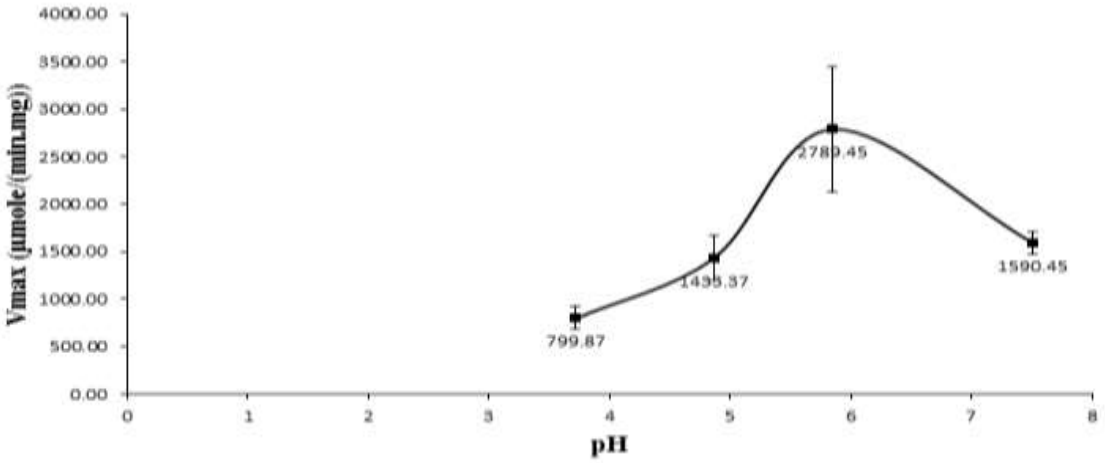

Figure 5 - 5 Activity of human prostatic acid phosphatase vs pH at T=37ºC. Error bars represent standard deviation.

5.3.6 In vitro drug release analysis

Figure 5.6 shows the release profile of the formulation F1 showing signanficant relatively to the controle under the influence of hPAP. The drug release of TFV under the influence of hPAP is significant woithin 6 hours.

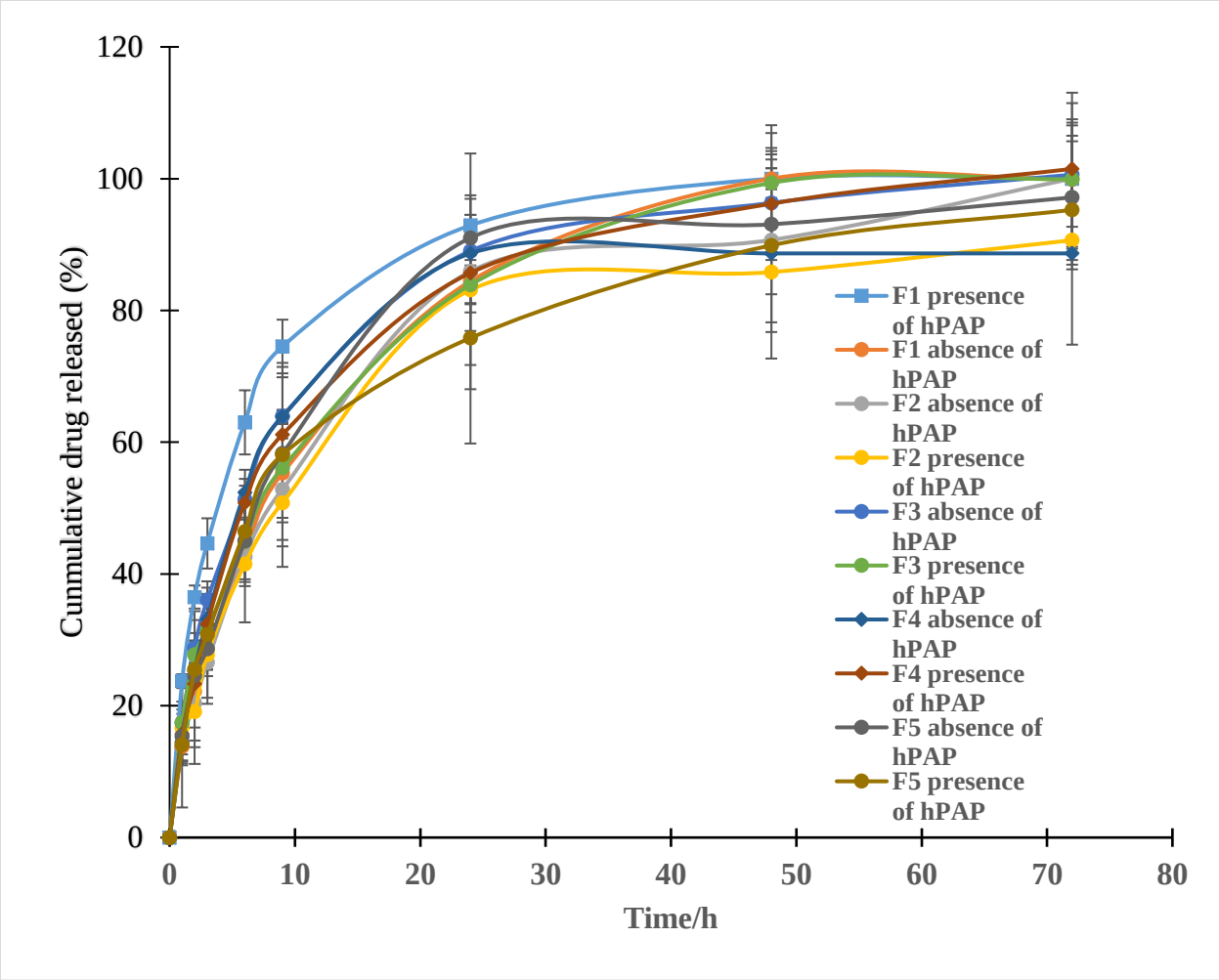

Figure 5 - 6 Release profile of chitosan NPs under/without the influence of human prostatic acid phosphatase for different formulation. Error bars represent the standard deviation.

Table 5-3 shows the release mechanism “n” for the 5 different formulaions. In addition, the the pairwise comparisons of the amount of drugs release within 6 hours in the presence or absence of hPAP are shown is table 5-3. The similarity factor (f1) and difference factor (f2) are used to validate the sameness or difference in drug percent release. From table 5-3, only F1 formulation exhibits a significant drug release in the presence of hPAP considering that f1=56.5 and f2=40.3, respectively.

Table 5- 3 Drug released mechanism "n", similarity factor (f1) and difference factor (f2) values

Formualtion	Drug released mechanism"n" value	Similarity factor (f1)	Difference factor (f2)
F1 absence of hPAP [c]	0.63 (R^2=0.998)	56.5	40.3
F1Presence of hPAP [d]	0.58 (R^2=0.997)		
F2 [c]	0.61 (R^2= 0.993)	8.6	77.1
F2 [d]	0.53 (R^2=0.939)		
F3 [c]	0.60 (R^2= 0.990)	9.0	71.1
F3 [d]	0.52 (R^2 = 0.986)		
F4 [c]	0.71 (R^2 = 0.997)	4.4	92.2
F4 [d]	0.66 (R^2 =0.997)		
F5 [c]	0.59 (R^2 =0.993)	5.2	90.8
F5 [d]	0.66 (R^2 =0.984)		

5.3.7 Cytotoxicity analysis

Figure 5-7 shows the cytotoxicity of formulation F1 and B1 on the vaginal epithelial cell line.

The formulation are non cytotoxic to the cells line

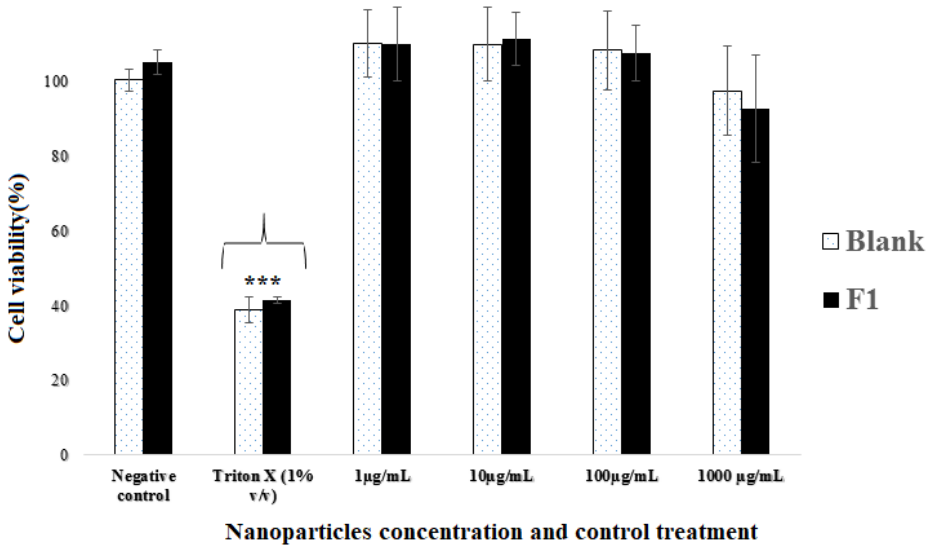

Figure 5 - 7 Percent VK2 E6E7 cell viability (% control) treated with B1 (pattern 5% fill) and F1 (solid fill black) respectively (n=3).*P<0.05 vs media, **P<0.01 vs media, ***P<0.001 vs media. Error bars represent the standard deviation.

5.4 Discussion

In this study, we investigated the effect of hPAP on chitosan NPs intended to trigger significantly the release of the anti-HIV microbicide in the presence of hPAP. The unknown Michaelis menten constant (Km) and velocity maximal of hPAP using TPP as a subtrate are also determined. In comparison to analogue acidic phosphatase, hPAP activity is affected by pH, substrate concentration, enzyme concentration[153]. At 37ºC, The maximum activity of hPAP using TPP as a subtrate, is attained in acid medium (pH=5.85) as shown in figure 5-5. This result is expected because acid phosphatase has a maximal acitivity in acid pH whereas alkaline phosphatase has a maximal pH in alkaline pH[154]. Even though, hPAP is an acid phosphatase, the activity observed in hydrolyzing TPP at neutral pH is very important for this study, as shown in figure 5-5. It is noteworthy that, male semen with alkaline pH has the propensity to neutralize the female vaginal fluid exhibiting an acidic pH[95]. Threfore, it is paramount important for the tiggerer to maintain as some extent an activity at neutral pH.

The freeze dried chitosan NPs particle mean diameter are in a nano-range in general except for formulation F3 and B3. The increase of the particle is due the high amount of chitosan and less amount aqueous solution of glacial acetic acid. It is well known that chitosan NPs usually aggregates during freeze drying. To overcome this undesirable properties either a cryoprotect such trehalose[114] can be used or a *in situ* formation of sodium acetate(SA)[145] can prevents the aggregation propensity of chitosan NPs. SA used as a cryprotectant and coating element exhibit several advantages in improving the physicoc chemical properties of chitosan NPs[145]. All the freeze dried chitosan NPs exhibit a high entrapment efficiciency as shown in table 5-2, because the TFV is *in situ* entrapped in chitosan NPs. In fact, the centrifugation process, during the preparation process of chitosan NPs, was avoided. This step is crucial to avoid the loss of the drug

in the supernatant. The release mechanism of all the formulaion are anomalous transport II conisdering that the drug release "n" value (0.5<n<1), as shown in table 5-3. Thus, the release of TFV from chitosan NPs is a synergic fickian and a swelling controlled TFV release from chitosan NPs[145]. Chitosan NPs exhibit a swelling behavior under the influence of the temperature as shown in figure 5-1 C with. The increase of chitosan NPs (F1) particle mean diameter from 131±0.9 nm to 306±55 nm (figure 5-1). In addition, the action of hPAP on chitosan Nps leads to the degradation of the nanoparticle as visuslized in **figure 5-4 d**.

It is notworthy that hPAP acts as a catalyst in hydrolyzing TPP. The gibbs free energy can be defined as:

$$\Delta G = \Delta H - T\Delta S \qquad (5.8)$$

Where, ΔG is the Gibbs free energy, ΔH is the enthalpy of reaction , ΔS is the entropy of reaction and T the temperature of the reaction.

If the value of ΔG is negative,the reaction can spontaneous. Such reaction is called exergonic. The change in free energy between the transitions state and and the substrate is called the Gibbs free energy of activation or the activation energy(.ΔG_a)

$$\Delta G_{a,unct} = \Delta G_{uncat} - \Delta G_s \qquad (5.9)$$

$$\Delta G_{a,cat} = \Delta G_{cat} - \Delta G_s \qquad (5.10)$$

In a typical hydrolysis reaction, as shown in eq. (5.8), the activation energy ($\Delta G_{a,cat}$) needed to hydrolyze TPP ($P_3O_{10}^{-5}$) into dipolyphospahte ($P_2O_4^{-4}$) and dihydrogen phophate ($H_2PO_4^-$) in the presence of hPAP will be less than its activation energy ($\Delta G_{a,uncat}$) in absence of enzyme.

$$(5N_a^+, P_3O_{10}^{-5}) + H_2O \leftrightarrows (4N_a^+,\ P_2O_4^{-4}) + (N_a^+, H_2PO_4^-) \qquad (5.9).$$

An approach of elucidating how hPAP catalyzed the hydrolisis of TPP can be explained as follows.

$$TPP \underset{}{\overset{k1}{\leftrightarrows}} \text{TPP-hPAP} \xrightarrow{k2} P, \qquad (5.10)$$

Where P is the product, V is the reaction velocity and k1 is reaction equilibrium constant and k2 the reaction rate constant.

A schematic representation of the activation energy of hPAP catalyzes the hydrolysis of TPP is shown in figure 5-8.

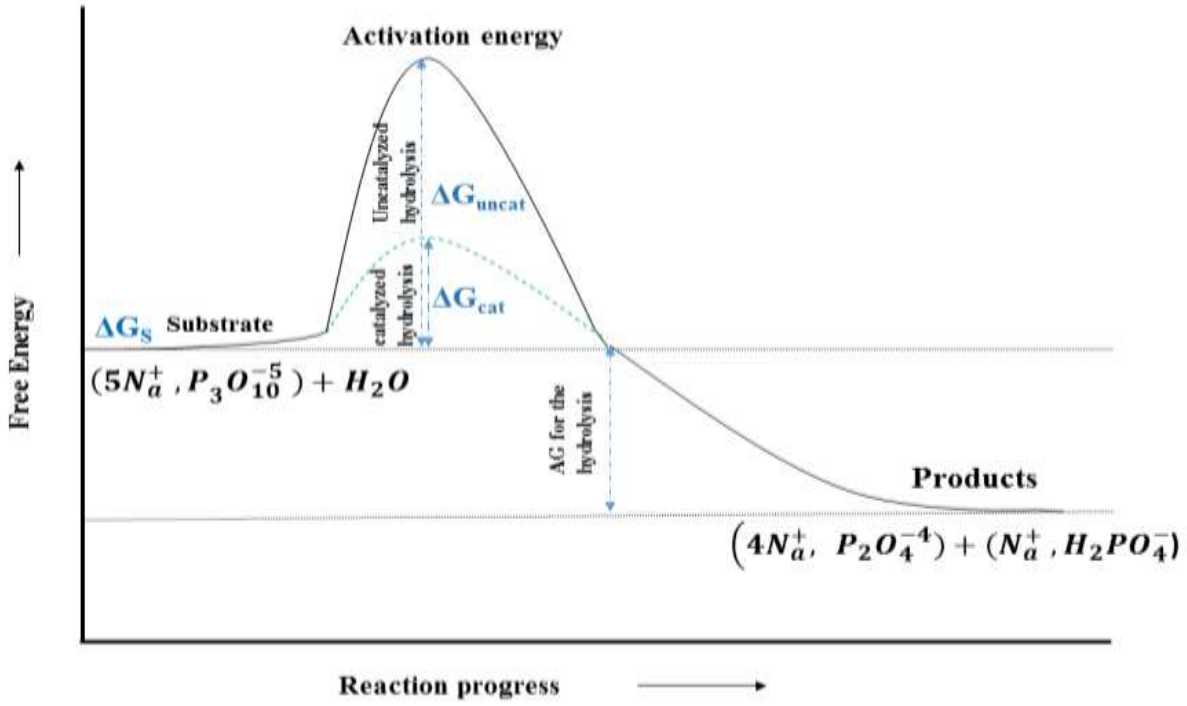

Figure 5 - 8 Schematic representation of the activation energy of tripolyphosphate in presence and absence of human prostatic acid phosphatase. Error bars represent the standard deviation.
The reaction velocity V can be written as follows

$$V = k2\,[TPP\text{-}hPAP] = \frac{kT}{h}[S]e^{\frac{-\Delta Ga}{RT}} \quad (5\text{-}11)$$

Where is the Balotsmann's constant and h is the Plank's constant.

Thus the rate of human prostati acid phosphatase catalyzes hydrolysis of TPP depends mainly on the activation energy.

$\Delta G_{a,cat}$ is less than $\Delta G_{a,uncat}$, therefore according to equation (5-11), the rate of hydrolysis of TPP under the influence of hPAP is greater than in absence of enzyme. The hydrolysis of TPP in chitosan NPs is evidenced by the degradation of chitosan NPs.

Combined swelling and degradation of Chitosan NPs (F1 formulation) exbibit different shape and a different population of NPs as shown in **figure 5-1 d** with an average higher polydispersivity index (0.7) relatively to the unincubated NPs with hPAP. This degradation of the chitosan NPs is materialized by the enhanced of TFV released from chitosan NPs as shown in figure 5-6. TPP has a dual property. It is used as the crosslink for chitosan NPs and as a substrate of hPAP for controlled released of TFV. The optimal formulation exhibiting higher drug release under the influence of hPAP within 6 hours (F1) as shown in figure 5-5. This formulation contains more enzyme substrate TPP, and less chitosan and SA. Thus, the steric hindrance might be less in this specific formulation and thereby allowing hPAP to hydrolyze TPP. The optimal chitosan NPs exhibiting significant release of TFV under the influence of hPAP is safe to the VK2 E6E7 cell line on based on International Organization for Standardization (ISO) ISO 10993-5 for cell viability[142].

5.5 Conclusion

A successful chitosan NPs sensitve to human prostatic acid phosphatase is engireered. At human physiological pH(7.4), triphosphate a substrate of hPAP is hydrolyzed suggesting that

hPAP maintains its activity at neutral pH. With no enzyme, the nanoparticle are spherical in nature and undergoes degradation in the presence of hPAP resulting in a significant drug released relatively to the control formulation. The entrapment efficiency of TFV in chitosan NPs is high (up to 90%) and the potential nanoformulation are safe to the vaginal epithelial cell line. This nanoformulation can be used as a topical vaginal anti- HIV microbicide for HIV/AIDS prevention.

CHAPTER 6

ENGINEERING FAST DISSOLVING SODIUM ACETATE MEDIATED DRUG CRYSTALLINE SOLID DISPERSION

(Adapted from Ngo et al International Journal of Pharmaceutics, 2018)

6.1 Rationale

In the drug development pipeline, nearly 90% of new active chemical entities are considered poorly water-soluble drugs based on the biopharmaceutics classification system (BCS) [155-156]. Hydrophobic drugs exhibit mostly crystalline structure. Those crystalline structures form tightly bonded atoms with high cohesive energy. In addition, hydrophobic drugs exhibit low aqueous solubility, poor absorption, limited dissolution and undesirable drug crystal size growth [157-161], resulting in low bioavailability and efficacy. These drugs are not suitable for intravenous (IV) administration because those poorly water-soluble solid aggregated drugs can potentially lead to thrombosis or stroke. The term solid dispersion in pharmaceutical formulation is defined as systems where the drug is finely dispersed in a carrier or excipient [162-165]. When the poorly water soluble drug is dispersed in a crystalline-carrier, amorphous-polymer-carrier, surfactant polymer carrier, and poorly water soluble -polymer carrier, the solid dispersion technique is called first, second, third and fourth generation solid dispersions, respectively[166]. In an amorphous solid dispersion (ASD), the hydrophobic drug is dispersed in an amorphous carrier [162, 167]. Classically, the ASD technique involves the dispersion the drug in amorphous polymeric matrix [158, 168-169]. In contrast to ASD, a crystalline solid dispersion (CSD) are systems where the carrier is crystalline not amorphous[162]. Sekiguchi and Obi, reported the first CSD where urea used as the carrier was blended with sulphathiazole following heating and fusion of the mixture above the eutectic point

and rapid cooling of the eutectic mixture [166, 170]. This latter process known as the *melting method* has the advantage of not using a solvent, however the fusion melting method exhibit several limitations. One limitation is the thermostability and physical degradation of the active pharmaceutical ingredient during the melting, crushing and milling of the resulting solid eutectic mass, respectively [166]. In addition, the dispersed drug has the propensity to rapidly crystallize when the carrier-drug mixture is not at the exact eutectic molar composition [166, 171]. A CSD system is a promising strategy to improve drugs bioavailability when they are, either, molecularly, amorphously or crystalline nanoparticulates dispersed in a highly water soluble carrier[172].There are three main methods for solid dispersion especially, the melting method, the solvent method and the melting/solvent method[166]. A *solvent method* involving freeze-drying technique (as implemented in this study) would potentially circumvent some of the limitations of the previous method because it involves less thermal degradation of the drugs [166, 173]. In addition, the technique proposed in this study is extremely desirable for CSD engineering because glacial acetic acid (AA, the solvent used as initial drug dissolution medium) is relatively non-toxic [174] and exhibits a high freezing point (FP) of 16. 68°C [145]. The high FP prevents the undesirable melting of the solvent during the freeze-drying process.

Sodium acetate (SA), is a well-known hydrotropic and a relatively safe chemical [135, 145]. The aqueous solution of SA is United States food and drugs administration (FDA) approved for intravenous (IV) infusion and mainly used to treat acidosis in patients [175-176]. The plasma concentration of sodium is in a range of 137-142 mEq/L [177] and the liver metabolizes acetate into bicarbonate[175]. It is a well-known antibacterial and preservative agent [106, 178]. SA is also used for taste masking [179-180]. It is highly water-soluble. SA does indeed have a surface active and efflorescent property. These intrinsic properties are used to improve the physio-chemical

properties of chitosan nanoparticles [145]. Up-to-date, little is known about the unique and intrinsic CSD property of SA for hydrophobic drugs.

Docetaxel (DXT) is a BCS class II[181-182] drug with a log P = 4.1[183] and is poorly water soluble[184]. It is used to treat different type of malignancy, especially breast, prostate, lung, head, neck, esophageal, squamous cell, and osteosarcoma cancer [185-186]. DXT binds to microtubules and prevents its depolymerization [187]. Current clinical formulation involves the use of vehicle known to have a systemic toxicity such as polysorbate [188-190] and solvent such as alcohol inducing patient intoxication[191].

It is hypothesized that a crystalline solid dispersion of DXT in SA crystal (C-DXT) can be engineered by dispersing native DXT in SA crystal matrix to reduce and prevent regrowth of DXT crystal size, enhanced DXT dissolution rate, resulting in enhanced DXT bioavailability, activity and safety. This hypothesis is tested with supporting physico-chemical characterization of the C-DXT formulation (e.g. powder X-ray analysis (PXRD), differential scanning calorimetry (DSC), scanning electron calorimetry (SEM), transmission electron microscopic (TEM), quartz crystal microbalance with dissipation monitoring (QCM-D), dynamic light scattering (DLS), and liquid chromatography tandem mass spectrometry (LC-MS/MS). The C-DXT formulation cytotoxicity on MCF-10A, MCF-7 and MDA-MB468 cells is assessed by MTS assay.

6.2 Material and Methods

6.2.1 Material

Docetaxel (DXT) is purchased from LC Laboratory (Woburn, Massachusetts). Sodium acetate (SA) anhydrous, Dulbecco modified eagle medium (DMEM) high glucose, DMEM/F12, Non-Essential Amino acid (NEAA), L-glutamine, cholera toxin, hydrocortisone, tween 80,

acetonitrile, and formic acid are purchased from Sigma Aldrich (Saint Louis, MO, USA). Glacial acetic acid (AA) (99.7%w/w), bovine insulin are purchased from Fisher Scientific (Pittsburgh, PA, USA). Fetal bovine serum (FBS) is obtained from Alphabioregen (Boston, MA, USA). Penicillin-streptomycin (Pen-Strep) solution is obtained from Invitrogen (Carlsbad, CA, USA). Horse serum, recombinant human Epidermal Growth Factor (EGF) are purchased from life technologies (Grand island, NY, USA). Rotometals, (San Leandro, CA, USA), supplies indium. Polyethylene glycol 300 MW (PEG300) and ethanol are obtained from Medisca (Plattsburgh, NY, USA).

MCF-7 (human breast adenocarcinoma) estrogen positive, MDA-MB-468 (human breast adenocarcinoma) triple negative, MCF10A (cell line mammary normal gland/breast) are purchased from ATCC (Manassas, VA, USA). All other chemicals used in this study are of analytical grade and used as received without further purification.

6.2.2 Engineering of Crystal Docetaxel Formulation

The C-DXT formulation engineering process is adjusted from the published method of coating chitosan nanoparticles with SA with a slight modification [145]. After a thorough screening and considering the hydrophobic nature of DXT, the following unique and three-steps process is used to engineer C-DXT:

Firstly, approximately 454 mg of SA anhydrous is dissolved in 8 mL of glacial acetic acid (AA) for 30 minutes to generate sodium *cation* and acetate *anion*. It is noteworthy that the deprotonated form of acetic acid (acetate *anions*) are the predominant chemical species. In fact, in this medium, there is negligible proton transfer from acetic acid to acetate anion due negligible water content (AA purity > 99.7%) and the weak acidic nature of glacial acetic acid solution with a pKa value of approximately 4.76 [124].

Secondly, DXT (32 mg) is dissolved in the resulting acetate solution for 10 minutes under continuous magnetic stirring. The drug containing acetate solution is colorless suggesting the complete dissolution of DXT.

Thirdly, DXT solution is frozen using liquid nitrogen and subsequently freeze-dried for 24 hours using the benchtop freeze-dryer (Labconco Corporation, Kansas City, Missouri, USA). During the freeze-drying process, there is a complete sublimation of AA, and recrystallization of SA that was initially dissolved in AA [145] as shown in Figure 6-1 [145].

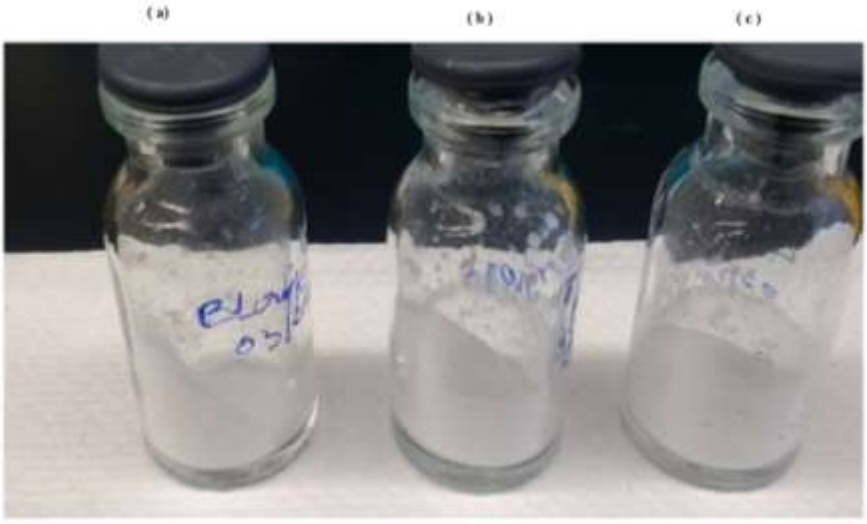

Figure 6- 1 Blank SA after freeze-drying of acetate solution (a), crystal solid dispersion of docetaxel formulation (b), and (c).

The freeze-dried product is the C-DXT formulation. The schematic representation of the preparation of C-DXT is shown in Figure 6-2.

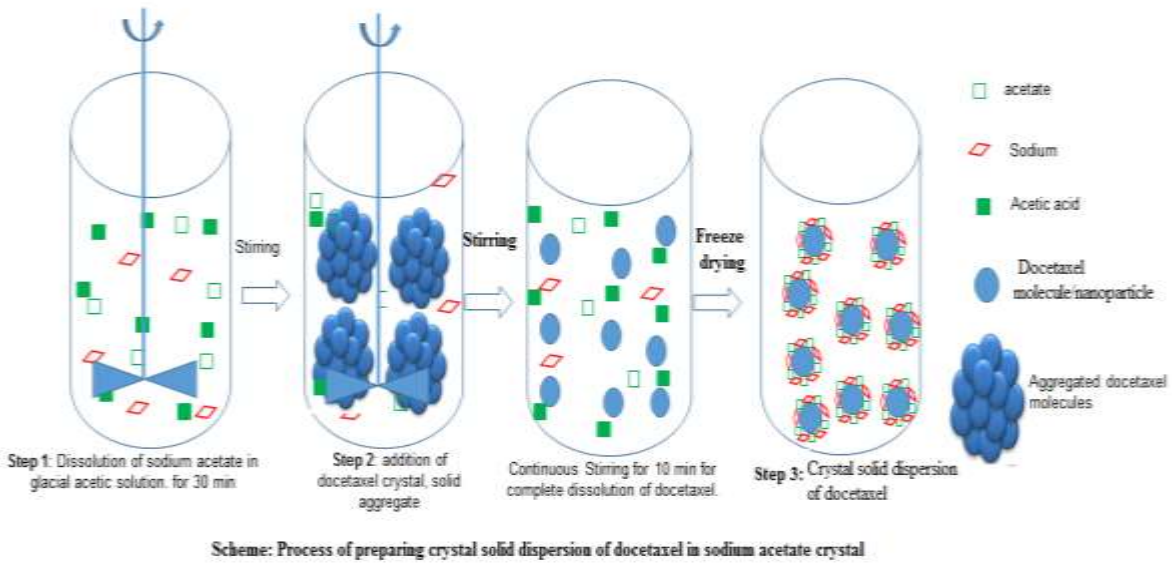

Figure 6- 2 Process of preparation of crystal solid dispersion of docetaxel in Sodium acetate Crystal.

6.2.3 Differential Scanning Calorimetry (DSC)

The DSC scan is performed to assess the CSD nature of the DXT molecularly dispersed in SA crystals. Briefly, approximately 4 mg of sample is added into an aluminum Tzero pan, sealed with a Tzero lid, and inserted in the left sample pan holder while the reference (empty) is placed into the right sample pan holder. The measurements are performed in a temperature range from 20°C to 350°C at a heating rate of 10°C/min under a continuous flow of liquid nitrogen using a Differential Scanning Calorimetry 8000 (PerkinElmer, Shelton, Connecticut, USA). The thermal analysis is performed using Pyris series software (PerkinElmer, Shelton, and Ct). The enthalpy of fusion of samples are calculated using indium with known enthalpy of fusion as a reference[192].

6.2.4 X-Ray Powder Diffractometric (XRD)

The XRD analysis is performed to confirm both the regeneration of SA crystal initially dissolved in AA upon freeze-dried and the inclusion of DXT in SA crystal matrix. Briefly, the powder XRD scans are achieved using a MiniFlex automated X-ray diffractometer (Rigaku, The Woodlands, TX) at room temperature. Ni-filtered Cu K -alpha radiation is used at 30 kV and 15 mA. The diffraction angle is from 2θ=5° to 2θ=60° with a step size of 0.05°/step, and a count time of 2.5 s/step (effectively 1.1°/ min for approximately 46 min/scan). The diffraction patterns are processed using Jade 8+ software (Materials Data, Inc., Livermore, CA) [145].

6.2.5 Liquid Chromatography (LC)-Tandem Mass Spectrometry (MS/MS)

The LC-MS/MS analysis is performed to confirm the chemical stability of DXT dispersed in SA crystal[193]. SA adduct is used to quantitate DXT [193-194]. Briefly, C-DXT formulation (10 µM of DXT) formulation is dissolved in a (49.95/49.95/0.1) % by volume of water/acetonitrile/formic acid, respectively. The control containing 10 µM of native DXT is dissolved in an aliquot of the above organic solvent. Mass spectrometry parameter optimization for multiple reaction monitoring (MRM) detection and quantification is achieved using preparative HPLC-purified samples. Detection optimization is achieved using the automated quantitative optimization routine in Analyst. The separation conditions, the MS conditions and the optimal parameters for the selected precursor/product ion pairs for DXT respectively are shown in Table 6-1.

Table 6- 1 LC-MS/MS conditions for docetaxel qualitative analysis

Separation conditions			
Instrumentations	HPLC system		
Column	C8		
Mobile phase A	100% Water + 0.1% Formic acid		
Mobile Phase B	30% Water + 70% Acetonitrile with 0.1% Formic acid		
Mobile phase C	100% Acetonitrile + 0.1% Formic Acid		
Gradient	Time (min)	Mobile Phase A (% v/v)	Mobile Phase C (% v/v)
	0.01	90	10
	4	90	10
	10	0	100
	10.5	90	10
	14.5	90	10
Flow rate	300 µL/min		
Cell temperature	40 C		
Injection volume	20 µL		
Injection wash solvent	25% methanol		
MS conditions			
Instrumentation	Qtrap		
Ionization condition	ESI		
Polarity	Positive		
Scan time (min)	14 min		
Compound transitions			
Parent(m/z)	830.26		
Products(m/z)	304.2		
Collision energy (V)	33		
Data processing software	Analyst version 1.6 software		
Retention time	11.38 min		

6.2.6 Morphology Analysis

6.2.6.1 Scanning Electron Microscopy (SEM) Size Analysis in Solid dry State

The SEM is performed to visualize the morphology of both native DXT crystal and amorphous DXT in solid powder state. Briefly, a small amount of the sample powder is mounted on 1/2-in. aluminum stubs with double sticky carbon tape and sputter coated (Emitech EMS575SX) with approximately 20 nm thickness of gold-palladium alloy. The sample is then visualized under a FEI/Philips XL30 Field-Emission Environmental SEM (Philips/FEI, Eindhoven, Netherlands) at 5 kV. Digital images are acquired with ORIUS™ SC 100 large format (II Megapixel) CCD camera (Gatan, Pleasanton, CA, USA). The length and width range of drugs crystal, C-DXT and control SA in the SEM images are assessed using Image Pro Plus software (Image Pro plus 6.0, Media Cybernetics, Silver Spring, MD, USA)[195].

6.2.6.2 Transmission electron microscopy (TEM), size analysis of C-DXT suspension

The TEM is performed to elucidate the surface morphology and the structural information of C-DXT. To get the specimens, the drops of native DXT and C-DXT aqueous suspensions are placed on a copper grid with a carbon support film and air dried. The suspensions are viewed under a scanning transmission electron microscope CM12 (FEI, Hillsboro, OR, USA) at 80 kV accelerating voltage. Digital images are acquired with an ORIUSTM SC 1000 11 Megapixel CCD camera (Gatan, Pleasanton, CA, USA) [145].

6.2.7 Particle Mean Diameter of C- DXT Nanosuspension

Dynamic light scattering (Zetasizer Nano ZS, Malvern Instruments Ltd, Worcestershire, UK) is used to measure the size of water dispersible nanosuspension of amorphous DXT in de-

ionized water. The experiment is carried out at 25°C. Samples with Polydispersity index (PDI) < 0.05 are considered monodispersed according to the National Institute of Standards [145].

6.2.8 Percent yield and Drug Loading

The amount of C-DXT dispersed in SA matrix and the yield with respect to DXT amount are determined using UV spectrophotometer (Spectronic Genesys 10 Bio, Thermo Electron Corporation, WI, USA) at a wavelength of 230 nm[196 197]. Briefly, 1 mg of C-DXT-SA, forming a nanosuspension in de-ionized water is dissolved in 13% v/v of ethanol/water solution. The percent drug loading (% DL) is calculated as follow:

$$\%DL = \frac{Amount\ of\ DXT}{Amount\ of\ (SA+DXT)} x100 \quad (6\text{-}1)$$

Where *amount of DXT* = amount of only DXT dispersed in SA matrix, and *Amount of (SA+DXT) i*s the mass of 1 mg amorphous formulation.

$$\%\ Yield = \frac{Experimental\ amount\ of\ DXT}{Theoretical\ amount\ of\ DXT} * 100 \quad (6\text{-}2)$$

The calibration curve of DXT is Y= 0.0164X -0.0053 (R^2=0.9999)

Where, Y is the absorbance of DXT, X is the concentration of DXT in µg/mL.

6.2.9 Quartz Crystal Microbalance with Dissipation Monitoring (QCM-D)

The structural information of C-DXT formulation in pure de-ionized water are monitored using QCM-D[198-199]. Blank SA, a well-known hydrophilic, highly water soluble salt is used as control. QCM-D experiments are performed using the Q-Sense Analyzer (previously known as QSense E4 Biolin Scientific Inc., NJ 07652), which allowed simultaneous monitoring of frequency (ΔF) and dissipation (ΔD) changes of four individual sensors. The gold-coated AT-cut quartz crystals (QSX301) with a fundamental resonance frequency of 5 MHz are used for all

measurements. The crystals are cleansed before each experiment by soaking in a 5:1:1 mixture of de-ionized water, hydrogen peroxide (30%, Sigma Aldrich), and ammonia (25%, Fisher Scientific) at a temperature of 75°C for 5 min followed by rinsing with DI water and drying with nitrogen gas. All experiments are carried out at a constant flow rate of 50 μL min^{-1} by means of a peristaltic pump (Ismatec IPC-N)[200]. The experimental temperature is maintained at 25°C. In each experiment, the gold-coated sensors are allowed to equilibrate in DI water at 25°C until a stable ΔF and ΔD are achieved. Then C-DXT and Blank SA aqueous solutions are flown and the changes in ΔF and ΔD are recorded in real time. Finally, the sensors are rinsed with DI water.

For any rigid and thin film adsorbed onto the sensor surface, the shift in frequency is linearly proportional to the change in mass as described by Sauerbrey equation[201]:

$$\Delta f = \frac{-n}{C}\Delta m \tag{6-3}$$

Where, "n" =overtone number and C = mass sensitivity constant (C=17.7 ng $cm^{-2}Hz^{-1}$for a 5 MHz AT cut quartz crystal at room temperature).

The dissipation factor D is defined as the inverse of the crystal's quality factor Q as described by the following equation [202-203]:

$$D = \frac{1}{Q} = \frac{E_{dissipated}}{2\pi E_{stored}} \tag{6-4}$$

Where $E_{dissipated}$ is the energy loss during one oscillation period and E_{stored} is the energy stored during one oscillation.

6.2.10 Dissolution Study

The dissolution is performed using a USP dissolution apparatus 2 (Scientific Instruments and Technology Corp., Piscataway, NJ) in 150 mL of 0.1N HCL. The paddle speed is set at 100 RPM. Briefly, 46 mg of C-DXT formulation containing 3 mg of DXT along with a control (physical mixture of native DXT and SA) is added to each dissolution vessel. At predetermined

time interval, 1 ml of sample was withdrawn and replaced with fresh media. Then, samples were centrifuged at 14,000 rpm for 10 min at 25ºC using a refrigerated microcentrifuge (VWR, Radnor, PA). The concentration of the drug in the supernatant is measured at 230 nm using the above UV spectrophotometer. The dissolution profile of native docetaxel and C-DXT formulations are compared using the difference factor (f_1) and the similarity factor (f_2) expressed below [151]:

$$f_1 = \left(\frac{\sum_{t=1}^{n}|R_t - T_t|}{\sum_{t=1}^{n} R_t}\right) * 100 \quad (6\text{-}5)$$

$$f_2 = 50 * \log_{10}\left[\frac{100}{\sqrt{1+\frac{\sum_{t=1}^{n}(R_t - T_t)^2}{n}}}\right] \quad (6\text{-}6)$$

Where, n is the number of time points, R_t is the mean dissolution value for the reference product (e.g. native DXT) and T_t is the mean dissolution value for the test product (e.g. C-DXT formulation). In general, a f_1 value less than 15 and a f_2 value greater than 50 indicate sameness or equivalence in dissolution profile [151].

6.2.11 Cell Culture and Medium

MCF-7 (human breast adenocarcinoma) Estrogen positive cells are grown in DMEM high glucose supplemented with 10% Fetal Bovine serum (FBS), 10µg/mL insulin, 1%v/v L-glutamine, 1% v/v penicillin-streptomycin (Pen-Strep) solution and, 1%v/v non-essential amino acid (NEAA). MDA-MB-468 (human breast adenocarcinoma) triple negative cells are grown in DMEM high glucose supplemented with 20% FBS, 1%v/v Pen-Strep and, 1% v/v L-glutamine. Control MCF-10A (normal gland /mammary cell lines) are grown in DMEM/F12 supplemented with 5% v/v Horse serum, 20 ng/mL EGF, 0.5 µg/mL of hydrocortisone, 100 ng/mL of cholera toxin, and 1% v/v pen-strep. Cells are grown and maintained in a monolayer culture, in 75 cm^2

culture flasks (Techno Plastic Product, Switzerland), at 37°C in a humidified atmosphere of 5% carbon dioxide (CO_2).[204]

6.2.12 Exposure Protocol

C-DXT and simulated clinical DXT formulations, nanosuspension and micellar suspension respectively [205] are added in DMEM high glucose /FBS (10%) or DMEM/F12/ Horse Serum (5%) at 65,800 ng/mL and sterilized for 30 min under UV light[145]. Different C-DXT and simulated DXT formulations concentration are prepared from the stock solutions 7 mg/mL (solvent=(50/50) %v/v water/PEG) and 20 mg/ml(solvent= (50/50) %v/v (ethanol/tween 80)[191], respectively. Then, the formulations are diluted 1:100; 1:10,000; 1:1,000,000; and 1:100,000,000. MDA-MB-468, MCF-7 ($1x10^4$ cells/100µL/well)[206-207], and MCF-10A ($1x10^5$ cells/100µL/well)[208-209] are seeded in 96 well plate and incubated overnight. The cells are exposed to the C-DXT and simulated clinical DXT at, 0.000658 ng/mL; 0.0658 ng/mL; 6.58 ng/mL; 658 ng/mL; and 65,800 ng/mL for 24hrs and 48hrs, respectively. Wells containing cells with the culture media only are used as the negative controls. As a positive control, the cells are treated with triton X (1% v/v).

6.2.13 Viable Cell Proliferation Assay

Cell proliferation level is determined by MTS assay. Viable cells bio-reduce MTS compound mix with PMS (cellTiter 96® AQ_{ueous}) into formazan[152]. After exposure to DXT/blank formulations, the old media containing cells is discarded, replaced with 100µL of fresh media, and equilibrated for 30 min at 37ºC. Then, 20µL cellTiter 96® AQ_{ueous} (Promega, Madison, WI, USA) is added to each well and incubated for 1 hour. The absorbance is read at 450 nm using a DTX 880 multimode microplate reader (Beckman Coulter, Brea, CA, USA).

$$Viability\ (\%) = \frac{aborbance\ (test)}{absorbance\ (control)} x100 \quad (6\text{-}7)$$

Where absorbance (test) and absorbance (control) denote the amount of formazan

6.2.14 Statistical Analysis

All values are expressed as mean ± standard deviations. One-way analysis of variance (ANOVA) in combination with Dunnett's post-hoc test are used to compare samples with unequal variances[210] and identify means of data that are significantly different from each other. A student t-test is used to compare the experimental to the theoretical yield. All statistical analyses are carried out using JMP software version 9, (SAS Institute, Cary, and North Carolina, USA). P-value below 0.05 is considered statistically significant and warrants the rejection of the null hypothesis.

6.3. Results and Discussion

6.3.1 Differential Scanning Calorimetry (DSC)

Figure 6-3 shows the heat flow curve versus temperature of C-DXT (a), physical mixture of DXT and SA (b), blank SA (c), native DXT (d), and indium (e). The endothermic melting peak of docetaxel is both visible in the native drug Figure 6-3b and the physical mixture Figure 6-3d, whereas, it disappears in the C-DXT formulation Figure 6-3a. The DSC curve of C-DXT and blank SA are alike as shown in figure 6-3a and figure 6-3c, respectively. These data suggest that DXT is in its might be coated with SA as shown in figure 6-3a.

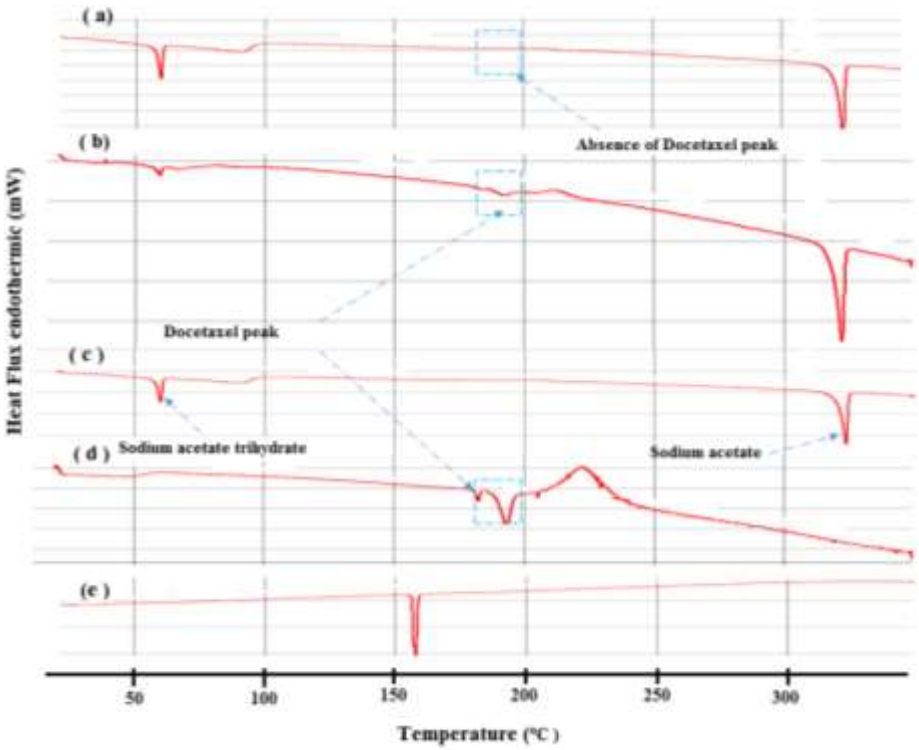

Figure 6- 3 DSC curve of crystal solid dispersion of docetaxel formulation (C-DXT) (a), physical mixture of DXT (b), blank (SA, Blank SA is obtained by dissolving sodium acetate anhydrous in glacial acetic acid and subsequently freeze-dried), (c), native DXT (d), and indium (e).

6.3.2 X-Ray Powder Diffractometric (P-XRD)

Figure 6-4 shows the P-XRD pattern of C-DXT (a), physical mixture of DXT and SA (b), blank SA (c), and native DXT (d), respectively. The characteristic peaks of DXT at 2 Braggs angle (2θ) equal 15.31°C and 23.04°C, respectively are present in the physical mixture figure 6-4b and native DXT figure 6-4d [211]. These DXT peaks disappear in the C-DXT formulation, as shown in figure 6-4a because DXT is coated with SA [145, 212].

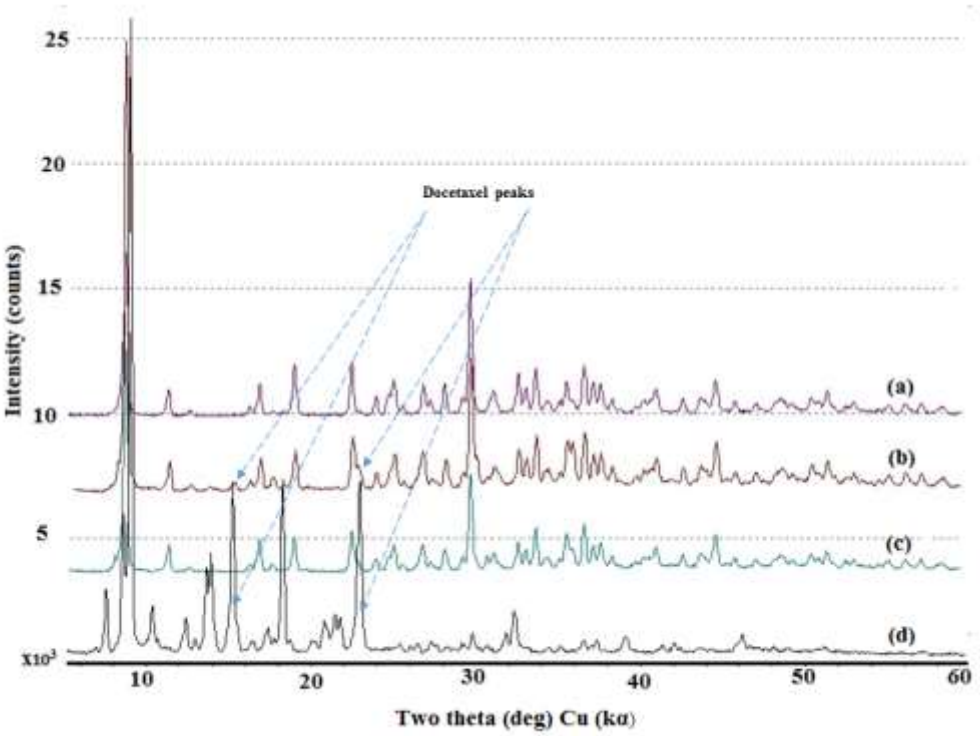

Figure 6- 4 P-XRD pattern of crystal solid dispersion of docetaxel (C-DXT) (a), physical mixture of DXT and SA (b), blank SA (c), and native DXT (d), respectively

6.3.3 Liquid Chromatography (LC)-Tandem Mass Spectrometry (MS/MS)

Figure 6-5 shows the chromatogram of native DXT (a) and C-DXT (b) with identical retention time (11.38 min). This suggests that the engineered CSD technique preserves the chemical stability of DXT. The result is indeed expected because DXT is stable in AA solution [213].

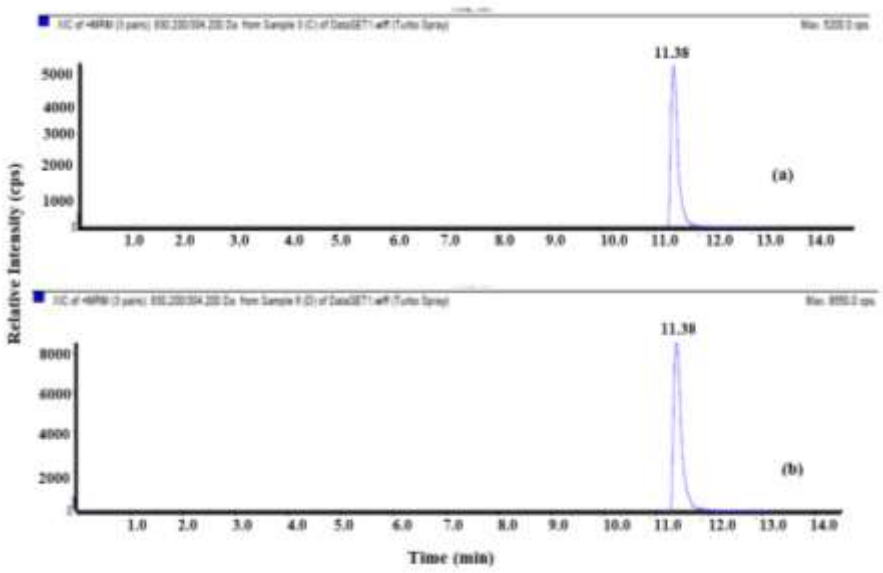

Figure 6- 5 Chromatogram of native docetaxel (a) and crystal solid dispersion of docetaxel (C-DXT) (b), MRM

6.3.4 Morphological Analysis: Scanning Electron Microscopy (SEM) And Transmission Electron Microscopy (TEM)

Figure 6-6 a1-3 shows the SEM morphological analysis of native DXT (Figure 6-6 a1), blank SA (Figure 6-6 a2), C-DXT in solid freeze-dried powder state (Figure 6-6 a3). Unlike native DXT morphology, the morphology of blank SA and C-DXT is identical due to the presence of SA crystals and their surface active property[145]. The maximum crystal size is 960.3 μm, 455.2 μm, and 302.8 μm, for native DXT, C- DXT and blank SA, respectively.

Figure 6-6b1-6 shows also the TEM morphological and structural analysis of native DXT (Figure 6-6 b1 and b4,) and C-DXT (Figure 6-6 b2, Figure. 6-6 b3, and Figure 6-6 b5 and Figure 6-6 b6) aqueous suspensions. There is a dramatic decrease of DXT particle size in the C-DXT formulation. Unlike native DXT made of uniform DXT crystal as shown in Figure 6-6 b1 and Figure 6-6 b4, C-DXT nanoparticle (size<200 nm) are made of DXT and blank SA as elucidate by the visual structural information shown in Figure 6-6 b6. C-DXT presumably contains drug

molecules and/or very small drug aggregates coated by SA due to SA surface-active propensity as shown in Figure 6-6 b6.

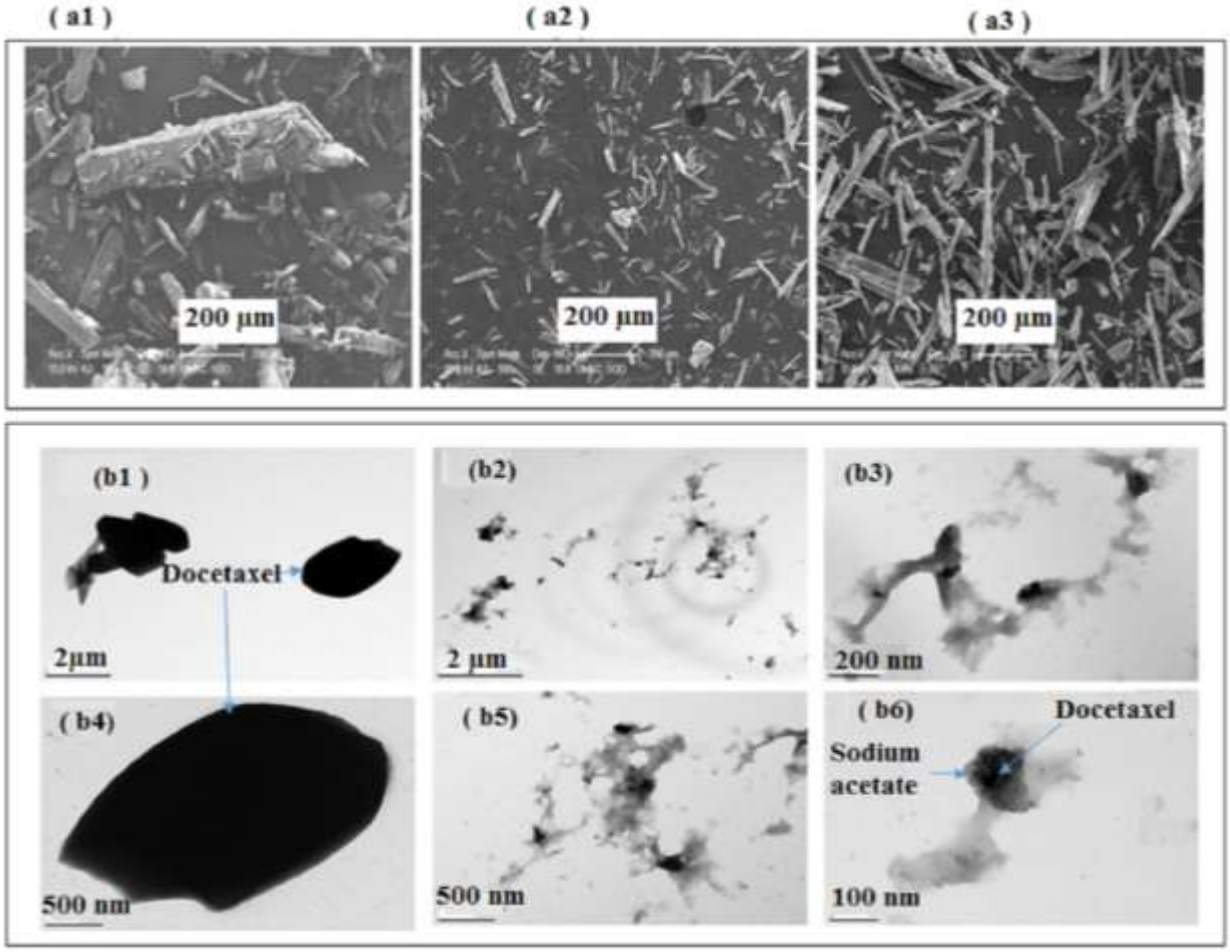

Figure 6- 6. Scanning electron microscopy (SEM) morphological analysis of native DXT in freeze dried state (a1), blank SA (a2), crystal solid dispersion of docetaxel (C-DXT) (a2) respectively, in dry powder solid state; Transmission electron microscopy (TEM) aqueous solution of native docetaxel (b1, b4), aqueous solution of crystal solid dispersion of docetaxel (C-DXT) (b2, b3, b5 and b6). A sample drop is placed on a copper grid with a carbon support film and air dried within 1 minute. Scale bar represents 200 µm for (a 1-3), 100 nm for (b 6), 200 nm for (b3), 500 nm for (b4, b5), and 2000 nm for (b1, b2) respectively.

6.3.5 Particle Size Distribution, Percent Yield And Drug Loading

In pure de-ionized water, C-DXT formulation forms a nanosuspension with an average size of approximately 161.3 ±11 nm as shown in Figure 6-7a-c. The percent drug yield is 95.2 ± 4.1%. The experimental and theoretical drug loading are 6.52 ± 0.48 % and 6.58%, respectively and are statistically identical based on student t-test analysis with df=2, t=0.22 and p-value=0.58.

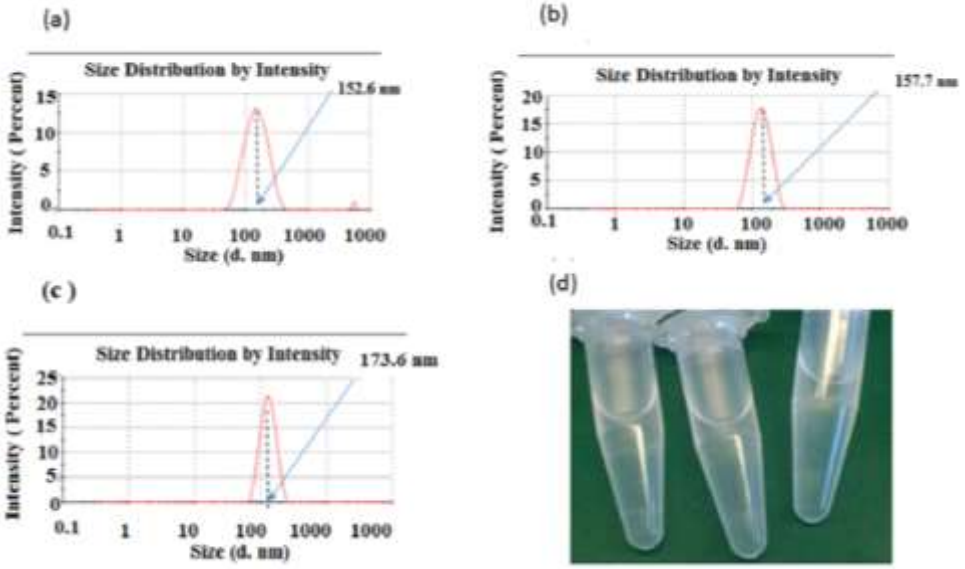

Figure 6- 7. Particle size distribution of crystal solid dispersion of DXT in pure deionized water (6a-c), Visual inspection of the nanosuspension (figure 6-7 d).

6.3.6 Quartz crystal microbalance with dissipation monitoring (QCM-D)

Figure 6-8 shows the QCM-D graph of both frequency and dissipation values versus time of blank SA (Figure 6-8a) and C-DXT (Figure 6-8b). The frequency and dissipation of oscillations energies values versus time for SA are constant. These data suggest that there is complete dissolution of SA in deionized water, as expected. The formation of soft or viscoelastic films cause dissipation of oscillation energy due to mechanical losses in the flexible mass[199] as shown in Figure 6-8b. These C-DXT molecules do not indeed bind tightly among themselves nor rigidly to the

QSX301 crystal surface as evidenced by the increase of both the dissipation factor and the frequency[199]. D1 and F1 are the fundamental dissipation and frequency respectively. D3, D5… D11, D13 and F3, F5...F11 and, F13 represent the odds overtone for the dissipation and frequency respectively.

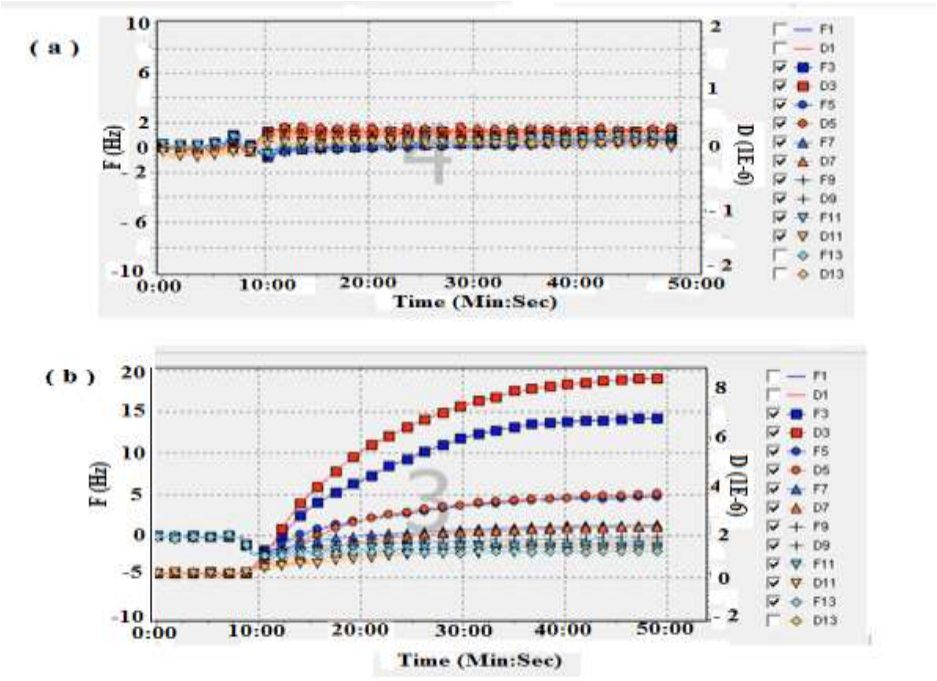

Figure 6- 8. QCM-D graph of both frequency and dissipation energy versus time of blank SA (a) and crystal solid dispersion of docetaxel (C-DXT) (b), in deionized water. D1 and F1 are the fundamental dissipation and frequency respectively. D3, D5…D11, D13 and F3, F5….F11 and F13 represent the odds overtone for the dissipation and frequency, respectively.

6.3.7 Dissolution Study

Figure 6-9 shows the cumulative dissolution profile of C-DXT formulation and native DXT. C-DXT exhibits a fast dissolving profile with 96 percent of drugs dissolved within 10 min.

The f_1 and f_2 values are 547.8 and 7.1 respectively, indicating a non-equivalence of the dissolution profile of C-DXT relatively to native DXT.

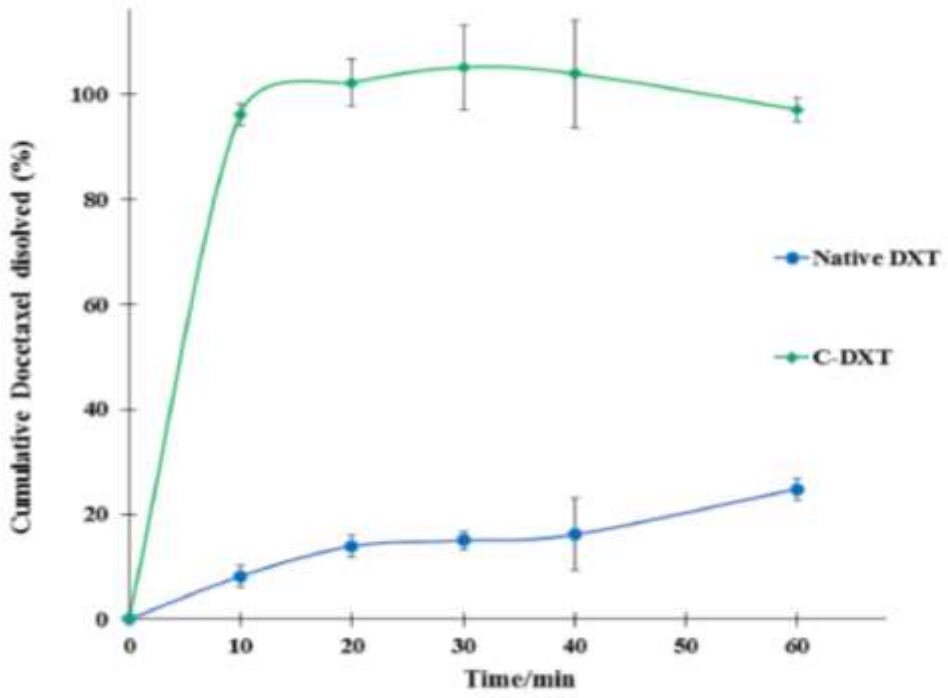

Figure 6- 9 Dissolution profile of native docetaxel and crystal solid dispersion of docetaxel (C-DXT) in 0.1 N HCl aqueous solution. Error bars represent the standard deviation.

6.3.8 Cytotoxicity assessment

6.3.8.1Cytotoxicity activity on MCF 10A

Figure 6-10 shows the percent cell viability of MCF 10A after treatment with different formulations. In general, the vehicle, blank SA/PEG300 is safer compared to the blank tween 80/EtOH at highest concentration as shown in Figure 6-10a, b. The cytotoxicity of C-DXT formulation on normal MCF-10A cells is weak over 48 hours, whereas a strong cytotoxicity is observed with the simulated clinical formulation DXT as shown in Figure 6-10b. The percent cell

viability data for simulated clinical DXT formulation (65,800 ng/mL), blank tween 80/EtOH containing both (0.17/0.17%) v/v Tween 80/EtOH are similar and are below 40%. Triton X (1% v/v) is strongly cytotoxic to the cell line as shown in Figure 6-10 and is well-known to induces apoptotic and necrotic cell deaths[214].

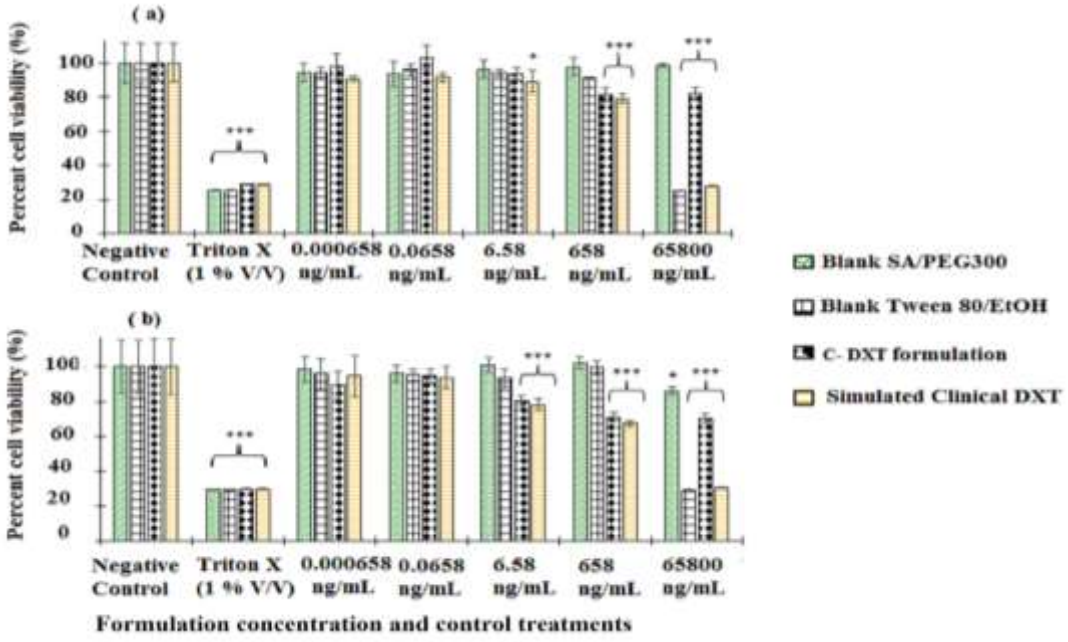

Figure 6- 10. (a) Percent MCF 10A cell viability (% control) treated 24 hours with the different formulations: Blank SA (pattern fill, weave), Blank Tween 80/EtOH (pattern fill, large grid), crystal solid dispersion of docetaxel (C-DXT) (pattern fill, solid diamond grid), and Simulated clinical DXT (pattern fill, Horizontal stripes: light) respectively (n=3). *P < 0.05 vs media, ** P < 0.01 vs media, *** P < 0.001 vs media. (b) Percent MCF 10A cell viability (% control) treated 48 hours with the different formulations: Blank SA (pattern fill, weave), Blank Tween 80/EtOH (pattern fill, large grid), crystal solid dispersion of docetaxel (C-DXT) (pattern fill, solid diamond grid), and Simulated clinical DXT (pattern fill, Horizontal stripes: light) respectively (n=3). *P < 0.05 vs media, **P < 0.01 vs media, ***P < 0.001 vs media. Error bars represent standard deviation.

6.3.8.1Cytotoxicity activity on MCF 7 and MDA-MB 468

Figure 6-11 shows the percent cell viability of MCF-7. After 24 hrs of treatments, the cytotoxicity is observed for the highest concentration of C-DXT and simulated clinical DXT formulations, blank SA/PEG300 and the blank Tween 80/EtOH as shown in Figure 6-11a. The

cytotoxicity of C-DXT on MCF-7 increases after 48hrs treatment. The blank tween 80/EtOH is also cytotoxic to MCF-7 at (0.17/0.17) % v/v (tween 80/EtOH). The cytotoxicity data of these formulations on MDA-MB-468 cells is shown in Figure. 6-12. Within 24 hrs, there is no observed cytotoxicity (Figure 6-12a). However, there is an increase of the cytotoxicity when DXT concentration is equal or greater than 6.58 ng/mL as shown in Figure 6- 12b over a time period of 48hrs

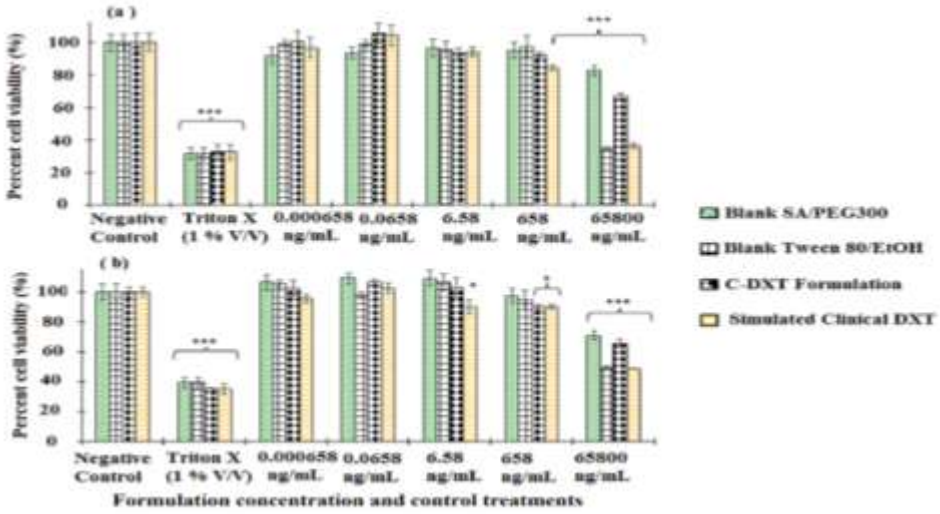

Figure 6- 11. (a) Percent MCF 7 cell viability (% control) treated 24 hours with the different formulations: Blank SA (pattern fill, weave), Blank Tween 80/EtOH (pattern fill, large grid), crystal solid dispersion of docetaxel (C-DXT) (pattern fill, solid diamond grid), and Simulated clinical DXT (pattern fill, Horizontal stripes: light) respectively (n=3). *P < 0.05 vs media, **P < 0.01 vs media, ***P < 0.001 vs media. (b) Percent MCF 10A cell viability (% control) treated 48 hours with the different formulations: Blank SA (pattern fill, weave), Blank Tween 80/EtOH (pattern fill, large grid), crystal solid dispersion of docetaxel (C-DXT) (pattern fill, solid diamond grid), and Simulated clinical DXT (pattern fill, Horizontal stripes: light) respectively (n=3). *P < 0.05 vs media, **P < 0.01 vs media, ***P < 0.001 vs media. Error bars represent standard deviation.

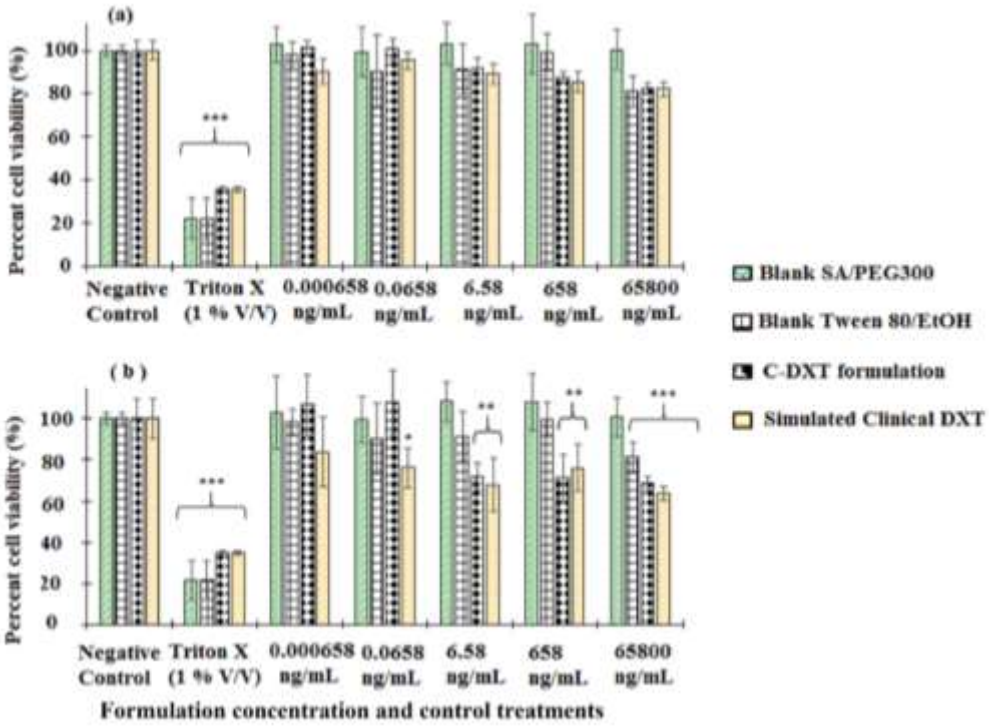

Figure 6- 12. (a) Percent MDA-MB 468 cell viability (% control) treated 24 hours with the different formulations: Blank SA (pattern fill, weave), Blank Tween 80/EtOH (pattern fill, large grid), crystal solid dispersion of docetaxel (C-DXT) (pattern fill, solid diamond grid), and Simulated clinical DXT (pattern fill, Horizontal stripes: light) respectively (n=3). *P < 0.05 vs media, **P < 0.01 vs media, ***P < 0.001 vs media. (b) Percent MCF 10A cell viability (% control) treated 48 hours with the different formulations: Blank SA (pattern fill, weave), Blank Tween 80/EtOH (pattern fill, large grid), crystal solid dispersion of docetaxel (C-DXT) (pattern fill, solid diamond grid), and Simulated clinical DXT (pattern fill, Horizontal stripes: light) respectively (n=3). *P < 0.05 vs media, **P < 0.01 vs media, ***P < 0.001 vs media. Error bars represent standard deviation.

6.4 Discussion

Based on the knowledge gained from our previous studies [145, 212], C-DXT formulation is successfully engineered by using a unique crystal solid dispersion technique.

The enthalpy of fusion and melting point (MP) of native DXT are 32 J/g and 193.4°C, respectively (Table 6-1). Native DXT exhibits endothermic melting peak at 193.4°C as shown in Figure 6-3b in the physical mixture. However, there is an absence of the endothermic melting peak

of DXT at 193.4°C on the DSC curve (Figure 6-3a) due to the coating and efflorescent property of SA.[145]. The C-DXT formulation is visualized by the SEM and TEM analysis (Figure 6-6). The MP of SA in final C-DXT formulation (MP=323.75°C) (Figure 6-3a) is less than that of blank SA (MP=329.06°C) with respect to SA anhydrous content as shown in Figure 6-3c. This result is consistent with Van't Hoff s Law stating that the MP of a pure compound (Blank SA) is always greater than the MP of an impure compound[215] (C-DXT formulation)[216].

The DSC scans of C-DXT formulation and blank SA are identical as shown in Figure 6-3a and 3c. The endothermic melting peak observed at 59.9°C suggests the formation of SA trihydrate (SAT) crystals during the freeze drying process (Figure 6-3a, 3b and 3c)[217] due to the hygroscopic nature of AA[218] and residual water in commercially available AA (0.1% max) used in the dissolution step of native DXT in AA. The result of this finding is also consistent with the XRD scans. The physical mixture (Figure 6-4b) made of blank SA and native DXT show characteristic peaks of DXT at two Braggs angle (2θ) equal 15.31°C and 23.04°C whereas, there are no characteristic peaks of DXT at two Braggs angle (2θ) equal 15.31°C and 23.04°C, shown (Figure6-4a) respectively[211]. The PXRD scans of C-DXT and blank SA are identical as shown in Figure 6-4a and 4c. It is noteworthy that the percent limit of crystallinity detection of the Rigaku Miniflex diffractometer instrument used in this study is in the range of 0.3-1%, which is significantly lower that the actual C-DXT drug loading of 6.52 %w/w [219]. This fact further supports the fact that DXT (in the C-DXT formulation) is mostly molecularly dispersed in blank SA and may be coated with blank SA as visually shown in (Figure 6-6 b6). This outcome is supported by the result of our previous work where the PXRD scan of blank SA coated chitosan nanoparticle shows only unique and identical pattern of blank SA with no visible drug characteristic peak [145]. By definition when the drug is dispersed in a crystalline carrier, the solid dispersion technique is called CSD.

Therefore, the physical state of C-DXT is a CSD of DXT in SA crystal [162] where DXT molecule or small nanoparticulate matter may be also coated with SA. The CSD of DXT may be ascribed to the following physio-chemical properties of glacial acetic acid (AA) and SA.

Firstly, AA and DXT crystals have a good solvation interaction, which is in agreement with Hansen solubility parameters (δ_{HAN}). The Hansen solubility parameter (δ_{HAN}) includes different types of inter-molecular forces and is expressed as follow [220]:

$$\delta_{HAN} = \sqrt{\delta_d^2 + \delta_p^2 + \delta_h^2} \quad (6\text{-}8)$$

Where, δ_{HAN}= Hansen solubility parameters, δ_d=energy of dispersions forces between molecules, δ_p= energy of dipolar intermolecular forces between molecules, δ_h= energy of hydrogen bonds between molecules.

δ_{HAN} of AA and DXT are 21.4[221] and 27.14 (J/cm^3)$^{1/2}$, respectively [222]. The difference $\Delta\delta_{HAN}$=5.74<7.5 (J/cm^3)$^{1/2}$ between DXT(δ_{HAN}) and AA (δ_{HAN}) indicates a good solubility of the drug in the selected solvent[222] whereas $\Delta\delta_{HAN}$ =20.66>7.5 (J/cm^3)$^{1/2}$ between water (δ_{HAN} = 47.8 (J/cm^3)$^{1/2}$), and DXT(δ_{HAN}) indicates a poor solvation of DXT or solubility (11.75 μg/mL) in deionized-water. This leads to a complete dissolution and surrounding of every single DXT molecule by AA molecules. The stabilization of DXT by the solvation shell formed by AA molecules leads to a colorless solution.

Secondly, DXT molecules are entrapped in AA crystal upon freezing the hygroscopic AA solution[218] with liquid nitrogen. In addition, the hydrophobic interaction between solvated DXT molecules is significantly reduced in frozen AA crystal.

Thirdly, in the SA solution prior freeze-drying, Debye-Hűckel theory states that species in solution, especially *ion*s of opposite charges, are likely to be found close to each other. Thus,

sodium *cation* and acetate *anion* are close to each other and surround DXT molecules [145]. Moreover, the long- range coulombic interaction between sodium *cation* and acetate anion leads to the formation of SA. In fact, during the freeze drying process, sodium *cation* attracts and physically binds to acetate *anion* through coulombic or charge-charge interaction[223]. The radii for SA formation, especially the bond length of sodium c*ation* Na^+ and oxygen (O) from the carboxylate group COO- is in the range of 2.354-2.56 Å[224]. Columbic forces and the free energy for the coulombic interaction between sodium cation and acetate anion can be expressed as:

$$F = \frac{Q_1 Q_2}{4\pi\varepsilon_0 \varepsilon r^2} = \frac{-e^2}{4\pi\varepsilon_0 \varepsilon r^2} \quad (6.9)$$

$$W(r) = \frac{Q_1 Q_2}{4\pi\varepsilon_0 \varepsilon r} = \frac{-e^2}{4\pi\varepsilon_0 \varepsilon r} \quad (6.10)$$

Where F = columbic force; W(r) = free energy for columbic interaction; e = elementary charge 1.602 x 10^{-19} C; Q1=+e and Q2 =-e are sodium *cation* and acetate *anion* charges, respectively; r = distance between two isolated sodium *cation* (Na^+) and acetate anion (CH_3COO^-); ε = relative permittivity or dielectric constant of the medium especially icy or crystal glacial acetic acid, and ε_0= 8.85 x 10^{-12} C^2/Nm^2, the vacuum permittivity [225].

In the freeze drying operating condition (0.06 mBar and, 225.15 K) [145], the thermal energy

$$kT=(1.38\times10^{-23})(225.15)=3.1\times10^{-21}J. \quad (6.11)$$

where, the Boltzmann constant, k=1.38x10^{-23} m^2 kg s^{-2} K^{-1} .

The dielectric constant (ε) of frozen or crystal acetic acid is 2.5 [226]. Thus, from equation (12) and (13), the value of r must be equal or greater to 297.6 Å (significantly higher than the above bond length) for the coulombic energy to be less than the operating thermal energy kT. This suggests the very long range and strong coulombic interaction between sodium *cation* and acetate

anion during the freeze-drying process[227]. This resulting strong and long-range coulombic force is materialized by the formation of SA.

Fourthly, and most importantly, the surface active and efflorescent properties of SA as demonstrated in our previous study[135, 145] not only favor crystal solid dispersion (CSD) of DXT but also the coating of DXT by SA crystal while volatile acetic acid is sublimated[145]. The coating and efflorescent property of SA is acetate *anion* intrinsic amphiphilic property with CH_3 the non-polar part oriented at the air solvent interface and COO^- the polar part oriented toward the bulk solution [135, 145]. Moreover, the removal of the solvent AA by sublimation favors the spontaneous formation and migration of SA salt on the surface of DXT to form a coating layer. This leads to C-DXT formation and distributed in SA crystal. The CSD of DXT in SA crystal can potentially prevent DXT recrystallization, a common problem inherent to different milling technologies for hydrophobic drugs crystal size reduction[228]. In future studies, it would be important to elucidate the physio-chemical stability of C-DXT over various drug loading and storage time period using ICH guideline for stability study[229].

The high yield CSD process does not chemically degrade DXT as shown in Figure 6-5 because DXT is chemically stable in glacial acetic acid[213]. The retention time of native DXT (Figure 6-5a) and native DXT (Figure 6-5b) are identical (t=11.38 min).

In pure de-ionized water, C-DXT forms a stable nanosuspension of DXT with a particle mean diameter of 161.3 ±11 nm for 65.6 µg/mL of DXT as shown in Figure 6-7a-c and visualized in Figure 6 7 d. The nanosuspension exhibit a faster dissolution rate with more than 96.17 % of DXT dissolved in 10 minutes as shown in Figure 6-8. This enhanced dissolution rate of C-DXT formulation is due to the synergic effect of the hydrotropy of blank SA, the coating of DXT by blank SA [145] and the reduction of DXT average particle size (~161.3 nm) in C-DXT formulation.

According to, Noyes-Whitney equation as shown below, the decrease of drugs particle size increase their surface area which in turn increase drugs dissolution rate[230-231].

$$\frac{dm}{dt} = A\frac{D}{d}(C_s - C_b), \text{ [232]}, \quad (6\text{-}12)$$

where, $\frac{dm}{dt} =$ solute dissolution rate $(kg.s^{-1})$, mass of dissolved material(kg), time((s) , A = surface area of the solute partilce $(m^{2)})$, D = diffusion coefficient($m.s^{-1}$).

In addition, it is noteworthy that, in this dissolution media, (Figure 6-9) the highly water soluble blank SA concentration (~0.0035 M, assuming "blank SA" MW=82.03 g/mol) enables C-DXT rapid dissolution. This effective SA concentration is 571-1143 fold less than the commonly used concentration of SA (2-4 M)[233-234] required to enhance the solubility of the hydrophobic drug by hydrotropy. Thus, this unique dual coating and CSD engineering process is extremely crucial to favor not only the rapid dissolution of the C-DXT formulation but also maintain DXT concentration above its supersaturation limit in an aqueous media for at least 1h as shown in (Figure 6-9). Indeed, the dissolution of C-DXT formulation is now similar that of the water soluble carrier blank SA. Futhermore, it is noteworthy that SA (150 mEq or 12.3g) [175] and DXT (200 mg)[235] are relatively safe and clinically used for intravenous infusion for acidosis and cancer treatment respectively. For intravenous administration of 200 mg of DXT containing this CSD formulation, in a clinical setting, the required amount of SA would be 2.87 g or 35 mEq which is lower than the clinically used 150 mEq or 12.3 g. It would be 4 fold less SA amount considering drug loading is 6.52% and assuming SA MW=82.03 g/mol suggesting future clinical safety, efficacy and translation feasibility.

For higher concentrations, 1 mg/mL and 7 mg/mL of DXT containing C-DXT formulation can be stabilized in 50/50 % v/v deionized water/PEG300 aqueous media for 1 month and 1 hour, respectively. This aqueous nanosuspension appears to be non-rigid in nature as revealed by the

QCM-D result considering the increase of both frequency and dissipation factor (Figure 6-8b) [199]. It is noteworthy that the nanosuspension size is less than 200 nm and acceptable for IV administration[236]. In future studies, a complete mechanistic understanding of the nanosuspension formation, strategies to increase drug loading and effect of drugs loading on the C-DXT particle size will be investigated.

Based on ISO 10993-5 for *in vitro* cytotoxicity test with 100% viability allotted to the control, samples cytotoxicity level are classified as not cytotoxic, weak, moderate, and strong for cell viability higher than 80%, within 80–60%, within 60–40%, and strong below 40% respectively[145, 237]. In this study, the blank SA/PEG 300 containing (0.093% w/v SA) and 0.47% v/v PEG 300, respectively appeared to be non-cytotoxic to MCF-10A, whereas the vehicle tween 80/EtOH (0.17/0.17) % v/v strong cytotoxic observed to MCF-10A cells, is mainly due to ethanol as reported in previous study[238-239]. Compared to other xenobiotics previously used to overcome drug solubility problems, acetate is a very attractive alternative because it is a relatively safer natural bioactive agents involved in normal cell biochemistry during the Krebs cycle[240]. In general, the cytotoxicity levels of C-DXT and Simulated clinical DXT formulation on MCF-10A, MCF-7 and MDA-MB-468 is dose dependent and increase over a period of 48 hrs in all cell lines as shown in Figure 6-10 , Figure 6-11 and Figure 6-12. Below, DXT concentration of 6.85 ng/mL (8.14 nM), both C-DXT and simulated clinical DXT formulation appeared to be non-cytotoxic to the different cell lines. The cytotoxicity of DXT is observed with DXT concentration equal to, or greater than 6.85 ng/mL for both simulated clinical DXT and C-DXT as shown in Figure 6-12b. The cytotoxicity observed up to 8.14 nM of DXT concentration is consistent with reported IC_{50} of DXT, which was 8.2 nM over an exposure time period of 72 in a previous study[241]. This result suggests that DXT nanosuspensions are uptaken by different cell line and the activity of DXT is

preserved after the formulation engineering. The formation of a nanosuspension may potentially and selectively accumulate in tumor tissue due the enhanced permeability and retention (EPR) effect [242-243] and may potentiate the activity and safety of DXT with less protein binding.

6-5 Conclusions

A novel crystal solid dispersion (CSD) of docetaxel (C-DXT) is successfully engineered by molecularly dispersing a model BCS class II drug, DXT in sodium acetate crystal matrix. The proposed CSD engineering process is relatively simple and preserved the drug chemical stability in the C-DXT formulation. In an aqueous media, C- DXT formulation forms a non-rigid nanosuspension exhibiting a faster dissolution kinetics. The physical stability of C-DXT is time and concentration dependent. The cytotoxicity of C-DXT are comparable to that of simulated clinical DXT. At higher dose the vehicle SA/PEG 300 is safer than the vehicle tween 80/ETOH for normal cell. Such drug CSD process using the highly water-soluble salt such as SA as a dispersion medium may potentially be used to prevent recrystallization of hydrophobic drugs (from BCS class II and IV) in solid state, reduce drug crystal size, enhance their aqueous dissolution rate resulting in enhanced bioavailability; potentiate their safety and efficacy.

CHAPTER 7

SUMMARY AND FUTURE DIRECTIONS

7.1 Summary

At the end of this study, we conclude that, HIV/AIDS is still the worst outburst of infectious disease in modern human history. The rate of male to female HIV infection is still very alarming. Several efforts especially vaginal topical anti-HIV/AIDS microbicide are investigated to stop the exponential spread of HIV/AIDS. Those future and potential anti-HIV microbicides known as pre-exposure prophylaxis (PreP) are design to prevent the infection of HIV-infected-male to HIV free female. It is noteworthy that PreP do not cure the disease itself but may help prevent infection to HIV or help infected HIV/AIDS patient live longer. United States Food and Drug Administration (US FDA) in his fight against HIV/AIDS has approved several anti-HIV/AIDS microbicides to reduce the spread of HIV/AIDS. Those microbicides include the combination of many anti-HIV drugs that blocs the virus at different stage of infection or its life cycle.

There are several emerging anti-HIV/AIDS gel microbicides and/or anti HIVAIDS polymeric nanoparticles development to stop the male to female infection to HIV[244].

At the end of this dissertation, we conclude that a responsive human prostatic acid phosphatase Nanocarrier is successfully engineered for topical application in order to prevent male-to-female HIV infection. In chapter 3 a method for better for analysis of an anti-HIV microbicide was developed for better analysis of xenobiotic compound such tenofovir interfering with a mixture of vaginal and seminal fluid. In chapter 4, sodium acetate, known as Krebbs cycle biochemical is used to improve the physical and chemical properties of the hPAP responsive nanoparticles. For instance, the drug encapsulation efficiency was increase from 5-11% to more

than 90%. In chapter 5, the hPAP responsive nanoparticle was optimize to enhance the release of the anti-HIV microbicide because of the presence of the shell SA which prevent the degradation of the responsive nanoparticle. The optimal hPAP responsive nanoparticles was found for chitosan the engineered chitosan nanoparticle using the following independents variables chitosan concentration (1.5 mg/mL), acetic acid concentration (1.3 % v/v) and tripolyphosphate (3.5 mg/mL). The responsive nanoparticles are spherical in nature and undergo degradation under the action of hPAP releasing 63% of drug within 6 hours, which is the maximal time HIV crosses layers of stratified squamous vaginal epithelial cells upon release in the vaginal tract.

In chapter 6, versatile fast dissolving crystal solid dispersion of drug was engineered to enhance the aqueous dissolution of hydrophobic drugs. This latter can be applying to anti-HIV microbicides which are poorly water soluble drugs[245].

7.2 Futures Direction

This study has shown that, hPAP responsive nanoparticle is a promising vaginal delivery system against male to female HIV.

First, at the end this study, it is paramount important to investigate the effectiveness of this formulation in a preclinical setting in order to assess the safety and efficacy of this formulation. In a preclinical study, it is very imperative to combine more than two anti-HIV microbicide, which blocks the virus at different level. For instance, a combination of a protease inhibitor, entry inhibitor and reverse transcriptase inhibitor can reduce the risk of male to female infection to HIV through vaginal route.

Second, A new process especially, the spray drying technique can also be investigated to assess the hPAP responsive nanoparticle physical, chemical properties and anti-HIV/AIDS activity.

Third, hPAP contains amyloid fibril fragments, which are known as semen-derived enhancer of virus infection (SEVI) capture the HIV and facilitate the infection to the host cells[24]. This property of SEVI can be used as an alternative solution againt HIV male to female HIV infection. For instance, HIV target cell, macrophage $CD4^+$ membrane coated nanoparticle can be engineered as an efficient solution to attach HIV to the hPAP responsive nanoparticles. This biomimetic platform [246]made of macraphage shell and hPAP responsive nanoparticle can be used as anti HIV microbicide to outsmart the HIV. This results in the attachement of HIV to the responsive nanoparticle and its destruction. This new directive is promissing because it acts as HIV vaginal entry inhibitor.

APPENDICES

SPRINGER NATURE LICENSE
TERMS AND CONDITIONS

Dec 18, 2017

This Agreement between UNIVERSITY OF MISSOURI KANSAS CITY -- Albert Nguessan Ngo ("You") and Springer Nature ("Springer Nature") consists of your license details and the terms and conditions provided by Springer Nature and Copyright Clearance Center.

License Number	4251980194567
License date	Dec 18, 2017
Licensed Content Publisher	Springer Nature
Licensed Content Publication	Pharmaceutical Research
Licensed Content Title	Sodium Acetate Coated Tenofovir-Loaded Chitosan Nanoparticles for Improved Physico-Chemical Properties
Licensed Content Author	Albert N. Ngo, Miezan J. M. Ezoulin, James B. Murowchick et al
Licensed Content Date	Jan 1, 2015
Licensed Content Volume	33
Licensed Content Issue	2
Type of Use	Thesis/Dissertation
Requestor type	academic/university or research institute
Format	print and electronic
Portion	full article/chapter
Will you be translating?	no
Circulation/distribution	<501
Author of this Springer Nature content	yes
Title	PhD candidate pharmaceutical sciences
Instructor name	Dr. Youan Bi-Botti Celestin
Institution name	University of Missouri Kansas City
Expected presentation date	May 2018
Portions	I will use this manuscript in the chapter 2 of my PhD dissertation.
Requestor Location	UNIVERSITY OF MISSOURI KANSAS CITY 105 N. gladstone blvd, Apt 10 Kansas City, MO 64123 Cote D'Ivoire Attn: UNIVERSITY OF MISSOURI KANSAS CITY
Billing Type	Invoice
Billing Address	UNIVERSITY OF MISSOURI KANSAS CITY 105 N. gladstone blvd, Apt 10

REFERENCES

1. HIV/AIDS, W. H. O., Prevalence of HIV amond adults aged 15 to 49, 2016 by WHO region/Global Health Observatory (GHO)/HIV/AIDS. **2017**.

2. Hecht R, Bollinger L, Stover J, McGreevey W, Muhib F, Madavo CE, de Ferranti D.Critical choices in financing the response to the global HIV/AIDS pandemic. . *Health affairs* **2009,** *28* (6), 1591-1605.

3. Schackman, B. R.; Fleishman, J. A.; Su, A. E.; Berkowitz, B. K.; Moore, R. D.; Walensky, R. P.; Becker, J. E.; Voss, C.; Paltiel, A. D.; Weinstein, M. C.; Freedberg, K. A.; Gebo, K. A.; Losina, E., The lifetime medical cost savings from preventing HIV in the United States. *Med Care* **2015,** *53* (4), 293-301.

4. Fauci, A. S., An HIV Vaccine Is Essential for Ending the HIV/AIDS Pandemic. *JAMA* **2017,** *318* (16), 1535-1536.

5. Shaw, G. M.; Hunter, E., HIV transmission. *Cold Spring Harb Perspect Med* **2012,** *2* (11).

6. Yu, M.; Vajdy, M., Mucosal HIV transmission and vaccination strategies through oral compared with vaginal and rectal routes. *Expert Opin Biol Ther* **2010,** *10* (8), 1181-95.

7. Subbarao, S.; Otten, R. A.; Ramos, A.; Kim, C.; Jackson, E.; Monsour, M.; Adams, D. R.; Bashirian, S.; Johnson, J.; Soriano, V.; Rendon, A.; Hudgens, M. G.; Butera, S.; Janssen, R.; Paxton, L.; Greenberg, A. E.; Folks, T. M., Chemoprophylaxis with tenofovir disoproxil fumarate provided partial protection against infection with simian human immunodeficiency virus in macaques given multiple virus challenges. *J Infect Dis* **2006,** *194* (7), 904-11.

8. Duan, J.; Zhang, Y.; Han, S.; Chen, Y.; Li, B.; Liao, M.; Chen, W.; Deng, X.; Zhao, J.; Huang, B., Synthesis and in vitro/in vivo anti-cancer evaluation of curcumin-loaded chitosan/poly(butyl cyanoacrylate) nanoparticles. *Int J Pharm* **2010,** *400* (1-2), 211-20.

9. Sogias, I. A.; Williams, A. C.; Khutoryanskiy, V. V., Why is chitosan mucoadhesive? *Biomacromolecules* **2008,** *9* (7), 1837-42..

10. Meng, J.; Sturgis, T. F.; Youan, B. B., Engineering tenofovir loaded chitosan nanoparticles to maximize microbicide mucoadhesion. *Eur J Pharm Sci* **2011,** *44* (1-2), 57-67.

11. Van Etten, R. L.; Waymack, P. P., Substrate specificity and pH dependence of homogeneous wheat germ acid phosphatase. *Arch Biochem Biophys* **1991,** *288* (2), 634-45.

12. Yukl, S. A.; Shergill, A. K.; Ho, T.; Killian, M.; Girling, V.; Epling, L.; Li, P.; Wong, L. K.; Crouch, P.; Deeks, S. G.; Havlir, D. V.; McQuaid, K.; Sinclair, E.; Wong, J. K., The distribution of HIV DNA and RNA in cell subsets differs in gut and blood of HIV-positive patients on ART: implications for viral persistence. *J Infect Dis* **2013,** *208* (8), 1212-20.

13. van Hemert, F. J.; Berkhout, B.; Zaaijer, H. L., Differential binding of tenofovir and adefovir to reverse transcriptase of hepatitis B virus. *PLoS One* **2014,** *9* (9), e106324.

14. Wainberg, M. A., The Need for Development of New HIV-1 Reverse Transcriptase and Integrase Inhibitors in the Aftermath of Antiviral Drug Resistance. *Scientifica (Cairo)* **2012,** *2012*, 238278.

15. Ngo, A. N.; Ezoulin, M. J.; Youm, I.; Youan, B. B., Optimal Concentration of 2,2,2-Trichloroacetic Acid for Protein Precipitation Based on Response Surface Methodology. *Journal of analytical & bioanalytical techniques* **2014,** *5* (4).

16. Jakob, C. G.; Lewinski, K.; Kuciel, R.; Ostrowski, W.; Lebioda, L., Crystal structure of human prostatic acid phosphatase. *Prostate* **2000,** *42* (3), 211-8.

17. Muniyan, S.; Chaturvedi, N. K.; Dwyer, J. G.; Lagrange, C. A.; Chaney, W. G.; Lin, M. F., Human prostatic acid phosphatase: structure, function and regulation. *Int J Mol Sci* **2013,** *14* (5), 10438-64.

18. Chuang, T. D.; Chen, S. J.; Lin, F. F.; Veeramani, S.; Kumar, S.; Batra, S. K.; Tu, Y.; Lin, M. F., Human prostatic acid phosphatase, an authentic tyrosine phosphatase, dephosphorylates ErbB-2 and regulates prostate cancer cell growth. *J Biol Chem* **2010,** *285* (31), 23598-606.

19. Kong, H. Y.; Byun, J., Emerging roles of human prostatic Acid phosphatase. *Biomol Ther (Seoul)* **2013,** *21* (1), 10-20.

20. McTigue, J. J.; Van Etten, R. L., An essential active-site histidine residue in human prostatic acid phosphatase. Ethoxyformylation by diethyl pyrocarbonate and phosphorylation by a substrate. *Biochim Biophys Acta* **1978,** *523* (2), 407-21.

21. Kavanagh, J. P.; Bardsley, W. G., The identity of the acid and alkaline phosphatases of human seminal plasma. *J Reprod Fertil* **1979,** *57* (1), 43-8.

22. LaCount, M. W.; Handy, G.; Lebioda, L., Structural origins of L(+)-tartrate inhibition of human prostatic acid phosphatase. *J Biol Chem* **1998,** *273* (46), 30406-9.

23. Gundlach, G.; Luttermann-Semmer, E., The effect of pH and temperature on the stability and enzymatic activity of prostatic acid phosphatase. Studies on the optimization of a continuous monitored determination of acid phosphatase, II. *J Clin Chem Clin Biochem* **1987,** *25* (7), 441-6.

24. Munch, J.; Rucker, E.; Standker, L.; Adermann, K.; Goffinet, C.; Schindler, M.; Wildum, S.; Chinnadurai, R.; Rajan, D.; Specht, A.; Gimenez-Gallego, G.; Sanchez, P. C.; Fowler, D. M.; Koulov, A.; Kelly, J. W.; Mothes, W.; Grivel, J. C.; Margolis, L.; Keppler, O. T.; Forssmann, W.

G.; Kirchhoff, F., Semen-derived amyloid fibrils drastically enhance HIV infection. *Cell* **2007,** *131* (6), 1059-71.

25. Abdool Karim, Q.; Abdool Karim, S. S.; Frohlich, J. A.; Grobler, A. C.; Baxter, C.; Mansoor, L. E.; Kharsany, A. B.; Sibeko, S.; Mlisana, K. P.; Omar, Z.; Gengiah, T. N.; Maarschalk, S.; Arulappan, N.; Mlotshwa, M.; Morris, L.; Taylor, D.; Group, C. T., Effectiveness and safety of tenofovir gel, an antiretroviral microbicide, for the prevention of HIV infection in women. *Science* **2010,** *329* (5996), 1168-74.

26. Layne, E., spectrophotometric and turbidimetric methods for measuring proteins. *Methods Enzymol* **1957,** *3*, 447-455.

27. Owen, D. H.; Katz, D. F., A review of the physical and chemical properties of human semen and the formulation of a semen simulant. *J Androl* **2005,** *26* (4), 459-69.

28. Gao, D.; Wu, J.; Wu, Y. T.; Du, F.; Aroh, C.; Yan, N.; Sun, L.; Chen, Z. J., Cyclic GMP-AMP synthase is an innate immune sensor of HIV and other retroviruses. *Science* **2013,** *341* (6148), 903-6.

29. James W Curran. Pneumocystis Pneumonia. *Morbidity and Mortality Weekly* **1981,** *30*, 250-252.

30. Walzer PD, P. D., Krosgstad DJ, Rawson G, Schutz MG. , Pneumocystis carinii Pneumonia in the United States. Epidemiologic, diagnistic, and clinical features. *Ann intern Med* **1974,** *80*, 83-93.

31. Various, HIV/AIDS Research: Its History and Future. *Office of NIH History* **2016**, 1-7.

32. Gentile, M.; Adrian, T.; Scheidler, A.; Ewald, M.; Dianzani, F.; Pauli, G.; Gelderblom, H. R., Determination of the size of HIV using adenovirus type 2 as an internal length marker. *J Virol Methods* **1994,** *48* (1), 43-52.

33. Various, HIV sequence Compendium 2008 Introduction, Retrived March 31, 2009. **2008**.

34. Bastian, A. R.; Ang, C. G.; Kamanna, K.; Shaheen, F.; Huang, Y. H.; McFadden, K.; Duffy, C.; Bailey, L. D.; Sundaram, R. V. K.; Chaiken, I., Targeting cell surface HIV-1 Env protein to suppress infectious virus formation. *Virus Res* **2017,** *235*, 33-36.

35. Nyamweya, S.; Hegedus, A.; Jaye, A.; Rowland-Jones, S.; Flanagan, K. L.; Macallan, D. C., Comparing HIV-1 and HIV-2 infection: Lessons for viral immunopathogenesis. *Rev Med Virol* **2013,** *23* (4), 221-40.

36. Lederman, M. M.; Offord, R. E.; Hartley, O., Microbicides and other topical strategies to prevent vaginal transmission of HIV. *Nat Rev Immunol* **2006,** *6* (5), 371-82.

37. Sewankambo, N.; Gray, R. H.; Wawer, M. J.; Paxton, L.; McNaim, D.; Wabwire-Mangen, F.; Serwadda, D.; Li, C.; Kiwanuka, N.; Hillier, S. L.; Rabe, L.; Gaydos, C. A.; Quinn, T. C.; Konde-Lule, J., HIV-1 infection associated with abnormal vaginal flora morphology and bacterial vaginosis. *Lancet* **1997,** *350* (9077), 546-50.

38. Haynes, B. F.; Shattock, R. J., Critical issues in mucosal immunity for HIV-1 vaccine development. *J Allergy Clin Immunol* **2008,** *122* (1), 3-9; quiz 10-1.

39. Samson, M.; Labbe, O.; Mollereau, C.; Vassart, G.; Parmentier, M., Molecular cloning and functional expression of a new human CC-chemokine receptor gene. *Biochemistry* **1996,** *35* (11), 3362-7.

40. Wyatt, R.; Sodroski, J., The HIV-1 envelope glycoproteins: fusogens, antigens, and immunogens. *Science* **1998,** *280* (5371), 1884-8.

41. D'Cruz, O. J.; Uckun, F. M., Vaginal microbicides and their delivery platforms. *Expert Opin Drug Deliv* **2014,** *11* (5), 723-40.

42. Capoulade-Metay, C.; Ayouba, A.; Kfutwah, A.; Lole, K.; Petres, S.; Dudoit, Y.; Deterre, P.; Menu, E.; Barre-Sinoussi, F.; Debre, P.; Theodorou, I., A natural CCL5/RANTES variant antagonist for CCR1 and CCR3. *Immunogenetics* **2006,** *58* (7), 533-41.

43. Donlon, T. A.; Krensky, A. M.; Wallace, M. R.; Collins, F. S.; Lovett, M.; Clayberger, C., Localization of a human T-cell-specific gene, RANTES (D17S136E), to chromosome 17q11.2-q12. *Genomics* **1990,** *6* (3), 548-53.

44. Leith, J. G.; Copeland, K. F.; McKay, P. J.; Richards, C. D.; Rosenthal, K. L., CD8+ T-cell-mediated suppression of HIV-1 long terminal repeat-driven gene expression is not modulated by the CC chemokines RANTES, macrophage inflammatory protein (MIP)-1 alpha and MIP-1 beta. *AIDS* **1997,** *11* (5), 575-80.

45. Vangelista, L.; Secchi, M.; Liu, X.; Bachi, A.; Jia, L.; Xu, Q.; Lusso, P., Engineering of Lactobacillus jensenii to secrete RANTES and a CCR5 antagonist analogue as live HIV-1 blockers. *Antimicrob Agents Chemother* **2010,** *54* (7), 2994-3001.

46. Lobritz, M. A.; Ratcliff, A. N.; Marozsan, A. J.; Dudley, D. M.; Tilton, J. C.; Arts, E. J., Multifaceted mechanisms of HIV inhibition and resistance to CCR5 inhibitors PSC-RANTES and Maraviroc. *Antimicrob Agents Chemother* **2013,** *57* (6), 2640-50.

47. McBride, J. W.; Dias, N.; Cameron, D.; Offord, R. E.; Hartley, O.; Boyd, P.; Kett, V. L.; Malcolm, R. K., Pharmacokinetics of the Protein Microbicide 5P12-RANTES in Sheep following Single-Dose Vaginal Gel Administration. *Antimicrob Agents Chemother* **2017,** *61* (10).

48. Nettles, R. E.; Schurmann, D.; Zhu, L.; Stonier, M.; Huang, S. P.; Chang, I.; Chien, C.; Krystal, M.; Wind-Rotolo, M.; Ray, N.; Hanna, G. J.; Bertz, R.; Grasela, D., Pharmacodynamics, safety, and pharmacokinetics of BMS-663068, an oral HIV-1 attachment inhibitor in HIV-1-infected subjects. *J Infect Dis* **2012,** *206* (7), 1002-11.

49. Zwick, M. B.; Parren, P. W.; Saphire, E. O.; Church, S.; Wang, M.; Scott, J. K.; Dawson, P. E.; Wilson, I. A.; Burton, D. R., Molecular features of the broadly neutralizing immunoglobulin G1 b12 required for recognition of human immunodeficiency virus type 1 gp120. *J Virol* **2003,** *77* (10), 5863-76.

50. Li, Y.; O'Dell, S.; Walker, L. M.; Wu, X.; Guenaga, J.; Feng, Y.; Schmidt, S. D.; McKee, K.; Louder, M. K.; Ledgerwood, J. E.; Graham, B. S.; Haynes, B. F.; Burton, D. R.; Wyatt, R. T.; Mascola, J. R., Mechanism of neutralization by the broadly neutralizing HIV-1 monoclonal antibody VRC01. *J Virol* **2011,** *85* (17), 8954-67.

51. Gorny, M. K.; Conley, A. J.; Karwowska, S.; Buchbinder, A.; Xu, J. Y.; Emini, E. A.; Koenig, S.; Zolla-Pazner, S., Neutralization of diverse human immunodeficiency virus type 1 variants by an anti-V3 human monoclonal antibody. *J Virol* **1992,** *66* (12), 7538-42.

52. Qin, Y.; Shi, H.; Banerjee, S.; Agrawal, A.; Banasik, M.; Cho, M. W., Detailed characterization of antibody responses against HIV-1 group M consensus gp120 in rabbits. *Retrovirology* **2014,** *11*, 125.

53. Trkola, A.; Purtscher, M.; Muster, T.; Ballaun, C.; Buchacher, A.; Sullivan, N.; Srinivasan, K.; Sodroski, J.; Moore, J. P.; Katinger, H., Human monoclonal antibody 2G12 defines a distinctive neutralization epitope on the gp120 glycoprotein of human immunodeficiency virus type 1. *J Virol* **1996,** *70* (2), 1100-8.

54. Ofek, G.; McKee, K.; Yang, Y.; Yang, Z. Y.; Skinner, J.; Guenaga, F. J.; Wyatt, R.; Zwick, M. B.; Nabel, G. J.; Mascola, J. R.; Kwong, P. D., Relationship between antibody 2F5 neutralization of HIV-1 and hydrophobicity of its heavy chain third complementarity-determining region. *J Virol* **2010,** *84* (6), 2955-62.

55. Dey, A. K.; Griffiths, C.; Lea, S. M.; James, W., Structural characterization of an anti-gp120 RNA aptamer that neutralizes R5 strains of HIV-1. *RNA* **2005,** *11* (6), 873-84.

56. Mufhandu, H. T.; Gray, E. S.; Madiga, M. C.; Tumba, N.; Alexandre, K. B.; Khoza, T.; Wibmer, C. K.; Moore, P. L.; Morris, L.; Khati, M., UCLA1, a synthetic derivative of a gp120 RNA aptamer, inhibits entry of human immunodeficiency virus type 1 subtype C. *J Virol* **2012,** *86* (9), 4989-99.

57. Spaulding, A.; Rutherford, G. W.; Siegfried, N., Tenofovir or zidovudine in three-drug combination therapy with one nucleoside reverse transcriptase inhibitor and one non-nucleoside reverse transcriptase inhibitor for initial treatment of HIV infection in antiretroviral-naive individuals. *Cochrane Database Syst Rev* **2010,** (10), CD008740.

58. Kurth, A. E.; Celum, C.; Baeten, J. M.; Vermund, S. H.; Wasserheit, J. N., Combination HIV prevention: significance, challenges, and opportunities. *Curr HIV/AIDS Rep* **2011,** *8* (1), 62-72.

59. Gulnik, S.; Erickson, J. W.; Xie, D., HIV protease: enzyme function and drug resistance. *Vitam Horm* **2000,** *58*, 213-56.

60. Various, Antiretroviral drugs used in the treatment of HIV infection. *US Food and Drug Administration* **2018**.

61. Doitsh, G.; Greene, W. C., Dissecting How CD4 T Cells Are Lost During HIV Infection. *Cell Host Microbe* **2016,** *19* (3), 280-91.

62. Benson, C. A.; Kaplan, J. E.; Masur, H.; Pau, A.; Holmes, K. K.; Cdc; National Institutes of, H.; Infectious Diseases Society of, A., Treating opportunistic infections among HIV-infected adults and adolescents: recommendations from CDC, the National Institutes of Health, and the

HIV Medicine Association/Infectious Diseases Society of America. *MMWR Recomm Rep* **2004,** *53* (RR-15), 1-112.

63. Zheng, H.; Tang, C.; Yin, C., Exploring advantages/disadvantages and improvements in overcoming gene delivery barriers of amino Acid modified trimethylated chitosan. *Pharm Res* **2015,** *32* (6), 2038-50.

64. Artan, M.; Karadeniz, F.; Karagozlu, M. Z.; Kim, M. M.; Kim, S. K., Anti-HIV-1 activity of low molecular weight sulfated chitooligosaccharides. *Carbohydr Res* **2010,** *345* (5), 656-62.

65. Boyapalle, S.; Xu, W.; Raulji, P.; Mohapatra, S.; Mohapatra, S. S., A Multiple siRNA-Based Anti-HIV/SHIV Microbicide Shows Protection in Both In Vitro and In Vivo Models. *PLoS One* **2015,** *10* (9), e0135288.

66. Kim, K.; Lee, S.; Ryu, S.; Han, D., Efficient isolation and elution of cellular proteins using aptamer-mediated protein precipitation assay. *Biochem Biophys Res Commun* **2014**.

67. Obri, A.; Ouararhni, K.; Papin, C.; Diebold, M. L.; Padmanabhan, K.; Marek, M.; Stoll, I.; Roy, L.; Reilly, P. T.; Mak, T. W.; Dimitrov, S.; Romier, C.; Hamiche, A., ANP32E is a histone chaperone that removes H2A.Z from chromatin. *Nature* **2014,** *505* (7485), 648-53.

68. Erde, J.; Loo, R. R.; Loo, J. A., Enhanced FASP (eFASP) to Increase Proteome Coverage and Sample Recovery for Quantitative Proteomic Experiments. *J Proteome Res* **2014,** *13* (4), 1885-95.

69. Manik, L. D.; Aftab , A., Agent for protein precipitation, a method of protein precipitation, a method of protein assay using protein precipitation agent, and a kit for protein assay. U.S. Patent 5,900,376, May 4, 1999.

70. Wisniewski, J. R.; Zougman, A.; Nagaraj, N.; Mann, M., Universal sample preparation method for proteome analysis. *Nat Methods* **2009,** *6* (5), 359-62.

71. Liebler, D. C.; Ham, A. J., Spin filter-based sample preparation for shotgun proteomics. *Nat Methods* **2009,** *6* (11), 785; author reply 785-6.

72. Kim, Y. J.; Lee, H. M.; Wang, Y.; Wu, J.; Kim, S. G.; Kang, K. Y.; Park, K. H.; Kim, Y. C.; Choi, I. S.; Agrawal, G. K.; Rakwal, R.; Kim, S. T., Depletion of abundant plant RuBisCO protein using the protamine sulfate precipitation method. *Proteomics* **2013,** *13* (14), 2176-9.

73. Schilcher, G.; Schlagenhauf, A.; Schneditz, D.; Scharnagl, H.; Ribitsch, W.; Krause, R.; Rosenkranz, A. R.; Stojakovic, T.; Horina, J. H., Ethanol causes protein precipitation--new safety issues for catheter locking techniques. *PLoS One* **2013,** *8* (12), e84869.

74. Wang, J.; Feng, L.; Yu, W.; Xu, J.; Yang, H.; Liu, X., [Removal of high-abundance proteins in plasma of the obese by improved TCA/acetone precipitation method]. *Wei Sheng Yan Jiu* **2013,** *42* (5), 741-7.

75. Crowell, A. M.; Wall, M. J.; Doucette, A. A., Maximizing recovery of water-soluble proteins through acetone precipitation. *Anal Chim Acta* **2013,** *796*, 48-54.

76. Capriotti, A. L.; Cavaliere, C.; Foglia, P.; Piovesana, S.; Samperi, R.; Stampachiacchiere, S.; Lagana, A., Proteomic platform for the identification of proteins in olive (Olea europaea) pulp. *Anal Chim Acta* **2013,** *800*, 36-42.

77. Alam, A. Aftab A. , Agent for protein precipitation, a method of protein precipitation, a method of protein assay using protein precipitation agent, and a kit for protein assay. U.S. Patent US 6,875,617 B2, April 5, 2005

78. Talei, D.; Valdiani, A.; Puad, M. A., An effective protein extraction method for two-dimensional electrophoresis in the anticancer herb Andrographis paniculata Nees. *Biotechnol Appl Biochem* **2013,** *60* (5), 521-6.

79. Nandakumar, M. P.; Shen, J.; Raman, B.; Marten, M. R., Solubilization of trichloroacetic acid (TCA) precipitated microbial proteins via naOH for two-dimensional electrophoresis. *J Proteome Res* **2003,** *2* (1), 89-93.

80. Nandakumar, M. P.; Cheung, A.; Marten, M. R., Proteomic analysis of extracellular proteins from Escherichia coli W3110. *J Proteome Res* **2006,** *5* (5), 1155-61.

81. Sivaraman, T.; Kumar, T. K.; Jayaraman, G.; Yu, C., The mechanism of 2,2,2-trichloroacetic acid-induced protein precipitation. *J Protein Chem* **1997,** *16* (4), 291-7.

82. Rajalingam, D.; Loftis, C.; Xu, J. J.; Kumar, T. K., Trichloroacetic acid-induced protein precipitation involves the reversible association of a stable partially structured intermediate. *Protein Sci* **2009,** *18* (5), 980-93.

83. Wang, A.; Wu, C. J.; Chen, S. H., Gold nanoparticle-assisted protein enrichment and electroelution for biological samples containing low protein concentration--a prelude of gel electrophoresis. *J Proteome Res* **2006,** *5* (6), 1488-92.

84. Asadollahzadeh, M.; Tavakoli, H.; Torab-Mostaedi, M.; Hosseini, G.; Hemmati, A., Response surface methodology based on central composite design as a chemometric tool for optimization of dispersive-solidification liquid-liquid microextraction for speciation of inorganic arsenic in environmental water samples. *Talanta* **2014,** *123*, 25-31.

85. Chen, M.; Sui, X.; Ma, X.; Feng, X.; Han, Y., Application of response surface methodology to optimize microbial inactivation of shrimp and conch by supercritical carbon dioxide. *J Sci Food Agric* **2014**.

86. Mirizadeh, S.; Yaghmaei, S.; Ghobadi Nejad, Z., Biodegradation of cyanide by a new isolated strain under alkaline conditions and optimization by response surface methodology (RSM). *J Environ Health Sci Eng* **2014,** *12*, 85.

87. Pandiyan, K.; Tiwari, R.; Singh, S.; Nain, P. K.; Rana, S.; Arora, A.; Singh, S. B.; Nain, L., Optimization of Enzymatic Saccharification of Alkali Pretreated Parthenium sp. Using Response Surface Methodology. *Enzyme Res* **2014,** *2014*, 764898.

88. Nandy, B. C.; Verma, V.; Dey, S.; Mazumder, B., Three Levels Face Centered Central Composite Design of Colon Targeted Micro-Particulates System of Celecoxib: Screening of Formulations Variables and in Vivo Studies. *Curr Drug Deliv* **2014**.

89. Liu, Y.; Chen, M.; Wang, S.; Lin, J.; Cai, L.; Song, L., New insight into the stereoselective interactions of quinine and quinidine, with bovine serum albumin. *J Mol Recognit* **2014,** *27* (5), 239-49.

90. Zunszain, P. A.; Ghuman, J.; Komatsu, T.; Tsuchida, E.; Curry, S., Crystal structural analysis of human serum albumin complexed with hemin and fatty acid. *BMC Struct Biol* **2003,** *3*, 6.

91. Peng, W.; Ding, F.; Jiang, Y. T.; Sun, Y.; Peng, Y. K., Evaluation of the biointeraction of colorant flavazin with human serum albumin: insights from multiple spectroscopic studies, in silico docking and molecular dynamics simulation. *Food Funct* **2014**.

92. Laemmli, U. K., Cleavage of structural proteins during the assembly of the head of bacteriophage T4. *Nature* **1970,** *227* (5259), 680-5.

93. Dincer, S.; Ozdurmus, S., Mathematical model for enteric film coating of tablets. *J Pharm Sci* **1977,** *66* (8), 1070-3.

94. Liu, S. B.; Qiao, L. P.; He, H. L.; Zhang, Q.; Chen, X. L.; Zhou, W. Z.; Zhou, B. C.; Zhang, Y. Z., Optimization of fermentation conditions and rheological properties of exopolysaccharide produced by deep-sea bacterium Zunongwangia profunda SM-A87. *PLoS One* **2011,** *6* (11), e26825.

95. Owen, D. H.; Katz, D. F., A review of the physical and chemical properties of human semen and the formulation of a semen simulant. *J Androl* **2005,** *26* (4), 459-69.

96. Sassi, A. B.; Isaacs, C. E.; Moncla, B. J.; Gupta, P.; Hillier, S. L.; Rohan, L. C., Effects of physiological fluids on physical-chemical characteristics and activity of topical vaginal microbicide products. *J Pharm Sci* **2008,** *97* (8), 3123-39.

97. Montgomery, D. C., *design and analysis of experiments, 6th edition; John Wiley & Sons,Inc. United States of America; P414-415, 2005.*

98. Montgomery, D. C., *Design and Analysis of experiments, 6th ed.;John Wiley & Sons , Inc, pp 412-413*. 2005.

99. Montgomery, D. C., *design and analysis of experiments, 6th edition; John Wiley & Sons,Inc. United States of America; P390-401, 2005.*

100. Ohgushi, M.; Wada, A., 'Molten-globule state': a compact form of globular proteins with mobile side-chains. *FEBS Lett* **1983,** *164* (1), 21-4.

101. Thongboonkerd, V.; McLeish, K. R.; Arthur, J. M.; Klein, J. B., Proteomic analysis of normal human urinary proteins isolated by acetone precipitation or ultracentrifugation. *Kidney Int* **2002,** *62* (4), 1461-9.

102. Leite, M.; Freitas, A.; Azul, A. M.; Barbosa, J.; Costa, S.; Ramos, F., Development, optimization and application of an analytical methodology by ultra performance liquid chromatography-tandem mass spectrometry for determination of amanitins in urine and liver samples. *Anal Chim Acta* **2013,** *799*, 77-87.

103. Leca, J. M.; Pereira, V.; Pereira, A. C.; Marques, J. C., Rapid and sensitive methodology for determination of ethyl carbamate in fortified wines using microextraction by packed sorbent and gas chromatography with mass spectrometric detection. *Anal Chim Acta* **2014,** *811*, 29-35.

104. Kearney, B. P.; Flaherty, J. F.; Shah, J., Tenofovir disoproxil fumarate: clinical pharmacology and pharmacokinetics. *Clin Pharmacokinet* **2004,** *43* (9), 595-612.

105. Lee, Y. L.; Cesario, T.; Owens, J.; Shanbrom, E.; Thrupp, L. D., Antibacterial activity of citrate and acetate. *Nutrition* **2002,** *18* (7-8), 665-6.

106. Frech, G.; Allen, L. V., Jr.; Stiles, M. L.; Levinson, R. S., Sodium acetate as a preservative in protein hydrolysate solutions. *American journal of hospital pharmacy* **1979,** *36* (12), 1672-5.

107. Karaca, H.; Perez-Gago, M. B.; Taberner, V.; Palou, L., Evaluating food additives as antifungal agents against Monilinia fructicola in vitro and in hydroxypropyl methylcellulose-lipid composite edible coatings for plums. *International journal of food microbiology* **2014,** *179*, 72-9.

108. Costa, C.; Conte, A.; Del Nobile, M. A., Effective preservation techniques to prolong the shelf life of ready-to-eat oysters. *J Sci Food Agric* **2014,** *94* (13), 2661-7.

109. Millard S. Larson, H., and John F. Henry, Process of producing sodium or potassium acetate, propionate or butyrate. *US patent 2,895,990* **1959**.

110. Date, A. A.; Destache, C. J., A review of nanotechnological approaches for the prophylaxis of HIV/AIDS. *Biomaterials* **2013,** *34* (26), 6202-28.

111. Rautio, J.; R.;, M.; Kubunyi, H.; Folkers, G., Prodrugs and Targeted delivery. *Wiley VCH: Hoboken; 2010* **2010,** *47*.

112. Solinova, V.; Kasicka, V.; Sazelova, P.; Holy, A., Chiral analysis of anti-acquired immunodeficiency syndrome drug, 9-(R)-[2-(phosphonomethoxy)propyl]adenine (tenofovir), and related antiviral acyclic nucleoside phosphonates by CE using beta-CD as chiral selector. *Electrophoresis* **2009,** *30* (12), 2245-54.

113. Wang, X.; Zheng, C.; Wu, Z.; Teng, D.; Zhang, X.; Wang, Z.; Li, C., Chitosan-NAC nanoparticles as a vehicle for nasal absorption enhancement of insulin. *Journal of biomedical materials research. Part B, Applied biomaterials* **2009,** *88* (1), 150-61.

114. Rampino, A.; Borgogna, M.; Blasi, P.; Bellich, B.; Cesaro, A., Chitosan nanoparticles: preparation, size evolution and stability. *Int J Pharm* **2013,** *455* (1-2), 219-28.

115. Cullity B, D. ,Stock S.R. , Elements X-Ray Diffraction. *Book, ISBN 0-201-61091-4* **2001**, 123.

116. BRUSS, D. B., Harlow G. A., Titration of Weak Acids in Nonaqueous Solvents: Potentiometric Studies in Inert Solvents. *Analytical Chemistry* **1958,** *30* (11).

117. Costa, P.; Sousa Lobo, J. M., Modeling and comparison of dissolution profiles. *Eur J Pharm Sci* **2001,** *13* (2), 123-33.

118. Wadajkar, A. S.; Kadapure, T.; Zhang, Y.; Cui, W.; Nguyen, K. T.; Yang, J., Dual-imaging enabled cancer-targeting nanoparticles. *Adv Healthc Mater* **2012,** *1* (4), 450-6.

119. Panda, S. K.; Kumar, S.; Tupperwar, N. C.; Vaidya, T.; George, A.; Rath, S.; Bal, V.; Ravindran, B., Chitohexaose activates macrophages by alternate pathway through TLR4 and blocks endotoxemia. *PLoS Pathog* **2012,** *8* (5), e1002717.

120. Connelly, L.; Palacios-Callender, M.; Ameixa, C.; Moncada, S.; Hobbs, A. J., Biphasic regulation of NF-kappa B activity underlies the pro- and anti-inflammatory actions of nitric oxide. *Journal of immunology* **2001,** *166* (6), 3873-81.

121. Vega-Avila, E.; Pugsley, M. K., An overview of colorimetric assay methods used to assess survival or proliferation of mammalian cells. *Proc West Pharmacol Soc* **2011,** *54*, 10-4.

122. Dana W. Mayo, F. A. M., Robert W. Hannah, Course notes on the interpretaion of Infrared and Raman Spectra. *Willey&sons Publication* **2004**, 210-213.

123. Cho, J.; Heuzey, M. C.; Begin, A.; Carreau, P. J., Physical gelation of chitosan in the presence of beta-glycerophosphate: the effect of temperature. *Biomacromolecules* **2005,** *6* (6), 3267-75.

124. Van Beilen, J. W.; Teixeira de Mattos, M. J.; Hellingwerf, K. J.; Brul, S., Distinct effects of sorbic acid and acetic acid on the electrophysiology and metabolism of Bacillus subtilis. *Applied and environmental microbiology* **2014,** *80* (19), 5918-26.

125. Senozan, H. N. P. a. N. M., The Henderson–Hasselbalch Equation: Its History and Limitations. *Journal of chemical education* **2001,** *78* (11), 1499-1503.

126. Bigucci, F.; Abruzzo, A.; Vitali, B.; Saladini, B.; Cerchiara, T.; Gallucci, M. C.; Luppi, B., Vaginal inserts based on chitosan and carboxymethylcellulose complexes for local delivery of chlorhexidine: preparation, characterization and antimicrobial activity. *Int J Pharm* **2015,** *478* (2), 456-63.

127. FWU-LONG MI, S.-S. S., TSUNG-BI WONG, SHIANG-FANG JANG, SUNG-TAO LEE, KAI-TAI LU, Chitosan–Polyelectrolyte Complexation for the Preparation of Gel Beads and Controlled Release of Anticancer Drug. II. Effect of pH-Dependent Ionic Crosslinking or Interpolymer Complex Using Tripolyphosphate or Polyphosphate as Reagent. *Journal of Applied Polymer Sciences* **1999,** *74*, 1093-1107.

128. Holleman, A. F., ; Wiberg, E, Inorganic Chemistry, . *Book, ISBN 0-12-352651-5* **2001**, 729.

129. Magder, S.; Emami, A., Practical approach to physical-chemical Acid-base management. Stewart at the bedside. *Annals of the American Thoracic Society* **2015,** *12* (1), 111-7.

130. Hu, W.; Ding, L.; Cao, J.; Liu, L.; Wei, Y.; Fang, Y., Protein binding-induced surfactant aggregation variation: a new strategy of developing fluorescent aqueous sensor for proteins. *ACS applied materials & interfaces* **2015,** *7* (8), 4728-36.

131. Tarak C. Padhiyar, D. S. B. T., Recovery of Acetic Acid From Effluent via Freeze Crystallization. *Internationnal Journal of Scientific Engineering and Technology* **2013,** *2* (4), 211-215.

132. Cengel, Y. A. T., Robert H, Fundamentals of thermal-fluid sciences. *Boston: McGraw-Hill ISBN 0-07-297675-6.* **2004**, 78.

133. Victor H. Agenda, J. R. Z., Acetic acid and its derivatives. *Book, ISBN 0-8247-8792-7* **1993,** *49*, 96.

134. Paula, P. A. J. d., Atkin's Physical Chemistry, ninth edition. *Book, ISBN 978-0-19-954337-3* **2010**, 196.

135. Babak Minofar, P. J., , Manash R. Das,‡ Werner Kunz,, and Sekh Mahiuddin, Propensity of Formate, Acetate, Benzoate, and Phenolate for the Aqueous Solution/Vapor Interface: Surface Tension Measurements and Molecular Dynamics Simulations. *J. Phys. Chem.* **2007,** *111*, 8242-8247.

136. Michael J. Barrow, M. C., Kenneth W. Muir, J. Clare Speakman and David N. J. White, Crystal Structures of Some Acid Salts of Monobasic Acids. Part XVII. Structure of Sodium Hydrogen Diacetate, redetermined by Neutron Diffraction. *Journal of Chemical Society. Perkin 2*, 15-17.

137. Cameron, T. S.;Mannan K. M.; Rahman M. O., The crystal structure of sodium acetate trihydrate. *Acta Crystallographica. Section B* **1976,** *32*, 87-90.

138. Bruss, D. C.;Stock, S.R., Elements X-Ray Diffraction *Book, ISBN 0-201-61091-4* **2001,** *3* 296.

139. Zambito, Y.; Pedreschi, E.; Di Colo, G., Is dialysis a reliable method for studying drug release from nanoparticulate systems?-A case study. *Int J Pharm* **2012,** *434* (1-2), 28-34.

140. Chavanpatil, M. D.; Jain, P.; Chaudhari, S.; Shear, R.; Vavia, P. R., Novel sustained release, swellable and bioadhesive gastroretentive drug delivery system for ofloxacin. *Int J Pharm* **2006,** *316* (1-2), 86-92.

141. Smith, A.; Perelman, M.; Hinchcliffe, M., Chitosan: a promising safe and immune-enhancing adjuvant for intranasal vaccines. *Human vaccines & immunotherapeutics* **2014,** *10* (3), 797-807.

142. Lopez-Garcia, J.; Lehocky, M.; Humpolicek, P.; Saha, P., HaCaT Keratinocytes Response on Antimicrobial Atelocollagen Substrates: Extent of Cytotoxicity, Cell Viability and Proliferation. *Journal of functional biomaterials* **2014,** *5* (2), 43-57.

143. Introini, A.; Vanpouille, C.; Lisco, A.; Grivel, J. C.; Margolis, L., Interleukin-7 facilitates HIV-1 transmission to cervico-vaginal tissue ex vivo. *PLoS pathogens* **2013,** *9* (2), e1003148.

144. Seyfarth, F.; Schliemann, S.; Elsner, P.; Hipler, U. C., Antifungal effect of high- and low-molecular-weight chitosan hydrochloride, carboxymethyl chitosan, chitosan oligosaccharide and N-acetyl-D-glucosamine against Candida albicans, Candida krusei and Candida glabrata. *Int J Pharm* **2008,** *353* (1-2), 139-48.

145. Ngo, A. N.; Ezoulin, M. J.; Murowchick, J. B.; Gounev, A. D.; Youan, B. B., Sodium Acetate Coated Tenofovir-Loaded Chitosan Nanoparticles for Improved Physico-Chemical Properties. *Pharm Res* **2016,** *33* (2), 367-83.

146. Cariani, L.; Thomas, L.; Brito, J.; del Castillo, J. R., Bismuth citrate in the quantification of inorganic phosphate and its utility in the determination of membrane-bound phosphatases. *Anal Biochem* **2004,** *324* (1), 79-83.

147. Saheki, S.; Takeda, A.; Shimazu, T., Assay of inorganic phosphate in the mild pH range, suitable for measurement of glycogen phosphorylase activity. *Anal Biochem* **1985,** *148* (2), 277-81.

148. Nollet, L. L., Chromatograhic analysis of the environment. **2005,** *93*, 270.

149. Prusakiewicz, J. J.; Ackermann, C.; Voorman, R., Comparison of skin esterase activities from different species. *Pharm Res* **2006,** *23* (7), 1517-24.

150. Du, N.; Chen, M.; Liu, Z.; Sheng, L.; Xu, H.; Chen, S., Kinetics and mechanism of jack bean urease inhibition by Hg2+. *Chem Cent J* **2012,** *6* (1), 154.

151. Diaz, D. A.; Colgan, S. T.; Langer, C. S.; Bandi, N. T.; Likar, M. D.; Van Alstine, L., Dissolution Similarity Requirements: How Similar or Dissimilar Are the Global Regulatory Expectations? *The AAPS journal* **2016,** *18* (1), 15-22.

152. Owen, T. C., Tetrazolium compound for cell viability assays. *US patenbt # 5185450A* **1993**.

153. Gundlach, G.; Luttermann-Semmer, E., The effect of pH and temperature on the stability and enzymatic activity of prostatic acid phosphatase. Studies on the optimization of a continuous monitored determination of acid phosphatase, II. *J Clin Chem Clin Biochem* **1987,** *25* (7), 441-6.

154. King, R. J., Acid and Alkaline phosphatases in their relation to malignant disease. *Post graduate medical journal* **1948**, 299-306.

155. Kalepu, S.; Nekkanti, V., Insoluble drug delivery strategies: review of recent advances and business prospects. *Acta pharmaceutica Sinica. B* **2015,** *5* (5), 442-53.

156. Tuomela, A.; Hirvonen, J.; Peltonen, L., Stabilizing Agents for Drug Nanocrystals: Effect on Bioavailability. *Pharmaceutics* **2016,** *8* (2).

157. Lobmann, K.; Laitinen, R.; Grohganz, H.; Gordon, K. C.; Strachan, C.; Rades, T., Coamorphous drug systems: enhanced physical stability and dissolution rate of indomethacin and naproxen. *Molecular pharmaceutics* **2011,** *8* (5), 1919-28.

158. Jensen, K. T.; Larsen, F. H.; Cornett, C.; Lobmann, K.; Grohganz, H.; Rades, T., Formation Mechanism of Coamorphous Drug-Amino Acid Mixtures. *Molecular pharmaceutics* **2015,** *12* (7), 2484-92.

159. Cheow, W. S.; Kiew, T. Y.; Yang, Y.; Hadinoto, K., Amorphization strategy affects the stability and supersaturation profile of amorphous drug nanoparticles. *Molecular pharmaceutics* **2014,** *11* (5), 1611-20.

160. Badal Tejedor, M.; Nordgren, N.; Schuleit, M.; Pazesh, S.; Alderborn, G.; Millqvist-Fureby, A.; Rutland, M. W., Determination of Interfacial Amorphicity in Functional Powders. *Langmuir : the ACS journal of surfaces and colloids* **2017,** *33* (4), 920-926.

161. Curtin, V.; Amharar, Y.; Hu, Y.; Erxleben, A.; McArdle, P.; Caron, V.; Tajber, L.; Corrigan, O. I.; Healy, A. M., Investigation of the capacity of low glass transition temperature excipients to minimize amorphization of sulfadimidine on comilling. *Molecular pharmaceutics* **2013,** *10* (1), 386-96.

162. Baird, J. A.; Taylor, L. S., Evaluation of amorphous solid dispersion properties using thermal analysis techniques. *Adv Drug Deliv Rev* **2012,** *64* (5), 396-421.

163. Martinez, L. M.; Videa, M.; Lopez Silva, T.; Castro, S.; Caballero, A.; Lara-Diaz, V. J.; Castorena-Torres, F., Two-phase amorphous-amorphous solid drug dispersion with enhanced

stability, solubility and bioavailability resulting from ultrasonic dispersion of an immiscible system. *Eur J Pharm Biopharm* **2017,** *119*, 243-252.

164. Marano, S.; Barker, S. A.; Raimi-Abraham, B. T.; Missaghi, S.; Rajabi-Siahboomi, A.; Craig, D. Q. M., Development of micro-fibrous solid dispersions of poorly water-soluble drugs in sucrose using temperature-controlled centrifugal spinning. *Eur J Pharm Biopharm* **2016,** *103*, 84-94.

165. Kauppinen, A.; Broekhuis, J.; Grasmeijer, N.; Tonnis, W.; Ketolainen, J.; Frijlink, H. W.; Hinrichs, W. L. J., Efficient production of solid dispersions by spray drying solutions of high solid content using a 3-fluid nozzle. *Eur J Pharm Biopharm* **2017**.

166. Vo, C. L.; Park, C.; Lee, B. J., Current trends and future perspectives of solid dispersions containing poorly water-soluble drugs. *Eur J Pharm Biopharm* **2013,** *85* (3 Pt B), 799-813.

167. LaFountaine, J. S.; Prasad, L. K.; Miller, D. A.; McGinity, J. W.; Williams, R. O., 3rd, Mucoadhesive amorphous solid dispersions for sustained release of poorly water soluble drugs. *Eur J Pharm Biopharm* **2017,** *113*, 157-167.

168. Saal, W.; Ross, A.; Wyttenbach, N.; Alsenz, J.; Kuentz, M., A Systematic Study of Molecular Interactions of Anionic Drugs with a Dimethylaminoethyl Methacrylate Copolymer Regarding Solubility Enhancement. *Molecular pharmaceutics* **2017,** *14* (4), 1243-1250.

169. Goncalves, C.; Gomez, J. P.; Meme, W.; Rasolonjatovo, B.; Gosset, D.; Nedellec, S.; Hulin, P.; Huin, C.; Le Gall, T.; Montier, T.; Lehn, P.; Pichon, C.; Guegan, P.; Cheradame, H.; Midoux, P., Curcumin/poly(2-methyl-2-oxazoline-b-tetrahydrofuran-b-2-methyl-2-oxazoline) formulation: An improved penetration and biological effect of curcumin in F508del-CFTR cell lines. *Eur J Pharm Biopharm* **2017**.

170. Chiou, W. L.; Riegelman, S., Pharmaceutical applications of solid dispersion systems. *J Pharm Sci* **1971,** *60* (9), 1281-302.

171. Craig, D. Q., The mechanisms of drug release from solid dispersions in water-soluble polymers. *Int J Pharm* **2002,** *231* (2), 131-44.

172. Kawabata, Y.; Yamamoto, K.; Debari, K.; Onoue, S.; Yamada, S., Novel crystalline solid dispersion of tranilast with high photostability and improved oral bioavailability. *Eur J Pharm Sci* **2010,** *39* (4), 256-62.

173. Van Drooge, D. J.; Hinrichs, W. L.; Visser, M. R.; Frijlink, H. W., Characterization of the molecular distribution of drugs in glassy solid dispersions at the nano-meter scale, using differential scanning calorimetry and gravimetric water vapour sorption techniques. *Int J Pharm* **2006,** *310* (1-2), 220-9.

174. Johnston, C. S.; Gaas, C. A., Vinegar: medicinal uses and antiglycemic effect. *MedGenMed* **2006,** *8* (2), 61.

175. Neavyn, M. J.; Boyer, E. W.; Bird, S. B.; Babu, K. M., Sodium acetate as a replacement for sodium bicarbonate in medical toxicology: a review. *J Med Toxicol* **2013,** *9* (3), 250-4.

176. Ekblad, H.; Kero, P.; Takala, J., Slow sodium acetate infusion in the correction of metabolic acidosis in premature infants. *Am J Dis Child* **1985,** *139* (7), 708-10.

177. Ackerman, G. L., Serum Sodium. In *Clinical Methods: The History, Physical, and Laboratory Examinations*, rd; Walker, H. K.; Hall, W. D.; Hurst, J. W., Eds. Boston, 1990.

178. Sallam, K. I., Antimicrobial and antioxidant effects of sodium acetate, sodium lactate, and sodium citrate in refrigerated sliced salmon. *Food control* **2007,** *18* (5), 566-575.

179. Zheng, J. Y.; Keeney, M. P., Taste masking analysis in pharmaceutical formulation development using an electronic tongue. *Int J Pharm* **2006,** *310* (1-2), 118-24.

180. Sharafi, M.; Hayes, J. E.; Duffy, V. B., Masking Vegetable Bitterness to Improve Palatability Depends on Vegetable Type and Taste Phenotype. *Chemosensory perception* **2013,** *6* (1), 8-19.

181. Selvamuthukumar, S.; Anandam, S.; Kannan, K.; Manavalan, R., Nanosponges: a novel class of drug delivery system--review. *Journal of pharmacy & pharmaceutical sciences : a publication of the Canadian Society for Pharmaceutical Sciences, Societe canadienne des sciences pharmaceutiques* **2012,** *15* (1), 103-11.

182. Shah, S. M.; Jain, A. S.; Kaushik, R.; Nagarsenker, M. S.; Nerurkar, M. J., Preclinical formulations: insight, strategies, and practical considerations. *AAPS PharmSciTech* **2014,** *15* (5), 1307-23.

183. Tang, X.; Wang, G.; Shi, R.; Jiang, K.; Meng, L.; Ren, H.; Wu, J.; Hu, Y., Enhanced tolerance and antitumor efficacy by docetaxel-loaded albumin nanoparticles. *Drug Deliv* **2016,** *23* (8), 2686-2696.

184. Malleswara Reddy, A.; Banda, N.; Govind Dagdu, S.; Venugopala Rao, D.; Kocherlakota, C. S.; Krishnamurthy, V., Evaluation of the pharmaceutical quality of docetaxel injection using new stability indicating chromatographic methods for assay and impurities. *Sci Pharm* **2010,** *78* (2), 215-31.

185. Zhai, G.; Wu, J.; Xiang, G.; Mao, W.; Yu, B.; Li, H.; Piao, L.; Lee, L. J.; Lee, R. J., Preparation, characterization and pharmacokinetics of folate receptor-targeted liposomes for docetaxel delivery. *Journal of nanoscience and nanotechnology* **2009,** *9* (3), 2155-61.

186. Amat, S.; Bougnoux, P.; Penault-Llorca, F.; Fetissof, F.; Cure, H.; Kwiatkowski, F.; Achard, J. L.; Body, G.; Dauplat, J.; Chollet, P., Neoadjuvant docetaxel for operable breast cancer

induces a high pathological response and breast-conservation rate. *British journal of cancer* **2003,** *88* (9), 1339-45.

187. Lyseng-Williamson, K. A.; Fenton, C., Docetaxel: a review of its use in metastatic breast cancer. *Drugs* **2005,** *65* (17), 2513-31.

188. De Weger, V. A.; Beijnen, J. H.; Schellens, J. H., Cellular and clinical pharmacology of the taxanes docetaxel and paclitaxel--a review. *Anticancer Drugs* **2014,** *25* (5), 488-94.

189. Engels, F. K.; Mathot, R. A.; Verweij, J., Alternative drug formulations of docetaxel: a review. *Anticancer Drugs* **2007,** *18* (2), 95-103.

190. Tan, Q.; Liu, X.; Fu, X.; Li, Q.; Dou, J.; Zhai, G., Current development in nanoformulations of docetaxel. *Expert Opin Drug Deliv* **2012,** *9* (8), 975-90.

191. Mirza, A.; Mithal, N., Alcohol intoxication with the new formulation of docetaxel. *Clinical oncology* **2011,** *23* (8), 560-1.

192. Donald G. Archer, S. R., Enthalpy of Fusion of Indium: A Certified Reference Material for Differential Scanning Calorimetry. *J. Chem. Eng.* **2003,** *48* (5), 1157-1163.

193. Mortier, K. A.; Renard, V.; Verstraete, A. G.; Van Gussem, A.; Van Belle, S.; Lambert, W. E., Development and validation of a liquid chromatography-tandem mass spectrometry assay for the quantification of docetaxel and paclitaxel in human plasma and oral fluid. *Anal Chem* **2005,** *77* (14), 4677-83.

194. J. Jones, J. D., LC-MS/MS Method for the Determinationof Docetaxel in Human Serum for Clinical Research. *Thermoscientific chromatography* **2012**.

195. Meng, J.; Agrahari, V.; Ezoulin, M. J.; Purohit, S. S.; Zhang, T.; Molteni, A.; Dim, D.; Oyler, N. A.; Youan, B. C., Spray-Dried Thiolated Chitosan-Coated Sodium Alginate Multilayer Microparticles for Vaginal HIV Microbicide Delivery. *The AAPS journal* **2017,** *19* (3), 692-702.

196. Loos, W. J.; Verweij, J.; Nooter, K.; Stoter, G.; Sparreboom, A., Sensitive determination of docetaxel in human plasma by liquid-liquid extraction and reversed-phase high-performance liquid chromatography. *J Chromatogr B Biomed Sci Appl* **1997,** *693* (2), 437-41.

197. Zhang, P.; Zhang, H.; He, W.; Zhao, D.; Song, A.; Luan, Y., Disulfide-Linked Amphiphilic Polymer-Docetaxel Conjugates Assembled Redox-Sensitive Micelles for Efficient Antitumor Drug Delivery. *Biomacromolecules* **2016,** *17* (5), 1621-32.

198. Ward, M. D.; Buttry, D. A., In situ interfacial mass detection with piezoelectric transducers. *Science* **1990,** *249* (4972), 1000-7.

199. Daniel A. Buttry, M. D. W., Measurement of interfacial processes at electrode surfaces with the electrochemical quartz crystal microbalance. *Chemical Reviews* **1992,** *92* (6), 1355-1379.

200. Weckman, N. E.; McRae, C.; Ko Ferrigno, P.; Seshia, A. A., Comparison of the specificity and affinity of surface immobilised Affimer binders using the quartz crystal microbalance. *Analyst* **2016,** *141* (22), 6278-6286.

201. Karczmarczyk, A.; Haupt, K.; Feller, K. H., Development of a QCM-D biosensor for Ochratoxin A detection in red wine. *Talanta* **2017,** *166*, 193-197.

202. Bing Wu, K. W., Ping wang, and Da-Ming Zhu, Adsorption Kinetics and Adsorption Isotherm of Poly(N-isopropylacrylamide) on GoldSurfaces Studied Using QCM-D. *J. Phys. Chem.* **2007,** *111*, 1131-1135.

203. Dutta, A. K.; Belfort, G., Adsorbed gels versus brushes: viscoelastic differences. *Langmuir : the ACS journal of surfaces and colloids* **2007,** *23* (6), 3088-94.

204. Kulkarni, Y. M.; Yakisich, J. S.; Azad, N.; Venkatadri, R.; Kaushik, V.; O'Doherty, G.; Iyer, A. K. V., Anti-tumorigenic effects of a novel digitoxin derivative on both estrogen receptor-positive and triple-negative breast cancer cells. *Tumour Biol* **2017,** *39* (6), 1010428317705331.

205. Naguib, Y. W.; Rodriguez, B. L.; Li, X.; Hursting, S. D.; Williams, R. O., 3rd; Cui, Z., Solid lipid nanoparticle formulations of docetaxel prepared with high melting point triglycerides: in vitro and in vivo evaluation. *Molecular pharmaceutics* **2014,** *11* (4), 1239-49.

206. Garg, N. K.; Singh, B.; Kushwah, V.; Tyagi, R. K.; Sharma, R.; Jain, S.; Katare, O. P., The ligand (s) anchored lipobrid nanoconstruct mediated delivery of methotrexate: an effective approach in breast cancer therapeutics. *Nanomedicine* **2016,** *12* (7), 2043-2060.

207. Garg, N. K.; Tyagi, R. K.; Sharma, G.; Jain, A.; Singh, B.; Jain, S.; Katare, O. P., Functionalized Lipid-Polymer Hybrid Nanoparticles Mediated Codelivery of Methotrexate and Aceclofenac: A Synergistic Effect in Breast Cancer with Improved Pharmacokinetics Attributes. *Molecular pharmaceutics* **2017,** *14* (6), 1883-1897.

208. Qu, Y.; Han, B.; Yu, Y.; Yao, W.; Bose, S.; Karlan, B. Y.; Giuliano, A. E.; Cui, X., Evaluation of MCF10A as a Reliable Model for Normal Human Mammary Epithelial Cells. *PLoS One* **2015,** *10* (7), e0131285.

209. Nikkhah, M.; Strobl, J. S.; Schmelz, E. M.; Roberts, P. C.; Zhou, H.; Agah, M., MCF10A and MDA-MB-231 human breast basal epithelial cell co-culture in silicon micro-arrays. *Biomaterials* **2011,** *32* (30), 7625-32.

210. Duneet, C. W., Pairwise Multiple Comparisons in the Unequal Variance Case. *Journal of the American Statistical Association* **1980,** *75* (372), 796-800.

211. L. Zaske, M.-A. P. e. F. L., Docetaxel: Solid state characterization by X-ray powder diffractionand thermogravimetry. *journal of phys. IV* **2001**, 221-226.

212. Ngo, A. N.; Youan, B. B. C., Formulations for pharmaceutical agents US 20160361327 A1. *US patent application No, 62/173,772* **2016**.

213. Palepu, N. R., Docetaxel formulations with lipoic acid. *US patent # US 20120129922 A1* **2011**.

214. Borner, M. M.; Schneider, E.; Pirnia, F.; Sartor, O.; Trepel, J. B.; Myers, C. E., The detergent Triton X-100 induces a death pattern in human carcinoma cell lines that resembles cytotoxic lymphocyte-induced apoptosis. *FEBS Lett* **1994,** *353* (2), 129-32.

215. Kiyo, Y.; Michihiko, M.; Seiji, K.; Kusuo, N., Determination of the purityof Multi-component organic Substacnces by DSC. *Analytical Sciences* **1998,** *14*, 599-602.

216. Chiu, M. H.; Prenner, E. J., Differential scanning calorimetry: An invaluable tool for a detailed thermodynamic characterization of macromolecules and their interactions. *J Pharm Bioallied Sci* **2011,** *3* (1), 39-59.

217. Green, W. F., The "Melting-Point" of Hydrated Sodium Acetate: Solubility Curves. *J. Phys. Chem.* **1908,** *12* (9), 655-660.

218. Doles, W.; Wilkerson, G.; Morrison, S.; Richmond, R. G., Glacial Acetic Acid Adverse Events: Case Reports and Review of the Literature. *Hosp Pharm* **2015,** *50* (4), 304-9.

219. Various, Desktop X-ray Diffractometer "Miniflex". *The Rigaku Journal* **1997,** *14*, 29-36.

220. Hansen, C. M., The three dimensional solubility parameter and solvent diffusion coefficient, their improtance in surface Coating formulation. *Copenhagen Danish Technical Press* **1967**.

221. Burke, J., Solubility Parameters: Theory and Application. *The Book and Paper Group, the American Institute for Conservation* **1984,** *3*.

222. Huynh, L.; Grant, J.; Leroux, J. C.; Delmas, P.; Allen, C., Predicting the solubility of the anti-cancer agent docetaxel in small molecule excipients using computational methods. *Pharm Res* **2008,** *25* (1), 147-57.

223. Wang, J.; Yan, Z.; Zhuo, K.; Lu, J., Partial molar volumes of some alpha-amino acids in aqueous sodium acetate solutions at 308.15 K. *Biophys Chem* **1999,** *80* (3), 179-88.

224. Cameron, T. S.; Mannan, K. M.; Rahman, M. O., The crystal structure of sodium acetate trihydrate. *Acta Crystallographica. Section B* **1976**, 87-90.

225. Israelachvili, J. N., *Intermolecular and surface forces*. 2nd ed. ed.; Academic: 1991.

226. Philippe, R. P. A. M., Recherches de Stoechiométrie VII(1) Contribution à l'étude de la constante diélectrique des composés organiques purs. *Bulletin des sociétés chimiques belges* **1955,** *64*, 600-627.

227. Israelachvili, J., *Intermolecular and surface forces*. 2nd ed. ed.; Academic Press London, 1991.

228. Rabinow, B. E., Nanosuspensions in drug delivery. *Nat Rev Drug Discov* **2004,** *3* (9), 785-96.

229. Various, Stability Testing of New Drug Substances and Products. *FDA, US-Federal Register 68*, 65717-65718.

230. Chen, H.; Khemtong, C.; Yang, X.; Chang, X.; Gao, J., Nanonization strategies for poorly water-soluble drugs. *Drug discovery today* **2011,** *16* (7-8), 354-60.

231. Nair, R; Sunder, S.; Methods of Nanonization of Drugs for Enhancing their Dissolution. *European Journal of Advances in Engineering and Technology* **2016,** *3* (8), 101-110.

232. Koya, Y.; Uchida, S.; Machi, Y.; Shobu, Y.; Namiki, N.; Kotegawa, T., Prediction of drug interaction between oral adsorbent AST-120 and concomitant drugs based on the in vitro dissolution and in vivo absorption behavior of the drugs. *European journal of clinical pharmacology* **2016,** *72* (11), 1353-1361.

233. Vividha Dhapte, P. M., Advanced in hydrotropic solutions: An updated review. **2015,** *1* (4), 424-436.

234. Kumar, V. S.; Raja, C.; Jayakumar, C., A review on solubility enhancement using hydrotropic phenomena. *International Journal of Pharmacy and Pharmaceutical Sciences* **2013,** *6* (6), 1-7.

235. FDA, Taxotere (docetaxel) injection Concentrated, Intravenous Infusion (IV), refence ID: 3421782. *FDA, US-Federal Register* **2013**.

236. Merkle, F.; Bottcher, W.; Hetzer, R., Prebypass filtration of cardiopulmonary bypass circuits: an outdated technique? *Perfusion* **2003,** *18 Suppl 1*, 81-8.

237. Garle, M. J.; Fentem, J. H.; Fry, J. R., In vitro cytotoxicity tests for the prediction of acute toxicity in vivo. *Toxicol In Vitro* **1994,** *8* (6), 1303-12.

238. Tapani, E.; Taavitsainen, M.; Lindros, K.; Vehmas, T.; Lehtonen, E., Toxicity of ethanol in low concentrations. Experimental evaluation in cell culture. *Acta Radiol* **1996,** *37* (6), 923-6.

239. Tsujino, I.; Yamazaki, T.; Masutani, M.; Sawada, U.; Horie, T., Effect of Tween-80 on cell killing by etoposide in human lung adenocarcinoma cells. *Cancer chemotherapy and pharmacology* **1999,** *43* (1), 29-34.

240. Spencer, E. K.; Ivan, G. J.; Owen, H. F.; Ballard, F. J., Production and Utilization of Acetate in Mammals. *Biochem. J.* **1974,** *142*, 401-411.

241. Kucukzeybek, Y.; Gul, M. K.; Cengiz, E.; Erten, C.; Karaca, B.; Gorumlu, G.; Atmaca, H.; Uzunoglu, S.; Karabulut, B.; Sanli, U. A.; Uslu, R., Enhancement of docetaxel-induced cytotoxicity and apoptosis by all-trans retinoic acid (ATRA) through downregulation of survivin (BIRC5), MCL-1 and LTbeta-R in hormone- and drug resistant prostate cancer cell line, DU-145. *J Exp Clin Cancer Res* **2008,** *27*, 37.

242. Yhee, J. Y.; Jeon, S.; Yoon, H. Y.; Shim, M. K.; Ko, H.; Min, J.; Na, J. H.; Chang, H.; Han, H.; Kim, J. H.; Suh, M.; Lee, H.; Park, J. H.; Kim, K.; Kwon, I. C., Effects of tumor microenvironments on targeted delivery of glycol chitosan nanoparticles. *Journal of controlled release : official journal of the Controlled Release Society* **2017**.

243. Sumer Bolu, B.; Manavoglu Gecici, E.; Sanyal, R., Combretastatin A-4 Conjugated Antiangiogenic Micellar Drug Delivery Systems Using Dendron-Polymer Conjugates. *Molecular pharmaceutics* **2016,** *13* (5), 1482-90.

244. Nutan; Gupta, S. K., Microbicides: a new hope for HIV prevention. *Indian J Med Res* **2011,** *134* (6), 939-49.

245. Haaland, R. E.; Evans-Strickfaden, T.; Holder, A.; Pau, C. P.; McNicholl, J. M.; Chaikummao, S.; Chonwattana, W.; Hart, C. E., UC781 microbicide gel retains anti-HIV activity in cervicovaginal lavage fluids collected following twice-daily vaginal application. *Antimicrob Agents Chemother* **2012,** *56* (7), 3592-6.

246. Kroll, A. V.; Fang, R. H.; Zhang, L., Biointerfacing and Applications of Cell Membrane-Coated Nanoparticles. *Bioconjug Chem* **2017,** *28* (1), 23-32.

VITA

Albert Nguessan was born on January 09, 1981, in Toumodi, Côte d'Ivoire (Ivory Coast). He was educated in local local public school and graduated from "Lycee Moderne Attecoube", Abidjan, Ivory Coast, in 2001. Then, he enrolled in the research Unit of Sciences of the Structures of the Matter and Technology of the University of Cocody, where he received his associate degree in physic and Chemistry in 2004. In 2005, he joined the the prestigious National institute Felix Houphoet Boigny-Yamoussoukro and he received his chemical engineering bachelor degree in 2008. In 2007, he received the best student award and he worked in the oil company "Societe Ivoirienne de Raffinage "for six months. From 2009 to 2012, he worked as a high school teacher in mathematics, physic and chemistry. In February 2012, he joined the University of Missouri-Kansas City as an intern where he conducted research in drug delivery area. In summer 2013, he enrolled in the interdisciplinary PhD program upon completion of the admission requirements. He obtained his PhD 5 years later in May 2018 in pharmaceutical Science and Chemistry. Dr. Albert Ngo plan to embrace research academia career in the area of cancer therapy, drug delivery and vaccine development against HIV and others infectious diseases. Dr. Ngo is a member of the American association pharmaceutical scientists (AAPS) and former member of Junior Chamber International (JCI, Ivory Coast).